



UNIVERSIDAD DE INVESTIGACIÓN DE TECNOLOGÍA EXPERIMENTAL YACHAY

Escuela de Ciencias Químicas e Ingeniería

TÍTULO: EXPERIMENTAL TECHNIQUES FOR THE STUDY OF THE DEGRADATION OF PLA AND ITS BLENDS

Trabajo de integración curricular presentado como requisito para
la obtención del título de:

Ingeniera de Polímeros

Autor:

Cindhya Jazmín Chamorro López

Tutor:

PhD. Michell Uribe Rose Mary Rita

Urcuquí, junio 2021

SECRETARÍA GENERAL
(Vicerrectorado Académico/Cancillería)
ESCUELA DE CIENCIAS QUÍMICAS E INGENIERÍA
CARRERA DE POLÍMEROS
ACTA DE DEFENSA No. UITEY-CHE-2021-00009-AD

A los 21 días del mes de junio de 2021, a las 14:00 horas, de manera virtual mediante videoconferencia, y ante el Tribunal Calificador, integrado por los docentes:

Presidente Tribunal de Defensa	Dra. GONZALEZ VAZQUEZ, GEMA , Ph.D.
Miembro No Tutor	Dr. DIAZ BARRIOS, ANTONIO , Ph.D.
Tutor	Dra. MICHELL URIBE, ROSE MARY RITA , Ph.D.

El(la) señor(ita) estudiante **CHAMORRO LOPEZ, CINDHY JAZMIN**, con cédula de identidad No. **0402048078**, de la **ESCUELA DE CIENCIAS QUÍMICAS E INGENIERÍA**, de la Carrera de **POLÍMEROS**, aprobada por el Consejo de Educación Superior (CES), mediante Resolución **RPC-SO-41-No.476-2014**, realiza a través de videoconferencia, la sustentación de su trabajo de titulación denominado: **EXPERIMENTAL TECHNIQUES FOR THE STUDY OF THE DEGRADATION IN PLA AND ITS BLENDS**, previa a la obtención del título de **INGENIERO/A DE POLÍMEROS**.

El citado trabajo de titulación, fue debidamente aprobado por el(los) docente(s):

Tutor	Dra. MICHELL URIBE, ROSE MARY RITA , Ph.D.
--------------	--

Y recibió las observaciones de los otros miembros del Tribunal Calificador, las mismas que han sido incorporadas por el(la) estudiante.

Previamente cumplidos los requisitos legales y reglamentarios, el trabajo de titulación fue sustentado por el(la) estudiante y examinado por los miembros del Tribunal Calificador. Escuchada la sustentación del trabajo de titulación a través de videoconferencia, que integró la exposición de el(la) estudiante sobre el contenido de la misma y las preguntas formuladas por los miembros del Tribunal, se califica la sustentación del trabajo de titulación con las siguientes calificaciones:

Tipo	Docente	Calificación
Miembro Tribunal De Defensa	Dr. DIAZ BARRIOS, ANTONIO , Ph.D.	9,6
Tutor	Dra. MICHELL URIBE, ROSE MARY RITA , Ph.D.	9,8
Presidente Tribunal De Defensa	Dra. GONZALEZ VAZQUEZ, GEMA , Ph.D.	9,5

Lo que da un promedio de: **9.6 (Nueve punto Seis)**, sobre 10 (diez), equivalente a: **APROBADO**

Para constancia de lo actuado, firman los miembros del Tribunal Calificador, el/la estudiante y el/la secretario ad-hoc.

Certifico que *en cumplimiento del Decreto Ejecutivo 1017 de 16 de marzo de 2020, la defensa de trabajo de titulación (o examen de grado modalidad teórico práctica) se realizó vía virtual, por lo que las firmas de los miembros del Tribunal de Defensa de Grado, constan en forma digital.*



CHAMORRO LOPEZ, CINDHY JAZMIN
Estudiante

GEMA GONZALEZ VAZQUEZ
 Digitally signed by
 GEMA GONZALEZ
 VAZQUEZ
 Date: 2021.07.06
 09:47:01 -05'00'

Dra. GONZALEZ VAZQUEZ, GEMA , Ph.D.
Presidente Tribunal de Defensa

ROSE MARY RITA MICHELL URIBE
 Firmado digitalmente por ROSE
 MARY RITA MICHELL URIBE
 Fecha: 2021.07.06 07:47:39 -05'00'

Dra. MICHELL URIBE, ROSE MARY RITA , Ph.D.
Tutor

ANTONIO
DIAZ BARRIOS

Firmado digitalmente por
ANTONIO DIAZ BARRIOS
Fecha: 2021.06.24
21:29:56 -05'00'

Dr. DIAZ BARRIOS, ANTONIO , Ph.D.
Miembro No Tutor

CARLA SOFIA
YASELGA NARANJO

Digitally signed by CARLA
SOFIA YASELGA NARANJO
Date: 2021.06.24 16:12:09
-05'00'

YASELGA NARANJO, CARLA
Secretario Ad-hoc

AUTORÍA

Yo, **CINDHY JAZMÍN CHAMORRO LÓPEZ**, con cédula de identidad 0402048078, declaro que las ideas, juicios, valoraciones, interpretaciones, consultas bibliográficas, definiciones y conceptualizaciones expuestas en el presente trabajo; así cómo, los procedimientos y herramientas utilizadas en la investigación, son de absoluta responsabilidad de el/la autora (a) del trabajo de integración curricular. Así mismo, me acojo a los reglamentos internos de la Universidad de Investigación de Tecnología Experimental Yachay.

Urcuquí, julio 2021.



Cindy Jazmín Chamorro López

CI: 0402048078

AUTORIZACIÓN DE PUBLICACIÓN

Yo, **CINDHY JAZMÍN CHAMORRO LÓPEZ**, con cédula de identidad 0402048078, cedo a la Universidad de Investigación de Tecnología Experimental Yachay, los derechos de publicación de la presente obra, sin que deba haber un reconocimiento económico por este concepto. Declaro además que el texto del presente trabajo de titulación no podrá ser cedido a ninguna empresa editorial para su publicación u otros fines, sin contar previamente con la autorización escrita de la Universidad.

Asimismo, autorizo a la Universidad que realice la digitalización y publicación de este trabajo de integración curricular en el repositorio virtual, de conformidad a lo dispuesto en el Art. 144 de la Ley Orgánica de Educación Superior

Urcuquí, julio 2021.



Cindy Jazmín Chamorro López

CI: 0402048078

DEDICATION

To my parents,

To my sisters,

To my friends,

For all the support and unconditional love.

Thank you so much.



ACKNOWLEDGMENTS

I want to express my deep and sincere gratitude to my lovely family. First of all, special thanks to my parents Yolanda and Cristóbal for their guidance, love and support throughout the entire career. Thanks to my sisters Adri and Pame for their wise advice and constant motivational support during my university experience. Thanks to my nephews Dome and Samuel for their continuous and unparalleled love during the pandemic year we share together.

Special thanks to my advisor PhD. Rose Mary Michell for his constant guidance and good predisposition to work with me in this thesis study.

Finally, I would like to express my greatest appreciation to all my friends who have helped and supported me throughout these five years at Yachay Tech. Especially to my best friend Bryan, Sam, and Paula, thanks for always being for me, you are my second family, and I will always carry you in my heart. Thanks also to Rossem, Kevin, and Anthony for your unconditional support during my final year at university. Their support was undoubtedly important to reach this goal.

Thank you all for believe in me and want the best for me.

Cindhy

RESUMEN

El poli (ácido láctico) (PLA) puede descomponerse en condiciones ambientales mediante la escisión de la cadena, formando subproductos no tóxicos. La influencia de los factores ambientales abióticos en la destrucción de polímeros biodegradables es importante para evaluar y predecir el período de su total degradación en el medio ambiente. Esta revisión muestra investigaciones recientes sobre la biodegradación en ambientes abióticos y estudia la influencia de la humedad, temperatura, radiación ultravioleta (UV), la luz solar y el pH, así como las técnicas experimentales empleadas para estudiar la degradación del PLA y sus mezclas, como son la Calorimetría Diferencial de Barrido (DSC), Análisis termogravimétrico (TGA), Difracción de Rayos X (XRD), Espectroscopia Infrarroja por Transformada de Fourier (FTIR), Resonancia Magnética Nuclear (RMN), Microscopía Electrónica de Barrido (SEM) y pruebas mecánicas. El deterioro de las propiedades del PLA se debe principalmente a las escisiones de la cadena en la matriz del PLA. Estos cambios pueden observarse a través de la disminución de la masa molar del PLA, que puede ser monitoreada mediante Cromatografía de Permeación en Gel (GPC) y ^1H NMR. Por otra parte, las transiciones térmicas, típicamente estudiadas mediante DSC, presentan modificaciones durante la degradación; la transición vítrea, los procesos de cristalización y fusión muestran comportamientos diferentes, dependiendo del tipo de degradación y de los componentes presentes en las mezclas. La técnica de DRX proporciona información relevante sobre la cristalización que puede ser utilizada para complementar los resultados de DSC. Ahora bien, la estabilidad térmica del PLA se ve afectada como consecuencia de la degradación abiótica, mostrando una disminución de las temperaturas de descomposición térmica en la mayoría de los casos, tal como es reportado en los ensayos de TGA. Los cambios químicos que se originan durante la degradación pueden ser observados mediante FTIR y RMN. La degradación también afecta la morfología del PLA y sus mezclas, tanto la superficie de las muestras, mostrando evidencias de erosión, como en la interacción de las fases. Finalmente, las pruebas mecánicas resultaron ser muy sensibles a los cambios originados por la degradación, pudiéndose evidenciar la degradación mucho antes que en las otras técnicas revisadas. Las recopilaciones de estos resultados demuestran que la combinación de todas las técnicas de caracterización son una estrategia útil para monitorear el proceso de degradación y evaluar los cambios en la estructura del PLA inducidos por diferentes tipos de degradación abiótica.

Palabras clave: PLA, biodegradación, condiciones abióticas, técnicas experimentales, hidrólisis, fotólisis.

ABSTRACT

Poly (lactic acid) (PLA) can decompose under environmental conditions through chain scission, forming non-toxic subproducts. The influence of abiotic environmental factors on the destruction of biodegradable polymers is important to evaluate and predict the period of their full degradation in the environment. This review shows recent research involving biodegradation in abiotic environments and studies the influence of moisture, temperature, ultraviolet (UV) radiation, sunlight, and pH, as well as the experimental techniques employed to analyze the degradation of PLA and its blends such as Differential Scanning Calorimetry (DSC), Thermogravimetric analysis (TGA), X-Ray diffraction (XRD), Fourier Transform Infrared Spectroscopy (FT-IR), Nuclear Magnetic Resonance (NMR), Scanning electron microscopy (SEM) and Mechanical tests. These changes can be observed through the decrease in the molar mass of PLA, which can be monitored by Gel Permeation Chromatography (GPC) and ^1H NMR. On the other hand, thermal transitions, typically studied by DSC, exhibit modifications during degradation; the glass transition, the crystallization and melting processes show different behaviors, depending on the type of degradation and the components present in the blends. The XRD technique provides relevant information on crystallization that can be used to complement DSC results. Meanwhile, the thermal stability of PLA is affected as a consequence of abiotic degradation, showing a decrease in thermal decomposition temperatures in most cases, as reported in the TGA tests. Chemical changes that occur during degradation can be observed by FTIR and NMR. Degradation also affects the morphology of PLA and its blends, both the surface of the samples, showing evidence of erosion, as in the interaction of the phases. Finally, the mechanical tests proved to be very sensitive to the changes caused by the degradation, being able to show the degradation much earlier than in the other techniques reviewed. The compilation of these results demonstrate that the combination of all characterization techniques is a useful strategy for monitoring the degradation process and assessing changes on PLA structure induced by different types of abiotic degradation.

Keywords: PLA, biodegradation, abiotic conditions, experimental techniques, hydrolysis, photolysis.

CONTENT

LIST OF FIGURES	iii
LIST OF TABLES	v
LIST OF ABBREVIATIONS	vi
1. GENERAL INTRODUCTION	1
1.1. Introduction.....	1
1.2. Problem Statement.....	4
1.3. Objectives	4
1.3.1. General Objectives	4
1.3.2. Specific Objectives	4
2. PLA BACKGROUND	4
2.1. PLA properties.....	4
2.2. Application of PLA.....	6
2.2.1. Biomedical applications	6
2.2.2. Packing application	7
2.3. Degradation of PLA.....	7
2.3.1. Hydrolytic degradation.....	8
2.3.2. Photo-degradation.....	11
2.4. Degradation of PLA in abiotic environments.....	12
3. CHARACTERIZATION TECHNIQUES.....	26
3.1. Molecular weight determination.....	26
3.2. Thermal Analysis.....	30
3.2.1. Differential scanning calorimetry (DSC)	30
3.2.2. Thermogravimetric analysis (TGA)	36
3.3. X Ray diffraction (XRD)	40
3.4. Fourier Transform Infrared Spectrometry (FTIR)	43

3.5. Nuclear Magnetic Resonance (NMR) Spectroscopy	49
3.6. Scanning electron microscopy (SEM)	53
3.7. Mechanical test	56
4. CONCLUSIONS	64
5. REFERENCES	67

LIST OF FIGURES

Figure 1. Chemical structures of poly (lactic acid) (PLA) ¹¹	1
Figure 2. PLA life cycle ¹⁰	2
Figure 3. Three stereochemical forms of PLA. Taken from: ⁵	5
Figure 4. Hydrolysis process of aliphatic polyesters. (a) Water absorption of the polyester. (b) Polymer hydrolysis and formation of oligomers and monomers. (c) Oligomers and monomers diffusion ⁵²	8
Figure 5. Surface vs. bulk erosion during polymer degradation ⁸⁸	9
Figure 6. Suggested mechanism of hydrolysis in alkaline environment ^{88,94}	10
Figure 7. Suggested mechanism of hydrolysis in acidic environment ^{88,94}	11
Figure 8. Photodegradation of PLA via the Norrish II mechanism ^{95,106}	11
Figure 9. Influence of humidity, temperature, UV radiation, and pH on the biodegradation of PLA in different environments	21
Figure 10. Schematic plot of a distribution of MWs.	28
Figure 11. Molecular weight distribution of PLA after exposure to UV-A, UV-B and UV-C radiations ¹⁸⁴	29
Figure 12. Polydispersity index (PDI) of PLA films stored at 50 % RH, 100 % RH, and immersed in liquid water at 50 °C during time ¹¹⁹	30
Figure 13. DSC first heating curves of neat PLA after accelerated weathering degradation ¹⁰⁷	32
Figure 14. The differential scanning calorimetry (DSC) curves of the secondary heating curves were obtained for the degraded samples immersing in phosphate buffer solution (PBS) at 37 °C for 3, 4, 5, 6, 8, and 12 months ¹⁵⁰	34
Figure 15. (a) TGA and (b) dTG results of the reference PLA and the treated samples (10 °C/min) ¹⁰³	37
Figure 16. Thermal decomposition of degraded samples containing 60 wt % PLA for 4 weeks under hydrolytic degradation in PBS solution ⁷¹	40
Figure 17. XRD profiles of PLA films during hydrolytic degradation in (A) water, (B) 50% ethanol, (C) 95% ethanol and in the 3 rd day of immersion in (D) 50% ethanol and (E) 95% ethanol at 40 °C. The number on each profile indicate days immersed ⁶	42
Figure 18. Alterations in FTIR spectra of the neat PLA specimens after each accelerated weathering period ¹⁰⁸	45
Figure 19. Hydrolysis reaction equation of PLA in alkali solution ¹⁶⁴	46

Figure 20. FTIR spectra for pure PLA and PLA/TiO ₂ at different irradiation time ⁹⁹ ..	47
Figure 21. ¹ H NMR spectrum (700 MHz, CDCl ₃) of PLA after 16h of UV exposure at 254 nm ¹⁸⁵	50
Figure 22. Molar mass of particular groups in PLA used for calculating <i>Mn</i> ¹⁸⁵	51
Figure 23. (a) ¹³ C NMR spectra of PLA before degradation and (b) ¹³ C NMR spectra of the C=O peaks of PLA after degradation at 50 °C and 60 °C under neutral pH condition ²¹⁷	52
Figure 24. SEM of PLA/PBS with 30 wt% of PBS. (a) before degradation, (b) after being degraded at 37 °C for 312 h. Cross-section direction of sample degraded at low (c) and high magnifications (d) ⁵⁶	53
Figure 25. Schematic representations of the hydrolytic degradation process of pure PLA and PLA/PBS blends ⁵⁶	54
Figure 26. SEM micrographs of PLA fiber surface morphology. (a) non- degraded PLA fibers, (b) degraded fiber for 12 weeks at pH = 4.98 and T = 25 °C, (c) degraded fiber for 12 weeks at pH = 7.40 and T = 25 °C and (d) degraded fiber for 12 weeks at pH = 8.50 and T = 25 °C ⁵⁰	56
Figure 27. Stress-strain curve.	58
Figure 28. Schematic illustration of flexural strength test of a material ²²⁴	58
Figure 29. Effect of hydrolysis time on mechanical properties of PLA and jute/PLA composites, a) tensile strength and b) Young's modulus at 50 °C ⁶⁹	60
Figure 30. Strain at break of PLA as a function of number average molar mass (<i>Mn</i>) during exposure at 100, 130 and 150 °C under air ²³⁴	62
Figure 31. Tensile stress curves of the PLA/PBAT with different degradation days ²³⁵	63

LIST OF TABLES

Table 1. Lactic acid-based polymers properties ^{21,23,27,28}	6
Table 2. Degradation environments for PLA.....	14
Table 3. Comparison of hydrolytic degradation of modified PLA with different nanofillers.	24
Table 4. Techniques of analysis of PLA blends during degradation ¹⁸²	26
Table 5. DSC data obtained for neat PLA ^{19,107,109,124}	31
Table 6. DSC data obtained for neat PLA after accelerated weathering degradation ¹⁰⁷	33
Table 7. Evaluated TGA curve values of reference PLA ^{103 74 126}	36
Table 8. Peak band assignment for reference PLA ^{19,84,162}	44
Table 9. Mechanical properties of different stereochemical forms of PLA ^{23,226}	59

LIST OF ABBREVIATIONS

PLA	Poly(lactic acid)	nHa	Hydroxyapatite nanorod
LA	Lactic acid	Ha	Halloysite
PE	Polyethylene	AgNP	Silver nanoparticles
PET	Poly(ethylene terephthalate)	PEO	Poly(ethylene oxide)
PP	Polypropylene	WF	Wood flour
PVC	Poly(vinyl chloride)	PMMA	Polymethylmethacrylate
PS	Polystyrene	FeCl₃	Ferric chloride
PCL	Poly(ϵ -caprolactone)	TPS	Thermoplastic starch
PEG	Poly(ethylene glycol)	SP	Sucrose palmitate
PHA	Poly(hydroxyalkanoate)	PBAT	Poly(butylene adipate- <i>co</i> -terephthalate)
PLLA	Poly(L-lactic acid)	PBS	Poly(butylene succinate)
PDLA	Poly(D-lactic acid)	PGF	Phosphate glass fibre
PDLLA	Poly(D-L-lactic acid)	POM	Polyoxymethylene
PBS	Phosphate buffered saline	DSC	Differential Scanning Calorimetry
SBF	Simulated body fluids	TGA	Thermogravimetric analysis
MMT	Montmorillonite	DTG	Derivative thermogravimetric curve
C30B	Cloisite C30B	FTIR	Fourier Transform Infrared Spectroscopy
CNT	Carbon nanotubes	XRD	X-Ray diffraction
HNT	Halloysites nanotubes	GPC	Gel Permeation Chromatography
TiO₂	Titanium dioxide	PDI	Polydispersity Index
CNC	Cellulose nanocrystal	NMR	Nuclear Magnetic Resonance
ZnO	Zinc oxide	SEM	Scanning Electron Microscopy
MgO	Magnesium oxide		

1. GENERAL INTRODUCTION

1.1. Introduction

In recent years, the world consumption of polymers has increased exponentially. Conventional plastics such as polyethylene (PE), poly (ethylene terephthalate) (PET), polypropylene (PP), poly (vinyl chloride) (PVC), and polystyrene (PS), have been used for decades in a diverse range of applications as they are easily processed and are available in large quantities ¹. However, the disposal of millions of tons of these products has caused severe environmental pollution due to its low degradation ². The dismal management of these polymeric wastes represents a threat to our planet and produces an enormous ecological and economic impact. As a renewable and sustainable resource, biodegradable materials are considered a solution to the current plastic waste problem. Thanks to biodegradability, biocompatibility, sustainability, and renewability, biodegradable polymers have emerged as an alternative to reduce our dependence on petroleum-based plastics and contribute to developing a greener economy ^{3,4}.

More than perhaps any biodegradable polymer class, poly (lactic acid) or polylactide (PLA) has shown explosive growth and underpin the global shift towards sustainability. Because of its excellent properties, PLA shows broad potential applications in many fields, such as biomedical devices, packaging, agricultural films, and automotive industries ⁵. Due to its biocompatibility with the human body, PLA has been used in biomedical applications such as tissue engineering, wound management, and drug delivery systems ⁶⁻⁹. In packaging, PLA is one of the most promising candidates for the market of biopolymers ¹⁰. Therefore, biodegradable PLA is seen by many as a promising solution to “white pollution” and energy problem because they are environmentally friendly ⁵.

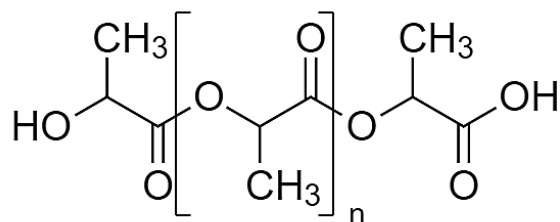


Figure 1. Chemical structures of poly (lactic acid) (PLA) ¹¹.

Poly (lactic acid) (Figure 1.) is a thermoplastic aliphatic polyester produced from non-fossil renewable natural resources by fermentation of polysaccharides or sugar extracted from corn, potato, cane molasses, and sugar-beet. PLA is industrially obtained through the polymerization of lactic acid (LA) or by the ring-opening polymerization (ROP) of lactide (the cyclic dimer of lactic acid) ¹⁰. Furthermore, PLA can be processed by film casting, extrusion, blow molding, and fiber spinning due to its greater thermal processability in comparison to other biomaterials such as poly(ϵ -caprolactone) (PCL), poly (ethylene glycol) (PEG), and poly(hydroxyalkanoates) (PHAs)¹². The life cycle of PLA is presented in Figure 2. Ordinarily, PLA is disposed of under composting conditions, which is how to biodegrade this polymer in a short time ¹³. This biodegradable material can decompose under environmental conditions and form sub-products more simple and non-toxic, mostly H_2O and CO_2 ¹⁴. Nevertheless, PLA offers other end-of-life options such as mechanical or chemical recycling and (renewable) energy recovery ¹⁵.

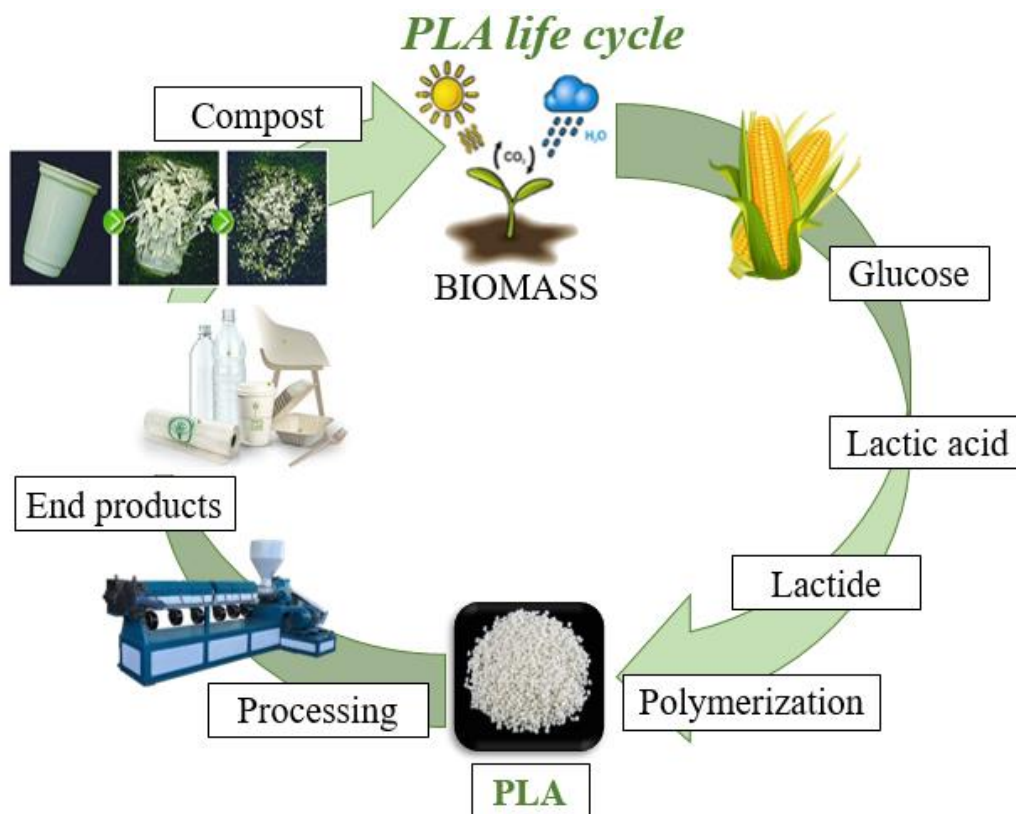


Figure 2. PLA life cycle ¹⁰.

PLA is affected by many abiotic environmental factors such as moisture, temperature, oxygen, ultraviolet (UV) radiation, sunlight, and catalytic species (influence by pH),

which cause the decomposition of these materials ¹⁶. PLA degraded faster in alkaline conditions because, during hydrolysis, cleavage of ester groups is catalyzed by hydroxide ions. Therefore, the high concentration of hydroxide ions in alkaline media enhances PLA degradation ¹⁷. UV light exposure also affects PLA degradation. Accelerated weathering tests are conducted in weathering chambers that mimic natural environmental conditions and the effects of prolonged outdoor exposure. The method is carried out by exposing the samples to UV radiation and controlled moisture/humidity and temperature ¹⁸. The primary degradation mechanism of ultraviolet (UV) irradiation is the “main chain scission” in the chemical bonds of the PLA backbone. This mechanism causes a decrease in the molecular weight of PLA to occur via “photolysis” of C–O and C–C bonds and/or “photo-oxidation” leading to the formation of carboxylic acid and ketones. Additionally, the main degradation mechanism of humidity is the “hydrolysis” of ester linkages of the PLA structure, resulting in a reduction of molecular weight ¹⁹.

This work review recent research involving biodegradation in abiotic environments and the experimental techniques employed for several authors to monitor the PLA degradation. This with the aim of characterize the changes occurring during its life cycle and predict how long it will degrade at long exposure times. The characterization techniques studied are Differential Scanning Calorimetry (DSC), Thermogravimetric analysis (TGA), X-Ray diffraction (XRD), Fourier Transform Infrared Spectroscopy (FT-IR), Nuclear Magnetic Resonance (NMR), Scanning electron microscopy (SEM), and determination of mechanical properties. Combining these analytical techniques provides parameters that monitor the degradation process and evaluate each degradation effect on the polylactide characteristics. Finally, it is important to determine the sensitivity of each technique to the advance of abiotic degradation in PLA and establish the most efficient and accessible technique that diagnoses the beginning of the degradation.

1.2. Problem Statement

Despite the enormous relevance of PLA at both scientific and industrial levels and the many reviews published on these materials, there is no bibliographic material where all the techniques used are summarized and how they help to determine the progress of degradation. For that reason, it is necessary to carry out an exhaustive review of the experimental techniques that study the degradation of PLA and its blends. This review will allow establishing protocols for the determination of useful life of PLA under abiotic degradative conditions which is studied using Differential Scanning Calorimetry (DSC), Thermogravimetric analysis (TGA), X-Ray diffraction (XRD), Fourier Transform Infrared Spectroscopy (FT-IR), Nuclear Magnetic Resonance (NMR), Scanning electron microscopy (SEM), and determination of mechanical properties.

1.3. Objectives

1.3.1. General Objectives

To review recent literature involving degradation in abiotic environments of PLA and its blends in the last five years

1.3.2. Specific Objectives

- To analyze the effect of the components of the blends on the degradation rate in abiotic conditions.
- To study the characterization techniques that monitor the PLA degradation.
- To summarize the changes induced in chemical structure, morphology, thermal, and mechanical properties of PLA during the degradation process.
- To establish the most sensitive technique that diagnoses the beginning of the degradation.

2. PLA BACKGROUND

2.1. PLA properties

Poly (lactic acid) (PLA) belongs to the family of aliphatic polyesters commonly made from hydroxy acids and are considered biodegradable and compostable²⁰. Lactic acid, a PLA monomer, has two optically active forms called L-lactic acid and D-lactic acid due

to an asymmetric carbon atom ⁵. There are three optical isomers of lactide, including L-lactide, D-lactide, and DL-lactide ²¹. Therefore, they are part of the family of polymers: poly-L-lactic acid (PLLA), poly-D-lactic acid (PDLA), and poly-D,L-lactic acid (PDLLA)²² (Figure 3).

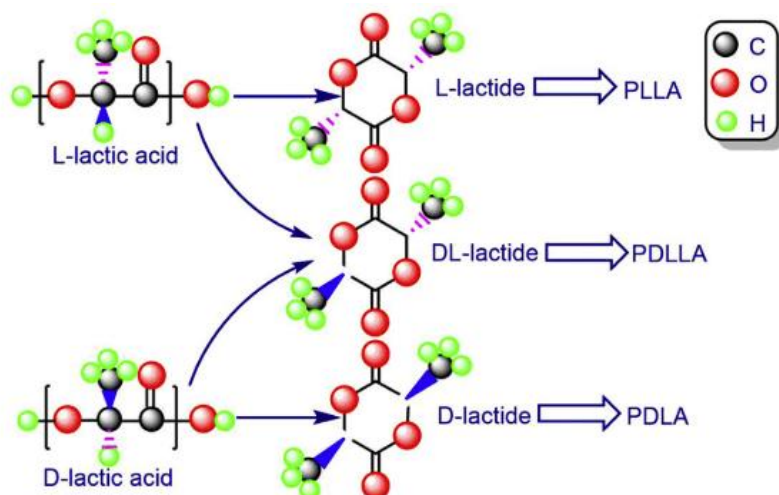


Figure 3. Three stereochemical forms of PLA. Taken from: ⁵.

PLA has achieved enormous acceptance due to its excellent biocompatibility and physical properties ²². PLA can be processed by conventional processing methods such as thermoforming, injection molding, blow molding, sheet extrusion, and fiber spinning ^{21,23}. Even PLA requires 25–55% less energy to produce than petroleum-based polymers ²³. On the other hand, PLLA has been used in applications as bioengineering and bone engineering ²¹. However, its high crystallinity and lengthy degradation periods have been the subject of study in recent years.

The physical characteristics of PLA depend on its molecular characteristics and the presence of ordered structures, such as crystallinity, lamellar thickness, spherulite size, morphology, and degree of chain orientation, also is to a great extent dependent on its transition temperatures.²⁴ In the solid-state, PLA can be either amorphous or semicrystalline, depending on the stereochemistry and thermal history. The glass transition temperature (T_g) of PLA is in ranges from 50-65 °C and melting point (T_m) ranges from 130°–180°C (depending on structure) ^{20,21}. PLA with higher than 90% PLLA tends to be crystalline, and the glass transition temperature and melting temperature of PLA increase with the amount of PLLA ^{26,27}. Moreover, the tensile strength and elastic modulus are comparable to poly (ethylene terephthalate) (PET). However, the low impact strength and brittleness indicate that they still are inadequate for use in many

applications^{21,23}. The density of amorphous and crystalline PLA has been reported as 1.248 g/cm^3 and 1.290 g/cm^3 , respectively²⁷. Generally, PLA is soluble in dichloroacetic acid, acetonitrile, chloroform, methylene chloride, 1,1,2-trichloroethane, dioxane²². Table 1 shows common properties of PLA, PLLA, PDLA, and PDLLA.

Table 1. Lactic acid-based polymers properties ^{21,23,27,28}.

Crystalline structure	PLA Semi- crystalline	PLLA Semi- crystalline	PDLA Crystalline	PDLLA Amorphous
Glass transition temperature, T_g (°C)	60-65	50-65	50-65	50-60
Melting temperature, T_m (°C)	150-162	170-180	120-150	120-170
Tensile modulus (GPA)	2.7-16	7-10	7-10	1.5-1.9
Tensile strength (MPA)	21-60	15.5-150	15.5-150	27.6-50
Elongation at break (%)	10-100	12-26	20-30	30-35
Density (g/cm^3)	1.21-1.25	1.33	1.36	1.25

2.2. Application of PLA

Exploring new materials based on PLA blends has resulted in considerable interest in the extensive research activities. The application of PLA blends can be highly affected by the composition of the blend and can vary based on the end-use requirements. For example, PLA blends have been used for several applications, such as food packaging²⁹⁻³⁸, drug delivery³⁹⁻⁴⁵, and tissue engineering^{26,27,43,44,46-48}, which can be attributed to their unique merits such as biodegradability, as well as mechanical and thermal properties⁴⁹.

2.2.1. Biomedical applications

PLA has been amply studied for medical applications because of its bioresorbability and biocompatible properties in the human body²⁴. The primary reported examples of medical or biomedical products are tissue engineering materials, implants for bone fixation devices like screws, surgical sutures, and drug delivery systems.

In tissue engineering, biopolymers such as PLA are an excellent substitute for traditional ceramic or metallic materials. PLA receives much attention because it is degraded in the human body by simple hydrolysis of the ester backbone to produce nontoxic and harmless compounds. The degradation sub-products are then eliminated through regular cellular activity and urine. Thus, they do not need a second surgery to remove the implant, reducing the medical cost and better recovering the tissue function as the device degrades^{24,26,27,46,47}.

Advances in polymer science have led to the development of several novel drug delivery systems. Delivery systems offer numerous advantages compared to conventional dosage forms; these include improved efficacy, low toxicity, and better patient convenience⁴². The PLA's drug carriers, such as liposomes, polymeric nanoparticles, micelles, and dendrimers, can encapsulate hydrophobic anti-tumor drugs. Small nanosized drug carriers are passively targeted to tumors, leading to a higher drug concentration at the tumor site and decreased toxicity than conventional administration. The liver and the kidneys rapidly eliminate these drugs with low molecular weight, and by loading them into nanoparticles, their bioavailability, payload, and anti-tumor effect increase³⁹.

2.2.2. Packing application

Market studies show that PLA is an economically feasible material for packaging. At present, PLA has positioned itself as the most consumed biopolymer for biodegradable packaging.²⁴ In general, the functional properties of PLA in terms of their mechanical and barrier properties are adapted to food requirements by using different strategies, such as physical or chemical modifications (crosslinking) or blending with other components, compatibilizers, or plasticizers³². Package applications include containers, sundae and salad cups, drinking cups, lamination films, wrappings for sweets, and water bottles²⁴. Currently, PLA is used in compostable yard bags to promote composting programs. Its degradation half-life goes from six months to two years, depending on its molecular weight and stereochemistry³².

2.3. Degradation of PLA

Polymer degradation is a desirable process to face pollution and prevent its accumulation in the environment. The degradation under abiotic environmental factors is determined by temperature, pH, humidity, and UV radiation. Their influence the degradation rate and decomposition of the polymers. Furthermore, the chemical and physical characteristics of the material, such as its morphology and molecular weight, are affected by degradation^{14,16}. The degradation of the polymer under an abiotic environment can be induced by processes as hydrolysis, photolysis, or photo-oxidation. Therefore, all these factors should be considered in the study of PLA degradation.

2.3.1. Hydrolytic degradation

Hydrolytic degradation of aliphatic polyesters occurs by the scission of chemical bonds along the backbone of the polymer. In aqueous solution, the hydrolytic mechanism proceeds through cleavage of the ester bond⁵⁰, water penetrates the polymer matrix and converts the long polymer chain to macromolecular oligomer fragments, then the formation of smaller oligomer fragments, and as the degradation progresses, the diffusion of oligomer fragments, and the formation of small molecular monomers^{51,52} (Figure 4). The presence of hydrophilic end groups as degradation products, such as hydroxyl and carboxyl, promotes polyester degradation. Increased hydrophilicity results in a greater water-absorbing capacity of the polymers, increasing the degradation rate. Also, it is established that carboxyl end groups formed by chain cleavage catalyze degradation and that amorphous regions are preferentially degraded⁵³. Many authors studied the hydrolytic degradation of PLA^{5,6,8,14,17,18,21,50-87}, and they have been found that the hydrolytic degradation of polyesters process occurs in two stages. The first stage occurs preferentially in the amorphous zones since these structures are less dense, and the hydrolytic attack facilitates the entire mass of molecular chains, the second stage results in the attack on the crystalline zones of the material, which take place once the amorphous zones have been degraded or eroded. This stage is slower than the first one due to the highly ordered structure of the crystalline zones makes the diffusion of the hydrolytic medium difficult⁵⁰.

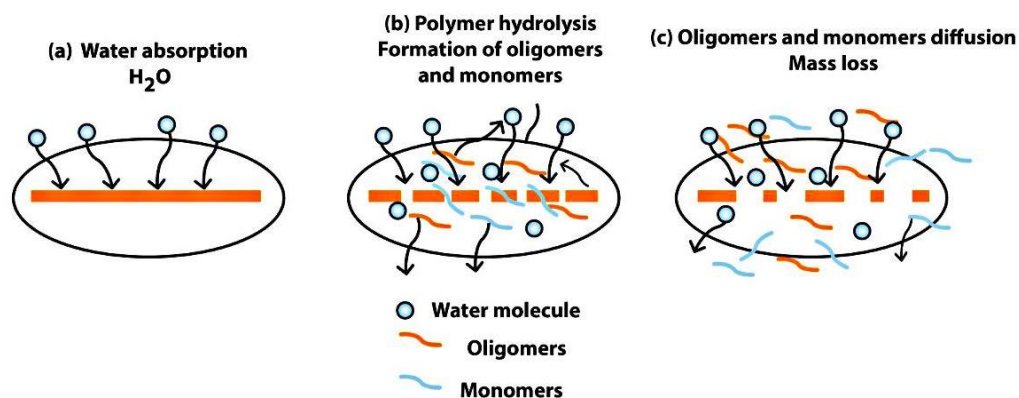


Figure 4. Hydrolysis process of aliphatic polyesters. (a) Water absorption of the polyester. (b) Polymer hydrolysis and formation of oligomers and monomers. (c) Oligomers and monomers diffusion⁵².

In general, the hydrolysis of material proceeds either via a bulk or surface erosion mechanism (Figure 5). Here, bulk erosion describes degradation that occurs uniformly through the thickness of a polymeric item, and surface erosion describes a decrease in the

surface thickness⁸⁸. Hydrolytic degradation is the result of the hydrolysis time of macromolecules into shorter chains (t_c) and the water diffusion in this time (D_T) through the material. D_T depends on crystallinity degree, hydrophobicity, and the medium characteristics as pH and temperature^{14,89}.

When the diffusion of water molecules is faster than the hydrolytic attack ($D_T > t_c$), bulk degradation occurs. At the beginning of this process, the molecular weight decreases, and crystallinity increases due to the higher mobility of shorter segments. When the chains are short enough, they become soluble in the surrounding medium resulting in weight loss.^{14,90} By contrast, when $D_T \leq t_c$, surface erosion occurs, and the material linearly loses as a consequence of chain cleavage⁹¹. The hydrolysis occurs near the surface of the sample being degraded, and the bulk remains barely unchanged¹⁴.

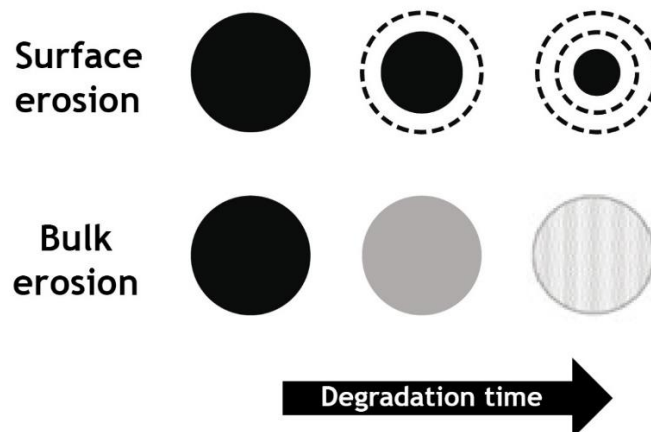


Figure 5. Surface vs. bulk erosion during polymer degradation⁸⁸.

2.3.1.1. Factors affecting the hydrolytic degradation

Factors as temperature and pH affect the hydrolytic degradation of PLA directly. Polymer chain mobility increases with medium temperature, increasing the susceptibility of ester bonds to undergo chain cleavage reactions¹⁴. For instance, PLA undergoes much faster degradation in an aqueous medium at 60 °C than at 37°C⁶².

Medium pH also influences the hydrolytic degradation mechanism of polyesters. For example, the hydrolysis of PLA is accelerated under both acidic and basic conditions. However, the polymer erosion mechanism changes at those two pH conditions from bulk erosion at low pH to surface erosion at high pH values⁸⁸. PLA degrades under basic conditions to the intermediate dilactide, while under acidic conditions, lactic acid is

directly generated⁸⁸. If the system is basic, the driving force for hydrolytic degradation changes to the formation of stable carboxylate anions⁷⁵. Chain degradation occurs via intramolecular transesterification. Such intramolecular degradation occurs by a random alkaline attack on the carbon of the ester group, followed by the hydrolysis of the ester link to release dilactide and decrease the molecular weight of PLA¹⁴ (Figure 6). While in acidic systems, an intramolecular hydrogen bond is formed due to the protonation of the hydroxyl end-group¹⁴. The hydrolysis process of ester bonds is highly dependent on the concentration of H⁺ ions in the solution (Figure 7). Therefore, a very acidic environment prevents the permeation of H⁺ ions into the structure leading to the reduction of the hydrolysis process of ester bonds because water penetrates the polymer at a slower rate, degradation occurs purely at the surface, the hydrolyzed surface by-products diffuse rapidly into the media. There is no opportunity for water molecules to reach the center of the matrix⁹². Consequently, at the higher pH condition is exhibits a more significant degradation with a greater weight loss. The simulated degradation in both environments leads to a faster mass loss; also, an aqueous environment generates pores or cracks that facilitate water diffusion within the polymeric matrix and accelerates degradation⁹³.

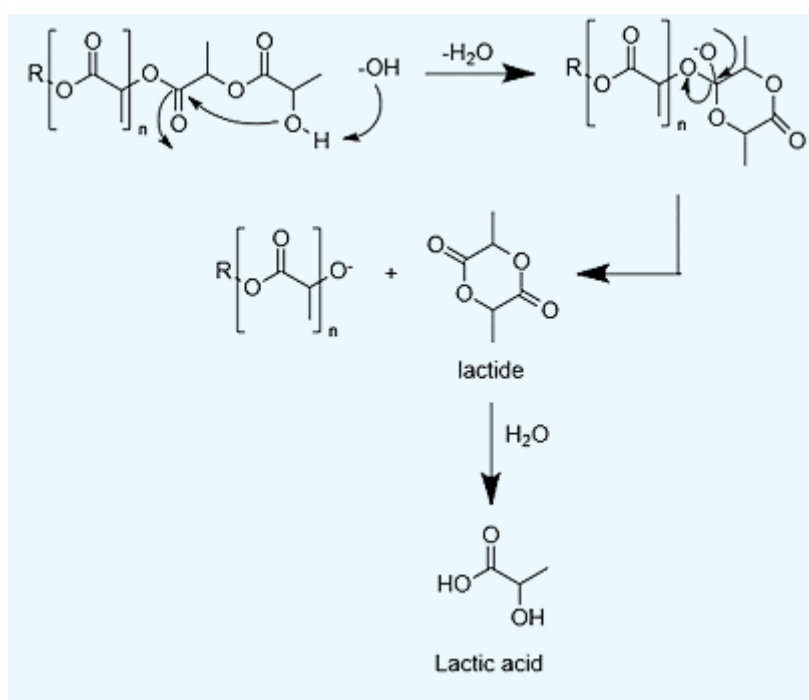


Figure 6. The suggested mechanism of hydrolysis in alkaline environment^{88,94}.

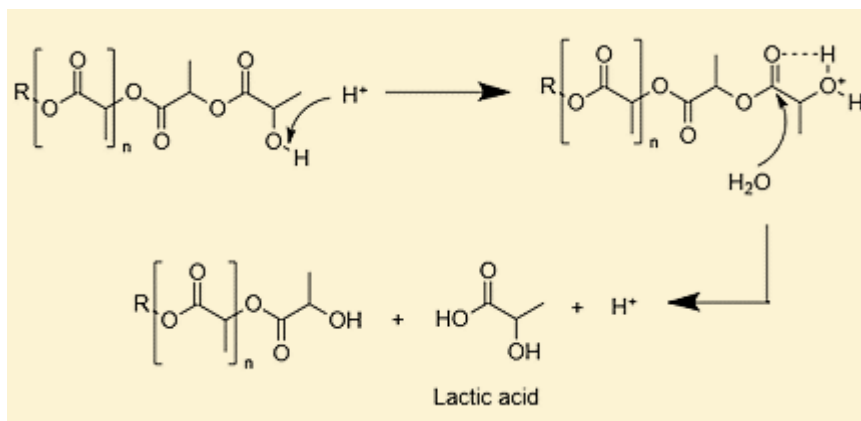


Figure 7. The suggested mechanism of hydrolysis in acidic environment ^{88,94}.

2.3.2. Photo-degradation

UV radiation induces degradation/modification of the surface chemistry in the composites, commonly known as photo-degradation or photo-catalysis ⁹⁵. Photo-degradation occurs with the absorption of UV photons by chromophore groups such as hydroperoxides, carbonyls, double and triple bonds. These activation processes initiated by UV photons causing a breakdown of polymer chains produces free radicals and reduces the molecular weight of polymers, resulting in a loss of surface gloss and the significant deterioration of many material properties with time ⁹⁶. The PLA has a sensibility to UV degradation because of the presence of carbonyl groups in its repetitive unit ⁹⁷. Various studies have been published that have investigated the photo-degradation of PLA ⁹³⁻¹⁰⁰. The degradation mechanisms in PLA reported in the literature are Norrish I and Norrish II ^{21,95,100}, and the most commonly reported is Norrish II mechanism ^{102,106-109} (Figure 8). Photolysis of PLA by Norrish II type photo-cleavage reaction resulting in decreased molecular weight by chain scission leads to the C=C double bond formation and hydroperoxide (O-H) at the new PLA chain terminals that produce a further degradation of the chain end groups ^{11,108}.

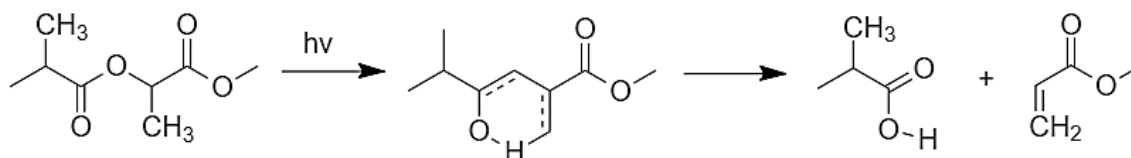


Figure 8. Photodegradation of PLA via the Norrish II mechanism ^{95,106}.

2.4. Degradation of PLA in abiotic environments

The environmental degradation process of PLA is affected by biotic and abiotic factors. Abiotic degradation includes non-living factors such as temperature, light, and moisture/water content or humidity, and it is a process that mainly occurs under the influences of hydrolysis and photolysis. At the same time, microorganisms such as fungi and bacteria are prime factors responsible for biotic degradation. In this study, we focus on investigating the degradation of PLA in abiotic environments.

Some researchers exposed the PLA materials only to UV-irradiation, some of them only to moisture, but in most of these studies, accelerated weathering conditions of UV-irradiation and moisture were applied together in consecutive cycles^{18,19,100,103,107,109–113}. Also, several authors report degradation in distilled water, demineralized water, deionized water, ethanol solutions, pure water, and simulating degradation in seawater^{114–123}. Moreover, it is reported simulating degradation in buffer solutions; pH can be varying from acid environments (low pH) until alkali environments (high pH)^{7,70,79,81,85,93,124–147}. Also, electron beam irradiation has been shown to affect PLA integrity. Pre-treating PLA by electron beam irradiation increased PLA brittleness and decreased molecular weight during degradation compared to non-irradiated samples¹⁷.

On the other hand, Thanh et al.¹⁴⁸ and Li et al.¹⁴⁹ reports the study of the PLA degradation process after being immersed in the simulated body fluids SBF and biocorrosion media for their potential bone implant applications. Finally, the biodegradation of PLA using digester sludge was estimated, and determine the specific gas production rate. These studies indicate that the properties reductions of the specimens were due to the degradation mechanisms of UV radiation in the form of photolysis and the hydrolysis reaction of moisture and aqueous solutions, all leading to the main chain scissions in PLA matrix¹⁰⁸.

In order to facilitate the biodegradation of PLA in these conditions, a range of strategies has been developed, including surface modification and the preparation of blends or composites with synthetic materials or biomass¹⁵⁰. The research about PLA composites mainly focuses on studying the hydrolytic degradation behavior of PLA composites. Various additives, plasticizers, and nanofillers can improve elasticity module, thermal stability, barrier properties, and influence in degradation process⁶⁸. Montmorillonite (MMT), Cloisite 30B, Nanofil2, carbon nanotubes (CNT), halloysites nanotubes (HNT),

titanium dioxide (TiO₂) nanoparticles are the most common fillers used in polylactide ⁷². Nanofillers have the functionality to create acid compounds and RCOOH by-products that can accelerate the degradation rate of filler-polymers. This acceleration is mainly because of the autocatalysis process. Nanofillers may alter water permeability, crystallinity, and glass transition temperature of polymers and therefore influence the degradation rate of filler-polymers^{56 52}.

This section aims to provide an updated summary of the degradation of PLA and its blends in different abiotic degradative environments. Determination of weight loss is the more most straightforward technique to monitor the biodegradation process. In this section, the weight loss changes will be analyzed to determine which degradative conditions accelerate the degradation of PLA. Also, the influence of nanofillers in PLA on their degradation rate will be compared. The degradation time of each polymer and medium characteristic is listed in (Table 2.).

Table 2. Degradation environments for PLA.

Material	Type of environment	Experimental conditions	Exposure time	Biodegradability (%)	Reference
PLA	(UV) irradiation	UV lamp (254 nm) at ambient temperature (25°C).	60 h	-	102
PLA	(UV) irradiation	UV radiation (254 nm)	100 h	-	151
PLA	(UV) irradiation	UV light (300–450 nm) at room temperature.	60 min	-	11
PLA	(UV) irradiation	UV radiation (254 nm)	50 min	86,9 from eq 1.	152
PLA-HNT	Accelerated photo-ageing	Mercury lamp (295 nm) at 60 °C.	240 h	-	153
PLA/ZnO	Accelerated photo-ageing	UV lamp (313 nm) at 60°C	500 h	-	154
PLA/PBS/Eversorb	Accelerated photo-ageing	Daylight irradiation for 8 hours at 60°C	480 h	-	155
PLA/PHB	Accelerated photo-ageing	Mercury arc with luminophore at 35–40 °C	125 days	33,3 from eq 2.	156
	Water vapor	Water at 60 °C	32 days	96,4 from eq 2.	
PLA	Humid Environments	50% RH at 50°C	70 days	~18,4 from eq 2.	58
		75% RH at 50°C		~47,4 from eq 2.	
		100% RH at 50°C		~94,7 from eq 2.	
PLA-S/C30B	Accelerated weathering testing	UVA-340 lamp with 8 h of UV exposure period at 60 ± 3 °C; followed by a condensation period of 4 h at 50 ± 3 °C.	360 h	77 from eq 2.	111
PLA-A/C30B				90 from eq 2.	
PLA	Accelerated weathering testing	UV radiation (300 to 400 nm) at 63 °C and 50% RH with dark period consists of 6 h at 95 %RH	72 days	-	110
PLA	Accelerated weathering testing	UVA-340 nm with cycles of 8 h UV irradiation, followed by 4 h dark condensation at 50 °C	2000 h	90 from eq 2.	107
PLA/TiO ₂				66 from eq 2.	
PLA	Accelerated weathering testing	UVB-313, at 50°C without humidity rate control.	100 days	1 from eq 1.	99
PLA/TiO ₂				16 from eq 1.	
PLA	Accelerated weathering testing	Xenon test chamber (300–400 nm) at 38 °C, dark condensation at 50 °C and 50% RH	200 h	1.8 from eq 2.	103
		Laser exposure irradiated (248 nm)		71.4 from eq 2	
PLA	Accelerated weathering testing	100 % RH at 50 °C	69 days	-	157
FR-PLA-C30B-30%	Accelerated weathering testing	75% RH at 50 °C	105 days	~85 from eq 2.	109
		UVA - 351 at 50 °C	125 days	~53,7 from eq 2.	
		UVA - 351 at 50 °C in water condensation	90 days	~90,7 from eq 2.	
PLA/PELU	Accelerated weathering testing	70% RH at 60 °C	96 h	-	158
EVA/PLA, EVA/PLA/TiO ₂	Accelerated weathering testing	UV light at 60°C and humidity condensation at 45°C.	672 h	-	16

PLA, clay/PLA,	Accelerated weathering testing	UV lamp at 65 °C and 50% RH	1000 h	-	112
PLA/Si69eBF/C30B	Accelerated weathering testing	UV radiation (300 to 400 nm) at 63 °C and 50% RH	90 days	-	159
PLA	Accelerated weathering testing	100% RH at 40, 60 and 80 °C	30 days	69 from eq 1.	160
PLA/HAp	Accelerated weathering testing	95% RH at 24 °C	30 days	50 from eq 2.	9
PLA amorphous	Accelerated weathering testing	80 % RH at 70°C	144 h	97 from eq 2.	51
PLA semi crystalline				88 from eq 2.	
PLA/HNT	Accelerated weathering testing	UVB-313 with cycles at 70°C and 4 h dark condensation at 50°C.	300 h	99 from eq 2.	19
PLA/talc	Accelerated weathering testing	UVB-313 at 70°C.	300 h	99,8 from eq 2.	161
CF/PALF/PLA	Accelerated weathering testing	UVA (340 nm) at 50 °C and 55% RH	250 h	2 from eq 1.	18
PLA				0.5 from eq 1.	
PLA	Gamma Ray Irradiation	Target dose 20 kGy in the presence of air at ambient temperature.	-	-	162
	Pulsed Light Irradiation	Linear lamp (190–700 nm) in the presence of air and at room temperature		-	
PLA	Electron beam irradiation	Target dose 10 kGy at room temperature	-	42,7 from eq 2.	163
PHBV/PLA				53,7 from eq 2.	
PHBV/PLA/C30B				43,6 from eq 2.	
PLA	Water solution	Water at 60 °C	4 weeks	21 from eq 1.	164
PLA/PHB				27 from eq 1.	
PLA/(R, S)-PHB/F	Water solution	Distilled water at 70°C	56 days	-	114
PLA/P(3HB-co-4HB)/jute	Water solution	Distilled water at 70°C	70 days	-	54
PLA/PTT/PEGMA	Water solution	Distilled water at 58 °C	120 days	40 from eq 1	59
PLA/PTT				96 from eq 1	
PLA/PHA	Water solution	Demineralized water (pH = 5.6) at 70°C	7 days	90 from eq 1.	115
PLA	Water solution	Demineralized water (pH = 5.6) at 70°C	7 days	98 from eq 1.	116
PLA/PHA				93 from eq 1.	
PLA	Water solution	Ultra-pure water at 58±2 °C	180 days	96 from eq 2.	83
PLA–Cotton_{TPS}	Water solution	Water-tube system at 70°C	120 days	100 from eq 1.	117
PLA_{TPS}-Cotton			145 days		
flax/PLLA	Water solution	Deionized water at 23 °C	8 weeks	-	118
AUL/PLA, AAL/PLA	Water solution	Distilled water at 25 and 50 °C	3 months	-	113

PLA	Water solution	Deionized water (pH 7.2) at 60 °C	90 days	37 from eq 1.	62
		Deionized water (pH 7.2) at 37 °C		~2 from eq 1	
PLA/PBAT	Water solution	Distilled water at 70 °C	70 days	50 from eq 1.	121
PLA	Water solution	Distilled water at 70 °C	365 days	-	119
PLA/ (R, S)-PHB	Water solution	Distilled water at 70 °C	70 days	-	120
PLA-OMMT, PLA-C	Water-ethanol solutions	Pure water, 50% and 95% ethanol at 40 °C.	180 days	-	67
PLA	Water and ethanol solution	Water at 90 °C	70 h	~100 from eq 2.	122
		50% ethanol at 80 °C	120 h	~100 from eq 2.	
		50% ethanol at 80 °C and pH 11 using sodium citrate	12 h	~95 from eq 2.	
		50% ethanol at 80 °C and pH 7 using sodium citrate	70 h	~95 from eq 2.	
		50% ethanol at 80 °C and pH 4 using sodium citrate	95 h	~100 from eq 2.	
PLA- montmorillonite PLA- Nanofil2	Lake water	Lake water (pH 8.4) at 20 °C	28 days	-	123
PLA	Natural seawater	Natural seawater, 12 h light-dark at 30°C	180 days	-	165
PLA/wood pulp	Simulating the marine environment	Euphotic zone (with light)	365 days	29.2 from eq 1.	166
		Aphotic zone (in darkness)		24,6 from eq 1.	
		Non-polluted sediment	128 days	100 from eq 1.	
		Sediment affected by organic pollution	140 days	100 from eq 1.	
lamine paper/PLA	Simulating the marine environment	Euphotic zone (with light)	365 days	5,6 from eq 1.	
		Aphotic zone (in darkness)		6 from eq 1.	
		Sediment affected by organic pollution		75,3 from eq 1.	
PLA	Simulating degradation in buffer solution	PBS (pH 7.2) at 37 °C	28 days	-	93
PLA	Simulating degradation in buffer solution	PBS (pH 7.4) at 37°C	8 weeks	0 from eq 1.	144
PLA	Simulating degradation in buffer solution	PBS (pH 7) at 37°C.	8 weeks	~23,8 from eq 1	145
I-L-PLA microspheres I-S-PLA microspheres	Simulating degradation in buffer solution	PBS (pH 7.4) at 37 °C	3 months	30 from eq 2 20 from eq 2	146
PLA scaffold	Simulating degradation in buffer solution	PBS (pH 7.4) at 37°C	360 days	95 from eq 2.	147
PLA/GNP-M composites PLA/GNP-C composites	Simulating degradation in buffer solution	PBS at 37 °C	6 months	88 from eq 2. 85,2 from eq 2.	124
Collagen/PLA	Simulating degradation in buffer solution	PBS at 37°C	28 days	-	125
Tet-CS/PLA	Simulating degradation in buffer solution	PBS (pH 7.2) at 37 °C	7 days	~85 from eq 1.	126
PLA/nHAp multiscale fiber scaffolds	Simulating degradation in buffer solution	PBS (pH 7.4) at 37 °C	5 months and 1 year	-	85
PLA- Montmorillonite,	Simulating degradation in buffer solution	PBS (pH 7.40) at 37 °C	180 days	-	68

PLA-Nanofil2						
PDLLA	Simulating degradation in buffer solution	PBS at 37°C	12 weeks	12 from eq 2.		127
PDLLA/PDLLA-COOH				60 from eq 2.		
Mg-SA-PLA	Simulating degradation in buffer solution	PBS (pH 7.40) at 37 °C	21 days	-		128
PLA	Simulating degradation in buffer solution	PBS at 37 °C	12 months	-97 from eq 2.		167
PLA/pMgO				-92 from eq 2.		
PLA/wMgO				-85 from eq 2.		
PLLA-Ha, PLLA-C30	Simulating degradation in buffer solution	PBS (pH 7.4) at 58 °C	13 days	-		7
PLA, PLA-PBG	Simulating degradation in buffer solution	PBS (pH 7.4) from 21 to 85 °C	56 days	-		168
PLA/CNC-ZnO PLA	Simulating degradation in buffer solution	PBS (pH 7.4) at 37 °C	70 days	25 from eq. 1		129
				8 from eq 1.		
PLA90/PBA10 PLA50/PBA50	Simulating degradation in buffer solution	PBS (pH 7.4). at 37±1 °C	5 days	1 from eq 1.		130
				12,5 from eq 1.		
PLA60/PEO40/CNT₂ PLA60/PEO40 PLA90/PEO10/CNT₂ PLA90/PEO10	Simulating degradation in buffer solution	PBS (pH 7)	4 weeks	42 from eq 1.		131
				32 from eq 1.		
				11 from eq 1.		
				7 from eq 1		
PLA/PEO PLA/PEO/CNT₁ PLA/PEO/CNT₂	Simulating degradation in buffer solution	PBS (pH 7) at room temperature	4 weeks	33 from eq 1		86
				38 from eq 1		
				41 from eq 1.		
PLA/PEO PLA/PEO/CNT	Simulating degradation in buffer solution	PBS (pH 7) at room temperature	4 weeks	-		71
PLA/PEO/CNT PLA/PEO/CNT	Simulating degradation in buffer solution	PBS solution (pH 7) at room temperature	4 weeks	-		132
	Simulating degradation in buffer solution	PBS solution (pH 7) at room temperature	4 weeks	-		72
PLA/nHA-Ag	Simulating degradation in buffer solution	PBS (pH 7.4) at 37°C	50 days	3 from eq 1.		133
PLLA/LATC30/nHA	Simulating degradation in buffer solution	PBS (pH 7.4) at 37 °C	15 months	100 from eq 1.		80
		PBS (pH 7.4) at 70°C	303 h			
PLA		PBS (pH 7.4) at 37 °C	22 months			
		PBS (pH 7.4) at 70°C	343 h			
LCB-PLA				-18 from eq 1.		
PLLA/Mg PLDA/Mg PLDA-cr/Mg	Simulating degradation in buffer solution	PBS at 37°C	28 days	13 from eq 1		93
				10.5 from eq 1		
				28 from eq 1.		

PLA/DCP/TAM	Simulating degradation in buffer solution	PBS (pH 7.3) at 60 °C	84 days	40 from eq 1. 28 from eq 1.	76
PLA					
PLA- Montmorillonite	Simulation degradation in buffer solution	Phosphate buffer and phosphate citric buffer solution (pH 7.40) at 60°C	30 days	-	94
PLA	Simulating degradation in buffer solution	PBS (pH 7.1) at 58°C	28 days	74 from eq 1. 68,7 from eq 1.	134
PLA/LG				57,4 from eq 1.	
	Simulating degradation in buffer solution and electron beam irradiation	PBS (pH 7.1) at 58°C and irradiated 90 kGy			
PLA	Simulating degradation in buffer solution	PBS (pH 7.1) at 58 °C	28 days	73 from eq 1. 74 from eq 1.	82
	Electron-beam irradiation and degradation in PBS solution.	Target dose 100 kGy then immersed in PBS (pH 7.1) at 58 °C			
PLA/PEGM	Simulating degradation in buffer solution	PBS (pH 7.1) at 58 °C		42 from eq 1.	
	Electron-beam irradiation and degradation in PBS solution.	Target dose 20 kGy then immersed in PBS (pH 7.1) at 58 °C		45 from eq 1.	
PLA/PEGM/HBN 5	Simulating degradation in buffer solution	PBS (pH 7.1) at 58 °C		36 from eq 1.	
	Electron-beam irradiation and degradation in PBS solution.	Target dose 100 kGy then immersed in PBS (pH 7.1) at 58 °C		49 from eq 1.	
PDLLA/Bioglass	Gamma irradiation and degradation in PBS solution.	Gamma irradiation at dose of 25 kGy, then PBS (pH 7.4) at 37°C	6 months	49 from eq 2.	135
PLA	Simulating degradation in buffer solution	Potassium phosphate buffers (pH 7.4) at 50 °C	8 weeks	15.8 from eq 1.	78
PLA + 2% BDICDI-stabilized	Simulating degradation in buffer solution	Sodium phosphate buffer (pH 7) at 58 °C	160 days	92,5 from eq 2.	61
PLA, PLA/ZnSt-Ag	Simulating degradation in buffer solution	Sodium phosphate buffer (pH 7) at 58 °C	25 days	100 from eq 2.	136
PLA/β-TCP	Simulating degradation in buffer solution	Sorensen's phosphate-buffered solution at 37°C	24 weeks	2,1 from eq 2.	79
MAWs/PLA	Simulating degradation in buffer solution	Sorensen's phosphate-buffered solution (pH 7.4) at 37°C	56 days	1 from eq 1.	137
		Sorensen's phosphate-buffered solution (pH 7.4) at 50°C	21 days	0.5 from eq 1	
PDLLA	Simulating degradation in solution	Titrisol buffer solution of either pH 3, pH 5, pH 7, pH 9, pH 11 and pH 13 (NaOH) at 37°C	426 h, 35 days	-	138
PLA	Simulating degradation in alkali solution	Ringer solution and distilled water (pH 8.16) at 37°C	100 days	-	139
PLA/PBS	Simulating degradation in alkali solution	NaOH (pH 13) at 37°C	312 h	-	56
PLA/WF/PMMA	Simulating degradation in alkali solution	NaOH (pH 12.5) at 50 °C	12 days	80 from eq. 1.	140
PLA				40 from eq 1.	

PLA/WF/PMMA	Simulating degradation in alkali solution	NaOH (pH 12.5) at 50 °C	66 h	80 from eq 1.	141
PLA			565 h	100 from eq 1.	
PLA/WF/PMMA	Simulating degradation in alkali solution	NaOH (pH 12.5) at 50 °C	10 days	80 from eq 1.	81
PLA/WF				100 from eq 1.	
PLA				30 from eq 1.	
PLA	Simulating degradation in alkali solution	NaOH (pH 13) at 30°C	10 weeks	11 from eq. 1	70
PLA/PBAT/TBT				7 from eq. 1	
PLA/PBAT/TBT/AgKT				6,5 from eq 1	
PLA	Simulating degradation in alkali solution	NaOH solution	29 days	100 from eq 1.	87
PLA-0.74 FeCl₃			31 days	95 from eq 1.	
PLA-3.69 FeCl₃			3 days	88 from eq 1.	
PLA	Simulating degradation in alkali solution and (UV) radiation	NaOH (pH= 14) at 60°C and UV irradiation (365 nm)	3 h	-	142
PLA-AIE	Simulating degradation in alkali solution	NaOH (pH 14) at 60°C	3 h	79 from eq. 1	142
		NaOH (pH 14) at 80 °C	2,7 h	96,1 from eq 1.	
PLA₄ChMA	Simulating degradation in alkali solution	D2O solution (pH 9) at 50°C and 85°C	75, 23 days	-	169
PLA/PBS-x	Simulating degradation in alkali solution	NaOH (pH 13) at 37°C	300 h	0.052 from eq 1.	56
PET/PLA-GO	Simulating degradation in acid solution	Sulfuric acid solution (pH 2) at 37°C	40 days	20 from eq 1.	66
		Sulfuric acid solution (pH 4) at 37°C		18 from eq 1.	
PLA/TPGS	Simulating degradation in acidic solution	Acetate buffer solution (pH 5.0) at 37 °C	12 h	-	143
PLA	Simulating degradation in solution	PBS (pH 7.3) at 37°C	90 h	3,75 from eq 1.	170
		HCl (pH 1)	90 h	3,5 from eq 1.	
		NaOH (pH 13) at 37°C	30 h	100 from eq 1.	
PLA-PMCP₂	Simulating degradation in solution	PBS (pH 7.3) at 37°C	90 h	1,25 from eq 1.	
		HCl (pH 1)	90 h	1,5 from eq 1.	
		NaOH (pH 13) at 37°C	70 h	100 from eq 1.	
PLA-PMCP₄	Simulating degradation in solution	PBS (pH 7.3) at 37°C	90 h	1 from eq 1.	
		HCl (pH 1)	90 h	1,5 from eq 1.	
		NaOH (pH 13) at 37°C	83 h	100 from eq 1.	
PLA/PCL	Simulating degradation in solution	PBS (pH 4) at 37°C	50 days	11 from eq. 1	84
PLA-SP	Simulation degradation in solution	PBS (pH 7) at 37 °C	120 h	16 from eq 1.	74
		PBS (pH 10) at 37°C		75 from eq 1.	
PCL60-PLLA40	Simulation degradation in solution	NaOH at 37 °C	24 h	93 from eq 2.	77
		PBS (pH 7.4) at 37 °C	56 weeks	14 from eq 2.	

PLA/PBAT/CEO	Simulating degradation in solution	Acetic acid buffer solution (pH 4.98) at 37° C	12 weeks	4 from eq 1.	50
		Acetic acid buffer solution (pH 4.98) at 25°C		1,4 from eq 1.	
		PBS (pH 7.40) at 37° C		5 from eq 1.	
		PBS (pH 7.40) at 25°C		5 from eq 1.	
		Ammonium buffer solution (pH 8.50) at 37° C		3,4 from eq 1.	
		Ammonium buffer solution (pH 8.50) at 25°C		3 from eq 1.	
PDLLA	Simulating degradation in solution	Titrisol buffer solution (pH 9) at 37 °C	426 h	100 from eq 1.	171
		Titrisol buffer solution (pH 11) at 37 °C	144 h	100 from eq 1.	
		NaOH (pH 13) at 37 °C	10-15 min	-	
PLA/TPS	Simulating degradation in solution	NaN3 solution incubated at 55 °C	28 days	25,8 from eq 1.	55
PLA/HAp	In vitro simulated body fluids (SBF)	SBF (pH 7.4) at 37 °C	28 days	-	148
Mg-PLA	In vitro simulated body fluids (SBF)	SBF at 37.5°C	8 weeks	-	172
PLA	In vitro simulated body fluids (SBF)	SBF and (Tris–HCl) solution (pH 7.4) at 37 °C	50 days	2 from eq 1	173
PLA/PGS				14 from eq 1.	
PLA	In vitro simulated body fluids (SBF)	Static degradation (SBF) at 37°C	12 weeks	42 from eq 1.	174
		Dynamic degradation (SBF) at 37°C		55 from eq 1.	
PBAT/PLA	Digestion sludge system	Respiratory test at 35°C	30 days	-	60
PLA/LA	Digestion sludge system	Filtered sludge at 37°C	30 days	50 from eq 2.	150
Mg/PLA	Biocorrosion media	Kirkland's biocorrosion media (KBM) pH 7.4, 37 °C	30 days	1,45 from eq 1.	149
PLA	Biocorrosion media			1,15 from eq 1.	
PLA	Biocorrosion media	Kirkland's biocorrosion media (KBM) at 37 °C	30 days	1,43 from eq 1	175
Mg wires/PLA	Biocorrosion media	Kirkland's biocorrosion media (KBM) at 37 °C	21 days	-	176
Mg wires/PLA	Biocorrosion media	Kirkland's biocorrosion media (KBM) at 37 °C	21 days	-	177

Equations:

$$\text{Weight loss}(\%) = \frac{W_0 - W_t}{W_0} \times 100 \quad (1) \quad ; \text{ where } W_0 \text{ is the initial weight, } W_t \text{ is the weight after a given time of degradation.}$$

$$\text{Molecular weight loss } \% = \frac{M_i - M_f}{M_i} \times 100 \quad (2) \quad ; \text{ where } M_i \text{ and } M_f \text{ are the initial and final molecular mass of the specimen, respectively.}$$

The most important aspect concerning biodegradation rates is probably the environment in which the polymer degrades. It is essential to compare the biodegradation rate of the same polymer in different environments to assess sustainable use and guarantee a reasonable degradation profile for the intended application or use in waste management⁸⁸. For instance, the biodegradation of PLA in accelerated weathering testing will differ when compared to PLA samples degraded in seawater or buffer solutions. The biodegradation rate depends on the concentration pH, humidity, temperature, light, and UV radiation. Figure 9 summarizes the biodegradability of PLA in different environmental conditions. In general, a rapid weight loss is observed in these studies, owing to different degradation mechanisms in the abiotic environments, which include the preferred degradation by random hydrolysis and photolysis of the ester bonds. Hereunder, it will be analyzed the degradative conditions that accelerates the degradation of PLA and the influence of nanofillers and its blends in PLA in their degradation rate.

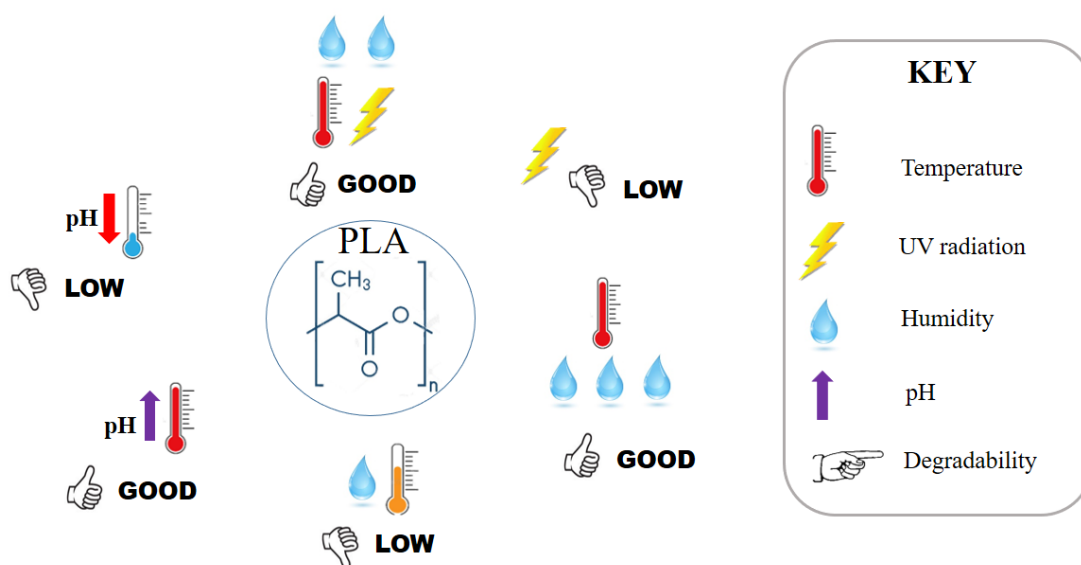


Figure 9. Influence of humidity, temperature, UV radiation, and pH on the biodegradation of PLA in different environments.

Regarding pH values, as mentioned above, some previous studies on the hydrolytic degradation of poly (lactic acid) suggest that PLA degrades faster in alkaline environments. For example, the degradation studies in buffer solutions carried out by Schusser et al.¹⁷¹ showed the PDLLA film exposed to pH 13 buffer solution degrades very fast, within 10–15 min. The polymer films exposed to pH 11 and pH 9 solutions can be considered completely degraded after 144 h and 426 h, respectively. In contrast, the PDLLA layers in contact with buffer solutions of pH 7, pH 5, and pH 3 are not completely degraded even after 35 days¹⁷¹. A similar trend is observed in the work of Xin et al.¹⁷⁰;

the degradation studies of PLA in phosphate buffer solutions showed slight weight loss in hydrochloric acid (pH=1), while the degradation in NaOH solutions (pH=13) need several days for complete degradation¹⁷⁰. Similar degradation behavior is reported for PLA concerning different pH conditions by Valapa et al.⁷⁴ and Woodard et al.⁷⁷. It is explained that the possible reason for this might be due to the decisive role played by terminal OH groups resulted during the hydrolytic degradation under basic conditions⁷⁴. These are also consistent with other works^{8,50,56,68,69,72,73,75,86,94,178,179}. In assessing the catalytic effect of elevated temperature. Xu et al.⁶² denote that relatively rapid mass loss was triggered for the films degraded at 60 °C displaying a weight loss of 63% after 90 days. By contrast, no evident mass loss was observed during the 90 days of degradation at 37 °C⁶². PLA exhibit a T_g around 60°C, by degrading the polymer at temperatures above the T_g , the chains in the amorphous regions of the polymer become flexible, due to the improvement in the mobility of PLA chains, water might diffuse into the PLA matrix more easily⁷⁴, which guarantees increasing the susceptibility of ester bonds to undergo chain cleavage reactions¹⁴. So, the number of carboxylic acid chain ends increases, making the hydrolysis a self-catalyzed reaction due to the accumulation of lactic acid monomers and oligomers in the specimens¹²². Additionally, we concluded that degradation process can be more critical in high medium showing more significant molecular weight reduction in less time¹²².

Many polymeric components in outdoor applications are exposed to ultraviolet (UV) light and atmospheric humidity leading to chemical degradation in the chain structure. Thus, it is crucial to determine the sensitivity of PLA structure under different weathering conditions in terms of outdoor applications. A certain number of researchers have studied atmospheric weathering studies of PLA and some composites under natural and artificial conditions. For instance, Lesaffre et al.¹⁰⁹ exposed PLA samples to three different accelerated aging tests: (i) 50 °C and UV-light (T/UV), (ii) 50 °C and relative humidity (T/ RH), and (iii) 50 °C , UV-light and relative humidity for 125 days (T/UV/RH). The results reported only slight bleaching of the material after 60 days exposure under T/UV conditions, whereas the material is completely disintegrated after 35 days and 10 days under T/RH and T/UV/ RH, respectively. It is an accelerated weight loss in T/UV/RH conditions because this phenomenon is autocatalyzed by the carboxylic acid end groups formed during hydrolysis and/or photo-oxidation¹⁰⁹. Rocca et al.⁵⁸ studied the modifications induced on PLA films when they are exposed to aquatic environments. The

PLA films were placed at 50, 75, 95, and 100% RH and immersed in liquid water at 50 °C. The weight loss change confirmed that PLA was subjected to hydrolysis reaction for all of the storage conditions. The kinetic analysis revealed that the reaction was accelerated when the chemical potential of water increased: 50% RH < 75% RH < liquid < 95% RH < 100% RH. Nevertheless, the reaction was significantly slower when PLA was immersed in liquid water conditions compared to the 100% RH. When PLA was exposed to water vapor, the degradation products were accumulated in the polymer matrix, accelerating the reaction. Simultaneously, these acidic molecules were transferred to the liquid media when PLA was immersed in liquid water, limiting or annihilating their action as catalysts⁵⁸. Furthermore, the authors who carried out the degradation at 100% relative humidity showed the highest percentages of weight and mass loss^{9,58,157,160}. In this sense, several authors reported a high biodegradability of PLA samples in accelerated weathering conditions^{16,18,19,51,103,112,153–159,161,180}.

On the other hand, only a few papers study PLA degradation in aquatic environments. Nazareth et al.¹⁶⁵ observed no weight loss after 180 days in natural seawater. However, Beltrán et al.¹⁶⁶ studied the degradation of PLA-based materials in marine habitats for a year and reported that UV light favored the degradation rate. In the case of PLA/wood pulp, the weight loss was much more noticeable with a value of 29.2% weight loss in conditions that simulate the light (wavelength and intensity) (WL) and a value of 24.6% weight loss in conditions where sunlight is totally attenuated (WD)¹⁶⁶.

In order to analyze the effects of filler type in the degradation rate of PLA, several authors have found a catalytic effect of nanofillers on the biodegradation of different PLA samples (Table 3), due to the high hydrophilicity of these nanoparticles⁵². Studies done by Luo et al.⁹⁹ show that the weight loss of PLA/TiO₂ nanocomposites decreased linearly with increasing UV irradiation time, while no significant weight change was noticed for pure PLA at the end of irradiation time. The weight loss of PLA/TiO₂ nanocomposites was about 17%. This loss implied that 2 wt % of TiO₂ nanoparticles in PLA had the highest photocatalytic degradation efficiency^{99,181}. The results of other authors confirm the strong influence of TiO₂ in accelerating the degradation of PLA^{16,107}. It was observed that the addition of clay favored PLA degradation in PLA, for that Chávez et al.¹¹¹ prepared nanocomposites of PLA mixing with Cloisite30B and reported a molecular decrease with the increase in the exposure time the specimens subjected to artificial weathering. A significant decrease in molecular weight can be attributed to the presence

of C30B. A weight loss of 90% in PLA/C30B (amorphous) while neat PLA showed a slight decrease¹¹¹.

Table 3. Comparison of hydrolytic degradation of modified PLA with different nanofillers.

Degradation time (under the same conditions)	Matrix	Weight loss (wt%)	Modified material	Weight loss (wt%)	Reference
80 days	PLA	1	PLA/TiO ₂	17	99
360 h	PLA	20	PLA/C30B	90	111
70 days	PLA	9	PLA/CNC-ZnO	25	129
50 days	PLA	0	PLA/nHA/ AgNP	3	133
4 weeks	PLA	6	PLA/PEO/CNTs	41	86
9 days	PLA	50	PLA/FeCl ₃	90	87

However, the artificial aging carried out by Rodríguez et al.¹⁵⁴ showed that the PLA/ZnO fibers exhibited a lower photo-degradation. While neat PLA showed a greater degradation extent with a weight loss of approximately 50% as the aging time was prolonged from 0 to 500 h, PLA/ZnO fiber was kept practically beyond 100 h. The addition of ZnO nanoparticles in PLA promoted a UV-shielding effect at relatively low concentrations (1-5 wt-%). This photo-degradation behavior could be related to aggregates of 3-5 µm in size on the PLA fibers, reducing the surface area prone to absorb UV rays¹⁵⁴.

Wang et al.¹²⁹ also studied the photo-degradation, in this case, nanocomposites films embedded with cellulose nanocrystal-zinc oxide (CNC-ZnO). This material proved a high ultraviolet protection factor value and faster degradation rate. By adding high content of 15wt %CNC-ZnO hybrids into the PLA matrix, the highest UV radiation was blocked out by (85.31%) of UV-A and (95.90%) UV-B. However, it is found that the weight loss of PLA nanocomposites after being degraded in PBS for 70 days increased from 9% for PLA to 25% with 15wt% CNC-ZnO hybrids. The improvement in the degradation rate can be attributable to the more hydroxyl groups on the surface of CNC in the CNC-ZnO hybrids, resulting in improved surface hydrophilicity for PLA nanocomposite¹²⁹.

On the other hand, several authors study the degradation rate of PLA for medical applications. Liu et al.¹³³ developed PLA composites with hydroxyapatite nanorod (nHA) and silver nanoparticles (AgNP) to improve mechanical properties and degradation rate and obtain polymer biomaterials for bone tissue engineering applications. PBS degradation studies showed that PLA shows negligible weight loss after 50 days

immersion, while PLA/nHA composite degrades continuously with immersion time. This difference implies that the nHA filler affects the degradation behavior of PLA by increasing its hydrophilicity and water uptake of the polymer matrix. The weight loss of PLA/nHA nanocomposite can be further increased by adding 18-25 wt% AgNPs. This increase demonstrates that AgNPs also facilitate PLA disintegration in PBS¹³³.

Some authors combined PLA with carbon nanotubes (CNTs) because CNTs advantageously improve the degradation rate and the mechanical and electrical properties of polymers^{71,72,86,131}. Zare et al.⁸⁶ reported a high degradation rate in PLA/PEO/CNTs nanocomposites, which largely depended on the CNT content. The hydrolytic degradation in PBS reported that the molecular weights of polymers decreased during degradation, but the molecular weight of PLA did not vary significantly in the degradation period. Moreover, CNTs and the addition of a water-soluble polymer like poly (ethylene oxide) (PEO) intensify the degradation fraction of samples. CNTs encourage the degradation of PLA/PEO blends due to the catalytic role of CNTs in the degradation of polymers⁸⁶. To enhance the mechanical properties and accelerating degradation, Wan et al.⁸¹ developed polylactic acid/wood flour/polymethylmethacrylate (PLA/WF/PMMA). Their studies of degradation showed that the PMMA and the WF synergistically modify the hydrolysis performance of the material, reporting a weight loss of 80% and 25% for pure PLA under the same conditions^{81,140,141}.

On the other hand, biodegradation studies carried out by Lee et al.¹⁵⁰ of PLA/LA blends reported that the inclusion of lactate in the PLA matrix might improve biodegradation and act as a control parameter for the polymer decomposition rate. The obtained results are expected to develop a strategy for improving the biodegradation rate of PLA blend materials and optimizing environmentally-friendly plastics¹⁵⁰. Finally, to accelerate the degradation rate of PLA, Li et al.⁸⁷ modified PLA with ferric chloride (FeCl_3), showing a degradation rate more than ten times higher than that of pure PLA. The results showed that FeCl_3 forms stable chemical bonds with C and O, which weakens the ester bond and leads to rapid degradation of PLA⁸⁷.

To identify the changes induced in chemical structure, morphology, thermal, and mechanical properties, a series of experimental techniques will be explained in the next section.

3. CHARACTERIZATION TECHNIQUES

Polymer degradation is a change in the chemical or physical properties of a polymer under the influence of one or more degradative factors. The degradation process can be helpful in establishing protocols and determine the progress of degradation and the useful life of a polymer by using some characterization techniques. This section provides a database about characterization techniques used during PLA degradation. Furthermore, it will show the main changes involved in the degradation of PLA, predict polymer durability in degradative abiotic environments, and suggest the aging parameters more effectively used in PLA degradation, corroborated by the characterization techniques shown in Table 4.

Table 4. Techniques of analysis of PLA blends during degradation ¹⁸².

Technique	Properties analyzed
<i>GPC</i>	Molecular weight distribution.
<i>DSC</i>	Melting and crystallization behavior.
<i>TGA</i>	Thermal stability.
<i>XRD</i>	Crystallization and orientation of polymer.
<i>FTIR</i>	Chemical structure of polymers. Identify quantitatively particular functional groups. Chain scission of polymer chain.
<i>NMR</i>	Characterization of degradation products. Molecular weight. Crystalline structures.
<i>SEM</i>	Morphology.
<i>Mechanical Test</i>	Young's modulus. Tensile strength. Elongation at the break.

3.1. Molecular weight determination

Gel permeation chromatography (GPC), also known as size-exclusion chromatography (SEC), is the most widely used technique for the analysis of polymers concerning other techniques of molecular weight (MW) measurement ¹⁸³. To determine chain scission and the molecular weight distribution of the polymer, we performed gel permeation chromatography (GPC). The GPC technique is very useful for the calculation of molecular weight, molecular weight, and polydispersity of polymers. The data concerning molecular weight allows predicting particular properties of investigated materials both

before and after degradation process^{68,103}. GPC analysis confirms the degradation phenomenon by displaying the reduction in molecular weight.

In general, PLA samples (≈ 50 mg) are placed in 10 mL vials; tetrahydrofuran (THF) is used as the solvent at a flow rate of 1.00 ml/min and temperature 35 °C. \bar{M}_n , \bar{M}_w and PDI were calculated from the resulted molecular weight distribution according to Equations 3, 4, and 5, respectively¹⁵⁷.

$$\bar{M}_n = \frac{\sum n_i M_i}{\sum n_i} \quad (3)$$

$$\bar{M}_w = \frac{\sum n_i M_i^2}{\sum n_i M_i} \quad (4)$$

$$PDI = \frac{\bar{M}_w}{\bar{M}_n} \quad (5)$$

Where M_i is the molecular weight (g/mol) of a molecule and n_i is the number of molecules having that molecular weight. The number average molecular weight (\bar{M}_n) is the total weight of all the polymer molecules in a sample, divided by the total number of polymer molecules in a sample. The weight average (\bar{M}_w) is based on the fact that a bigger molecule contains more of the total mass of the polymer sample than the smaller molecules do. The more massive the chain, the more the chain contributes to \bar{M}_w . The different average MWs obtained by GPC can be represented in an MWD curve, as appreciated in Figure 10. The change in molecular weight after degradation was calculated according to equation 2.

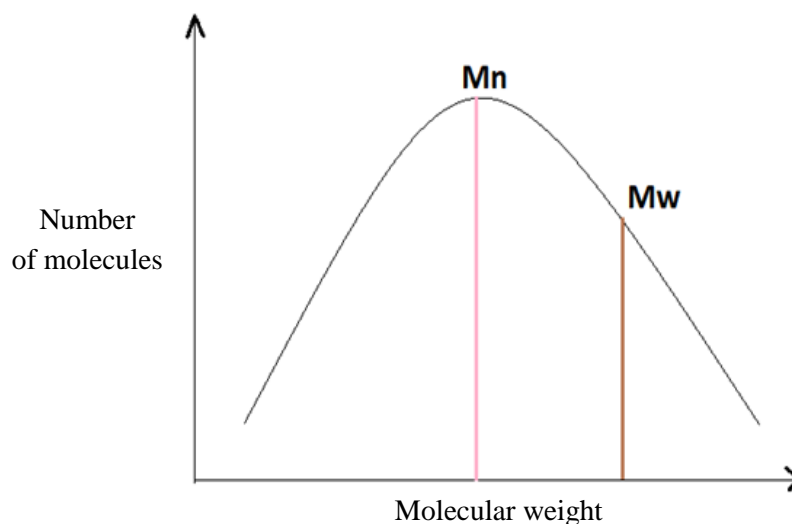


Figure 10. Schematic plot of a distribution of MWs.

Pattanasuttichonlakul et al.¹⁸⁴ used Ultraviolet (UV) irradiation to reduce the molecular weight of commercial polylactic acid. The results showed the \bar{M}_n and \bar{M}_w of PLA after UV-A, UV-B, and UV-C exposure for 120 min significantly decreased, as shown in Figure 11¹⁸⁴. Increasing the UV-C exposure time decreased the \bar{M}_n of PLA, indicating that the long chains of PLA were fragmented by UV-C irradiation. UV-C irradiation causes the cleavages of ester bonds in the PLA polymer, resulting in a decrease in the molecular weights and an increase in the brittleness of PLA¹⁸⁴. Although wavelengths of more than 300 nm are commonly used for photo-degradation of plastics, the intensity of sunlight is still strong at 245 nm. Also, the energy at wavelengths 254 nm is much higher than the energy at 300 nm¹⁸⁵. In the work of Litauszki et al.¹⁰³ the PLA film sample was artificially aged with a laser beam (248 nm). After 200 h of weathering, \bar{M}_w decreased a 65.8% reduction and polydispersity grew to 2.137, which is a 19.7% increase; this change is probably due to the hydrolysis of the matrix and the formation of the degradation product with a lower \bar{M}_w from the amorphous areas in the PLA sample¹⁶⁷. This significant breaking of the chains may have enabled the polymer chains of the original amorphous PLA to get ordered at an increased temperature and form a semicrystalline morphology during the cold crystallization process¹⁰³.

On the other hand, studies realized by Jiang et al.⁶⁹ reported that the \bar{M}_w during hydrolytic degradation in jute/PLA composites, was higher than that of pure PLA at the same temperature after aging, which suggested that the addition of jute fibers delayed the degradation of PLA, since the addition of jute fibers hindered the motion of molecular

chains⁶⁹. In general, A significant decrease in \bar{M}_n and \bar{M}_w was observed in all of the conditions^{63,67,76,83,86,114,135,154,161,167,186}. These results show the dominance of chain scission mechanism, which confirmed that all PLA films were subjected to hydrolysis⁵⁸.

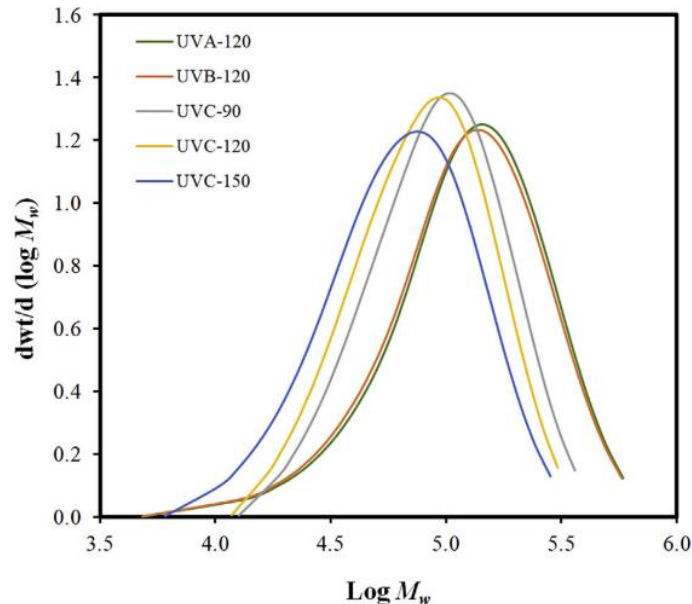


Figure 11. Molecular weight distribution of PLA after exposure to UV-A, UV-B and UV-C radiations¹⁸⁴.

When the polymer chain is cut preferentially, increasing or decreasing PDI trends are expected. During hydrolysis in studies carried out by Rocca et al.¹⁵⁷ in different humidity conditions, the PDI values were similar to the initial one (≈ 2.3) (Figure 12). No big changes were observed, suggesting that the degradation mechanism did not favor the formation of small or big oligomers in a preferential way, but randomly and/or end chain degraded the polymer^{58,157}. The authors concluded that the hydrolysis of PLA is carried out by a combination of random and end chain scission mechanisms. The random scission mechanism is behind the fast decrease in molecular weight of PLA, while the end chain scission mechanism is behind the mass reduction of the polymer, as it produces soluble monomers¹⁸⁷.

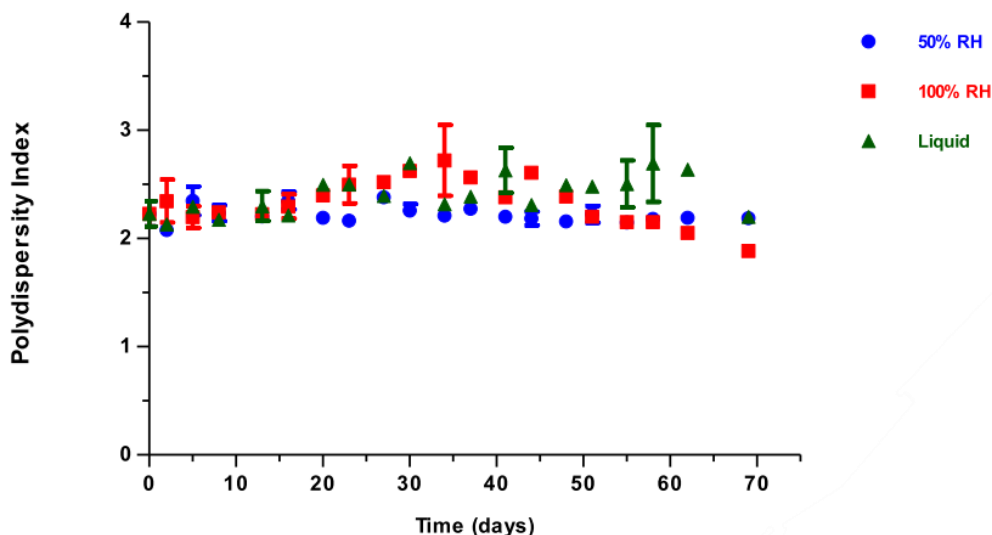


Figure 12. Polydispersity index (PDI) of PLA films stored at 50 % RH, 100 % RH, and immersed in liquid water at 50 °C during time ¹⁵⁷.

On the other hand, degradation studies carried out by Diani et al.¹⁶⁰ at elevated temperature and humidity showed the samples degraded at 60°C showed an increase in the PDI up to 4.0 at day 7. This increase in PDI can be attributed to the favored degradation in the amorphous regions of the samples, indicating the random scission of the chains rather than preferential degradation at the chain ends ¹⁸⁸. Following day 7, the PDI decreased as the amorphous regions are further degraded, the crystalline regions begin to degrade, showing lower molecular weight values¹⁶⁰.

3.2. Thermal Analysis

Thermal analysis (TA) comprises a family of measuring techniques that share a common feature; they measure a material's response to being heated or cooled (or, in some cases, held isothermally). The goal is to establish a connection between temperature and specific physical properties of materials ¹⁸⁹. The techniques that are the subject of this section are differential scanning calorimetry (DSC) and thermogravimetric analysis (TGA).

3.2.1. Differential scanning calorimetry (DSC)

Differential scanning calorimetry (DSC) is a useful analytical tool to characterize the physical properties of a polymer ¹⁹⁰. Also, DSC is an excellent technique to monitor the degradability of polymers since it determines the thermal properties, such as the glass transition (T_g), cold crystallization (T_{cc}), and melting (T_m) temperatures, enthalpies, and crystallinity ¹⁶⁶.

DSC analysis was carried out to determine possible changes of PLA thermal events induced by the degradation conditions applied. Taking as reference the work of Ren et al.⁶⁰ the experimental conditions were a sample of about 4–6 mg and tested in a nitrogen atmosphere. Heating them to 190 °C, kept the temperature for 3 min to eliminate the thermal history, then the temperature was reduced to 20 °C at a rate of 10 °C/min, and kept the temperature for 2 min. Finally, it was heated to 190 °C at a rate of 10 °C/min⁶⁰.

The melting enthalpies of PLA were determined from the DSC curves, and Equation (6) was used to calculate the degrees of crystallinity of PLA, where ΔH_m is the measured melting enthalpy, ΔH_{cc} is the measured cold crystallization enthalpy, $\Delta H_m^{100\%}$ is the theoretical melting enthalpy for PLA with 100 % of crystallinity, given as 93.1 J/g according to the literature¹⁹¹, and W is the polymer mass fraction in the analyzed sample¹⁹.

$$\chi_c(\%) = \frac{\Delta H_m - \Delta H_{cc}}{W_{PLA} \Delta H_m^{100\%}} \times 100 \quad (6)$$

Results reported in the literature about DSC analysis of neat PLA (melting and cold crystallization enthalpy and temperature, glass transition, and degree of crystallinity, respectively, ΔH_m , ΔH_{cc} , T_m , T_{cc} , T_g , and X_c) are summarized in Table 5.

Table 5. DSC data obtained for neat PLA^{19,107,109,161}

Sample	Glass	Melting		Cold Crystallization		Degree of Crystallinity
	Transition	Temperature	Enthalpy	Temperature	Enthalpy	
PLA	T_g (°C)	T_m (°C)	ΔH_m (J g ⁻¹)	T_{cc} (°C)	ΔH_{cc} (J g ⁻¹)	X_c (%)
	62.9	149,8	15,3	117	7.1	8.8

The DSC results of PLA studied by Antunes et al.¹⁰⁷ after accelerated weathering by ultraviolet (UV) and moisture at 50°C for 2000 h shows in Figure 13¹⁰⁷. The results show an increase in the melting and cold crystallization enthalpy of PLA, while T_{cc} , T_g , and T_m decreasing at the end of the weathering¹⁰⁷ (Table 6). T_g increased in the first time of weathering due to the increased of the degree of crystallinity which reduces the mobility of the amorphous zone. A second melting peak started to develop with increasing weathering exposure time, reflecting the melting of β and α crystallites, which have different melting temperatures due to different sizes and perfection¹⁰⁷. Moreover, T_{cc} shifts to a lower temperature when PLA starts to degrade. This change can be attributed

to the improvement of chain segment mobility, facilitating nucleation and growth of PLA crystals⁶. An increase in the cold crystallization enthalpy (ΔH_{cc}) indicates an increase in the number of polymer chains involved in the crystallization process during degradation, allowing the crystallization to begin at a lower temperature¹¹⁶. Additionally, the reduction in T_g at the end of weathering value can also be explained by increase in mobility of the chains that leads to a reduction in molecular weight of PLA due to the plasticizing effect of poly (lactic acid) oligomers formed during hydrolysis process⁶⁸. Similar results reported other authors in accelerated weathering tests^{19,109,151}.

In the work of Kaynak et al.¹⁹ they observed the decrease in T_g values up to 7 °C and T_m only 1-2 °C used UV radiation at 50°C for 300 h¹⁹. Gong et al.⁸⁷ reported that due to the addition of $FeCl_3$, the glass transition temperature of the modified samples decreased significantly compared with that of pure PLA. When $FeCl_3$ was added, the PLA molecular chain was degraded due to weakening of the ester bond, resulting in a decrease in the molecular weight of the PLA⁸⁷. In the other hand, Girdthep et al. reported an increase of T_g observed at the beginning of hydrolysis. T_g increase in the initial stage of hydrolytic degradation followed by a decrease afterwards. Such a T_g increase was attributed to polymer chain packing (polymer crystals) that reduce the mobility of the chains in the amorphous zone¹⁹² and probable formation of an intermediate phase from the hydrolyzed amorphous region¹⁹³, which restricted polymer chain mobility⁷⁰.

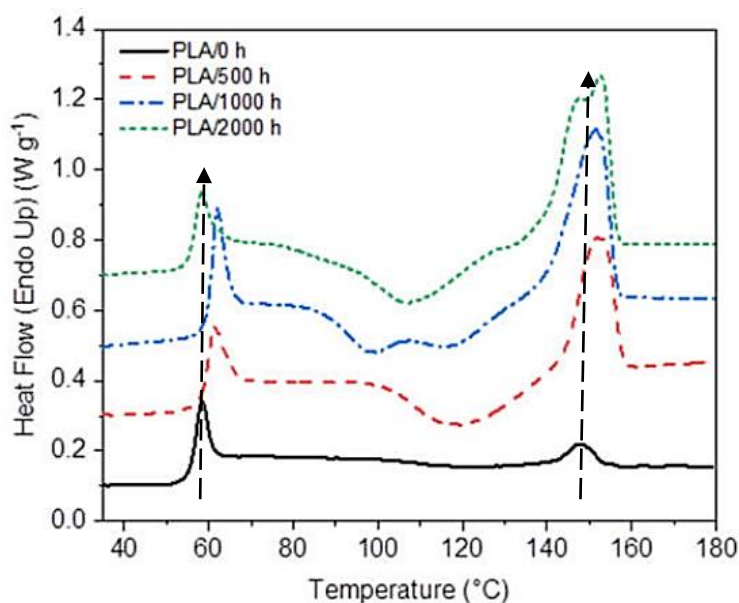


Figure 13. DSC first heating curves of neat PLA after accelerated weathering degradation¹⁰⁷.

Table 6. DSC data obtained for neat PLA after accelerated weathering degradation¹⁰⁷.

Sample	Glass Transition	Melting			Cold Crystallization	
	T_g (°C)	Temperature		Enthalpy	Temperature	Enthalpy
	T_g (°C)	T_{m1} (°C)	T_{m2} (°C)	ΔH_m (Jg ⁻¹)	T_{cc} (°C)	ΔH_{cc} (Jg ⁻¹)
PLA/ 0 h	56.9	147.7		2.3	121.2	2.2
PLA/ 500 h	59.9		152	21.6	119.8	19.1
PLA/1000 h	60.8		151.9	30.4	98.9/116.7	27.4
PLA/2000 h	56.7	147.3	152.7	34.8	107	24.6

Several authors analyze the changes in T_m after degradation^{7,61,68,71,76,78,79,94,145,167}. For instance, Rocca et al.¹⁵⁷ reported that in PLA materials exposed to humidity conditions at 50 °C, no significant changes were observed in T_m values of samples stored at 50% of relative humidity (RH)¹⁵⁷. The decrease was pronounced as PLA was stored in environments at high RH¹⁵⁷ and exposed to T/ UV/RH¹⁰⁹. As the degradation proceeds further, the crystalline zone is affected by degradation since the thickness of the crystalline regions decreases, leading to a reduction of the melting temperature (T_m). The reduction in melting temperature indicated low molecular weight fragments, caused by chain scission of ester bonds in the polymer matrix⁶¹. The value of T_m depends on the molar mass, the chain stiffness, and the branching degree of the chain. Slower molar mass loss generates fewer carboxy-terminal groups in the polymer chain, which lowers the melting temperature of the polymer crystals to a lesser extent than for other specimens¹¹⁶. Kruszkowska et al.⁹⁴ mentioned T_m changes in samples degraded of polylactide and polylactide filled with montmorillonite. In this case, T_m is slightly lower in the phosphate-citric buffer solution compared with degraded samples in phosphate buffer solution. The phosphate-citric buffer solution can affect the pH of the buffer solution more easily than in the case of the phosphate buffer since it has a lower capacity value. It causes an increase in the concentration of carboxyl-terminal groups, leading to the formation of oligomers of lactic acid in a greater quantity known to have a catalytical effect in hydrolytic degradation.⁹⁴ Also, the melting enthalpy of the specimens increased, followed by a decrease during the degradation process, and similar results show in all degradation experiments in water solutions^{6,62,67,83,116,120,121,123,159,166}.

Several authors reported a bimodal peak during the degradation process, indicating the formation of two fractions of different molecular weights during degradation^{6,7,67,68,123,167}. For instance, Gonzalez et al.¹¹⁶ reported two melting peaks, a lower-sized lamella, 138 °C (T_m), and the higher temperature peak, corresponding to the crystalline conformations

have a larger size lamella appears at 142 °C (T_{m2})¹¹⁶. According to the literature, the appearance of double melting peaks could be attributed to the development of two different crystals during the heating process of DSC, α and β -forms. The high T_m corresponds to the melting of the more stable structure, which is the α -crystal, while the low T_m is ascribed to the less perfect small crystals β ^{7,67,68,120,167}. The double-peak could also have been the result of a melting–recrystallization–melting process, or the melting of different sized lamellae formed during the degradation process¹⁰⁷. In the study of Zhao et al.¹⁶⁷ the bimodal peak can be observed during the degradation process, and the DSC curves obtained for the degraded samples are showed in Figure 14¹⁶⁷.

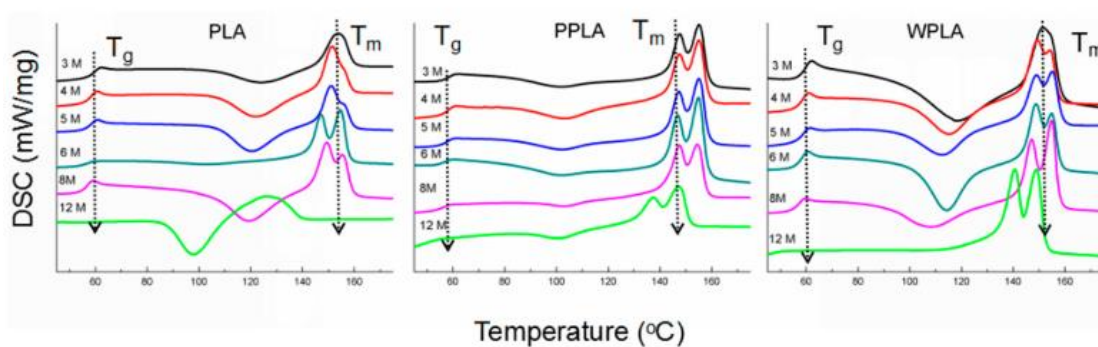


Figure 14. The differential scanning calorimetry (DSC) curves of the secondary heating curves were obtained for the degraded samples, PPLA corresponding to PLA/MgO nanoparticles and WPLA corresponding to PLA/MgO whiskers, immersed in phosphate buffer solution (PBS) at 37 °C for 3, 4, 5, 6, 8, and 12 months¹⁶⁷.

First, T_g peaks observed for the samples are gradually shifted to the lower value, and the same variation is also observed for T_m . There are also two endothermic peaks for some curves, and this is a common phenomenon for PLA degradation due to the recrystallization process of the defective crystals as decomposed products¹⁷⁸. The degrading process starts with an amorphous zone degradation and then gradually combines with the destruction of the crystalline structure in a long-term degradation, causing a molecular weight decline proved by the GPC results¹⁶⁷. The lower value of T_m shows the PLA sample in 12 months, and according to the GPC results, it implies the formation of a decomposed product with a low molecular weight during the long-term degradation¹⁶⁷. Initially, there is no intensively significant difference between the composites and PLA. However, with the extension of the immersing time, it is noticeable a variation of the curves in the PLA/MgO nanoparticles (PPLA) and PLA/MgO whiskers (WPLA). The variation in the DSC curve for WPLA implies the lower degrading rate, there is a prominent difference in the crystalline structure of WPLA formed in the degradation process. The MgO, especially the whiskers, is favorable for forming more

complete crystal regions, which lead to a higher crystallinity, resulting in it effectively inhibiting the degradation of the specimen¹⁷⁸. This also indicates that the large amount of water entering the matrix is apt to accelerate the hydrolyzing of the amorphous material, but it slightly impacts on the crystal area even for the long-term degradation. Finally, the double endothermic peaks are maintained in all the curves of PLA/MgO nanoparticles (PPLA) sample and WPLA after 12 months of degradation. These is due to, as mention above, the relatively denser or more compact crystalline network structure in the PLA matrix after the short-term degradation, caused by the MgO nanoparticles and whiskers¹⁷⁸, which may help delay its degradation¹⁶⁷.

The crystallinity of PLA samples after degradation varies depending on the degradation environment and the blends of PLA with different nanocomposites, additives, plasticizers, or nanofillers. Kaynak et al.¹⁹ reported DSC results during UV irradiation cycles at 70°C, the total crystallinity amount of the specimens increased significantly, e.g., from 14% to 48% in neat PLA and 59% in PLA/Halloysite nanotubes (PLA/HNT) specimen¹⁹. López et al.¹⁶⁰ show a maximum decrease of 12% of the percentage of crystallinity in blends of PLLA with cassava thermoplastic starch (PLLA/TPS) after 21 days of irradiation, suggesting that photo-degradation has advanced the point of arriving to affect the folded chains within the crystalline zone⁹⁷. For samples degraded at 80°C with 100% relative humidity, the percent crystallinity for the PLA sample peaked between 5 and 6 days increased to 73% while, at 14 days, the crystallinity had fallen to 52%¹⁶⁰. In studies carried out by Iñiquez et al.,⁶ the crystallinity of samples exposed to water increased from 2.8 to 7.3% after 6 months of immersion. For PLA films exposed to ethanol solutions, the crystallinity increased dramatically⁶.

Other authors reported an increased in crystallinity after different environment degradation^{6,7,63,65,67,70,72,74,75,78,79,83,15,101,103,107,110,112,123,125,128,130,47,132,134,142,143,145,146,155,158,174,176,49,178–182,53,55–57,62}. According to the literature, the increased in crystallinity indicates that hydrolytic fission of the chain takes place preferentially in the amorphous phase of the polymer⁹⁴. During the degradation of PLA, water diffuses into the amorphous regions initially, which are less packed and allow water to penetrate more easily than the crystalline regions. After the degradation of most or all the amorphous regions, the water slowly penetrates into the crystalline regions and its percentage of crystallinity decreases^{7,58,60,62,76,79,83,94,116,157,160,163,167,168,191}. However, no significant changes in crystallinity were observed in PLA samples after immersion in marine environment¹⁶⁶.

3.2.2. Thermogravimetric analysis (TGA)

Thermogravimetric analysis (TGA) is a technique used to study the thermal stability and the fraction of volatile components in a sample by monitoring the mass change as it is heated. TGA measurements can be performed in either inert (argon or nitrogen) or oxidant atmosphere (air or oxygen) ^{189,199–204}. Output data are collected as changes in mass due to increasing temperature (dynamic experiments) or time (isothermal experiments). It is also widespread to calculate the derivative thermogravimetric curve (DTG), corresponding to the actual mass (or mass percentage) derivative concerning time or temperature²⁰⁵.

Mass loss may be categorized as volatile components such as low molecular mass additives or oligomers that generally evaporate between ambient and 300 ° C; and generation of volatile degradation products resulting from chain scission that generally require temperatures above 200 ° C but not more than 800 ° C. All of these mass loss processes may be characterized by TGA to yield information such as composition, and thermal stability¹⁸⁹. It is important to understand the thermal degradation pathways of polymers and the effect of additives on this degradation in order to either accelerate or retard the degradative process. In some cases, such as a landfill, it is advantageous to accelerate degradation, while in other applications, such as in processing or reducing flammability, it would be desirable to retard it ²⁰¹.

Taking as reference the work of Taiatele et al. ⁵⁵, the thermal stability of samples was performed in protective nitrogen gas (20 ml/min) and with an industrial air measuring atmosphere (60 ml/min). Samples were heated from 30 °C to 600 °C at a heating rate was 10 °C/min, the weight of the samples was between 10 to 12 mg ⁵⁵. In table 7 are summarized TGA analysis of some authors about reference initial degradation of PLA with the temperature value corresponding to 5% weight reduction ($T_{5\%}$ [°C]), the temperature value corresponding to 10% weight reduction ($T_{10\%}$ [°C]), the temperature value corresponding to 50% weight reduction ($T_{50\%}$ [°C]), and the maximum temperature degradation rate (T_{\max} [°C]) ¹⁰³.

Table 7. Evaluated TGA curve values of reference PLA ^{103 74 163}.

$T_{5\%}$ (°C)	$T_{10\%}$ (°C)	$T_{50\%}$ (°C)	T_{\max} (°C)
320-332	341	356-360	362-368

To prove degradation and examine its extent, Litauszki et al.¹⁰³ performed thermogravimetric analysis to degraded samples under accelerated test aging and observed that laser treatment caused more intensive degradation than xenon treatment. The thermograms in Figure 15 (a) indicate that the PLA samples degrade in one step. While weight reduction starts ($T_{5\%}$) at 320 °C in the untreated PLA film, this temperature is lower 317 °C for the sample aged in the xenon test chamber and 258 °C for laser-aged PLA sample. Xenon test aging showed a 16 °C (ΔT) decrease in the maximum temperature degradation rate (DTG) compared to untested PLA, laser aging produced a 59 °C (ΔT) decrease. Also, the shape of the curves show that molecular weight values shifted towards even lower values, and the distribution of molecular weight widened (Figure 15 (b))¹⁰³.

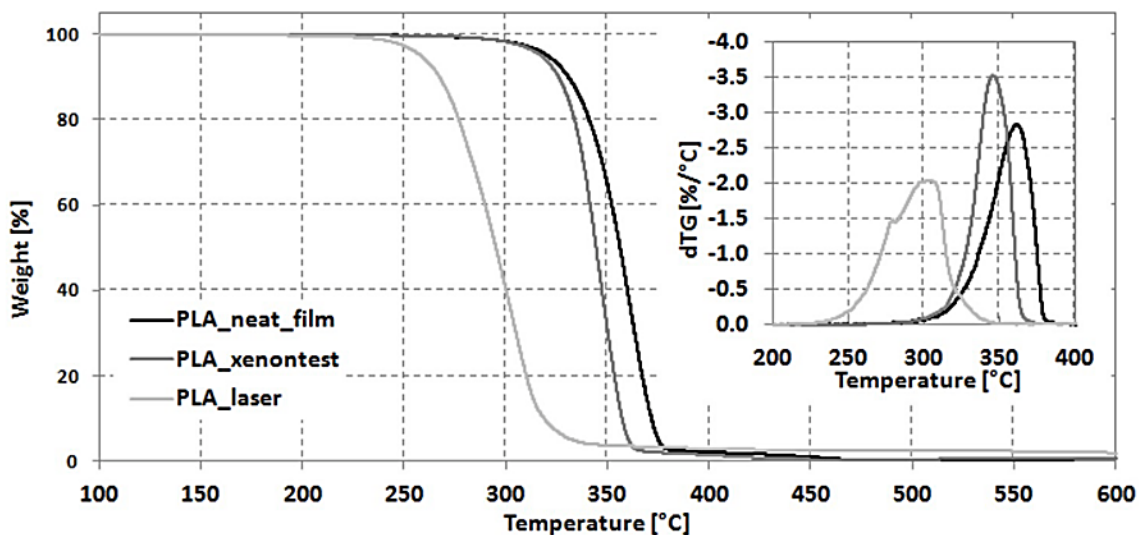


Figure 15. (a) TGA and (b) dTG results of the reference PLA and the treated samples (10 °C/min)¹⁰³.

The thermal stability study of Shalumon et al.⁸⁵ reported that PLA scaffolds after one year of in vitro degradation showed a reduction of decomposition temperature at 5% ($T_{5\%}$) of 125 °C (ΔT) and 65 °C for $T_{90\%}$ with respect to the initial value before degradation. This gradual decrease in thermal stability implies the reduction of structural stability and breaking of bonds in PLA scaffolds during degradation. In short, the stability evaluation of fibers before and after degradation, PLA fibers show faster degradation while PCL shows very slow one⁸⁵. This difference denotes that PLA fibers degrade faster than PCL fibers and could be a good candidate for tissue engineering scaffold⁸⁵. In another study, Valapa et al.⁷⁴ reported the TGA curves for PLA after degradation under different pH conditions. The results showed that after degradation time of 108 h, $T_{50\%}$ for PLA samples

hydrolyzed under acidic, neutral, and basic conditions at 35°C is determined to be 353, 356, and 343 °C, respectively. With the increasing temperature at 55°C, the $T_{50\%}$ further decreases to ~351, 354, and 313 °C, respectively. Confirming that PLA exhibits a faster rate of hydrolytic degradation under basic pH conditions and high temperatures⁷⁴.

Several authors showed a general displacement of the curve towards lower temperatures was found, traduced in a slightly lower thermo-oxidative stability as a function of the exposition time⁸³. It is the cause of Taiatele et al.⁵⁵ and López et al. that showed that thermal stability of PLA is affected by the presence of thermoplastic starch, even after degradation^{55,97}. In the work of Valapa et al.⁷⁴ the authors studied the thermal degradation profile of PLA-SP nanocomposite reveals that the addition of sucrose palmitate (SP) in the PLA matrix influences the faster rate of hydrolytic degradation process as compared to neat PLA under basic pH condition at 55 °C. The possible reason for the behavior exhibited by PLA-SP nanocomposite is that with increasing temperature during the thermal degradation analysis, decomposition of SP starts before PLA. H^+ ions released during the degradation of SP further triggers the autocatalytic cleavage of PLA backbone, which leads to an earlier degradation of PLA-SP nanocomposite compared to PLA, when subjected to TGA analysis⁷⁴. Also, Musioł et al.⁵⁴ reported that blends containing polylactide and poly(3- hydroxybutyrate-co-4-hydroxybutyrate) (PLA/P(3HB-co-4HB)) with jute fibers showed a further reduction in decomposition temperatures after 21 days of incubation in water at 70 °C, which may indicate a greater impact of the jute fibers additive in the composite on the biodegradation process⁵⁴.

The presence of a nanofiller can affect the degradation of nanocomposites and, therefore, their thermal properties. In the case of studied samples by Kruszkowska et al.¹²³ one of the used nanofillers was pure montmorillonite^{68,123}. The values of $T_{10\%}$ and $T_{50\%}$ of composites were lower compared to those of pure PLA in buffer solutions. This can be attributed to the fact that during the thermogravimetric analysis the nanofiller can constitute a barrier for the gas products forming in the sample and in this way the changes in the $T_{10\%}$ and $T_{50\%}$ values can be less significant for the investigated composites^{68,123}. It is widely supported argument that the improved thermal stability for polymer clay nanocomposites is mainly due to the formation of char which hinders the out-diffusion of the volatile decomposition products, as a direct result of the decrease in permeability⁹⁴. So, the results of Kruszkowska et al.¹²³ showed that the thermostability of nanocomposite PLA-Nanofil2 after hydrolytic degradation decreases more in comparison with PLA-

Montmorillonite sample, which can be determined based on the ΔT value (46.6 °C and 14.0 °C respectively). The phenomenon mentioned above is related to amine cation in the interlayer spaces of montmorillonite which alters the properties of the filler. It can be deduced that better dispersion of nanofiller in the polymer matrix enables penetration of nanomaterials by water and causes a decrease of the average molecular weight.

For this reason, the lower values of $T_{10\%}$ for the PLA-Nanofil2 sample have been observed in comparison with the PLA-Montmorillonite system^{68,123}. The thermal stability of PLA is improved upon the addition of clays, as previously shown. Studies carried out by Bergstrom et al.¹⁶³ showed increasing onset and maximum weight loss temperatures in the PLA/C30B sample. Thermogravimetric analysis after degradation in PBS at 37°C showed a decrease of $T_{5\%}$ by 45°C and 40 °C for neat PLA and PLA/C30B, respectively. This is due probably to chain scissions resulting from hydrolytic degradation. However, PLA/C30B nanocomposite is more thermally stable. This demonstrates that C30B can absorb volatile products emitted during the thermal degradation and simultaneously may act as an insulating barrier¹⁶³.

On the other hand, thermogravimetric analysis doing by Zare et al.⁷¹ showed that the addition of 1% wt % CNTs can improve the thermal stability of the PLA75/PEO25 blend, while further addition of CNTs accelerated the thermal decomposition (Figure 16). Therefore, the small concentration of CNTs has a protective role against the thermal decomposition of this system, but the high content of CNTs quickens the decomposition, because the high number of thermally conductive CNTs increases the heat transfer to the polymers⁷¹. The case of studies carried out by Pinto et al.¹²⁴ thermal properties of PLA loaded with graphene-related materials is not influenced by degradation, since reported slight changes after six months in vitro degradation¹²⁴. One may hypothesize that this is due to graphene improving thermal homogenization of the melt, minimizing hot-spots, and consequent polymer degradation¹²⁴. Likewise, the thermal stability of PLA/TiO₂ degraded specimens has been improved¹⁰⁷. $T_{5\%}$ before and after 2000 h of weathering were 239 and 295°C, and T_{max} before and after weathering were 318 and 357 °C, respectively. The same shift towards a higher indicates an increase in polymer stability after this weathering time. The PLA/TiO₂ samples, after weathering exposure, had lower \bar{M}_w values, as discussed before, but they were also organized in crystalline domains that degraded more slowly during TGA analysis. TiO₂ nanoparticles could improve the thermal stability of the PLA, acting as thermal blockers against heat diffusion¹⁰⁷.

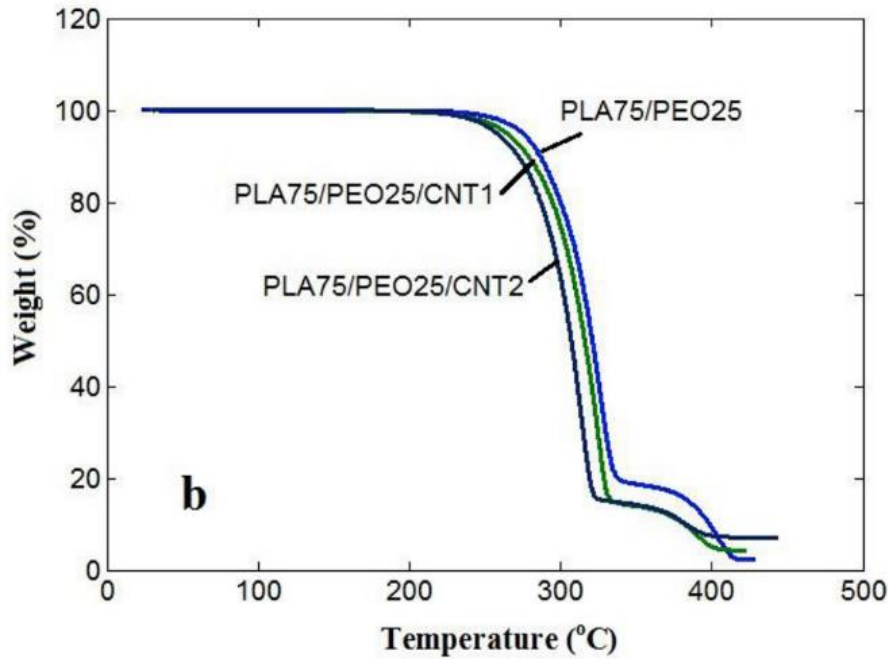


Figure 16. Thermal decomposition of degraded samples containing 75 wt % PLA for 4 weeks under hydrolytic degradation in PBS solution ⁷¹.

3.3. X Ray diffraction (XRD)

The XRD has been used to study polymer structures and monitor the changes in morphology and percent crystallinity of PLA after degradation²⁰⁶. Typically, the X-ray beam is directed onto the material to be tested at room temperature. The incident ray is then partially absorbed and partially scattered because of the interaction of the rays with the electrons, resulting in a diffraction pattern indicative of the atomic order of the material.

In general, measurement conditions there are usually at 40 kV and 45 mA with Cu Ka radiation (1.5406 Å), and the scanning range was from 0° to 80°¹⁷⁹. The results are plotted with intensity against the diffraction angle, degree 2 theta (°2θ). In this way, the scattering intensity can be measured and used to calculate the degree of crystallinity (X_c)²⁰⁷. Generally, the X_c was calculated using the equation:

$$X_c = \frac{A_c}{A_c + A_a} \times 100\% \quad (7)$$

where A_c and A_a are the area of the crystalline peaks and the area of the amorphous phase, respectively^{7,207}.

Iñiguez et al.⁶ studied the PLA immersed in ethanol and pure water and the XRD profiles of PLA films during hydrolytic degradation are shown in Figure 17. The results showed

that PLA immersed in pure water remained amorphous during hydrolysis since the profiles showed only broad peaks during hydrolysis, without the appearance of crystals⁶. In contrast, some sharp peaks began to appear after 3 days of exposure to 50% and 95% ethanol (Figure 17 D and E). The diffraction peaks observed in Figure 17 correspond to the formation of α -form crystals (orthorhombic unit cell with parameters $a = 1.06$ nm, $b = 0.61$ nm, and $c = 2.88$ nm)²⁰⁸. In 50% and 95% ethanol, it is observed diffraction peaks at 14.8° , 16.8° , 19.1° , and 22.4° which coincided with the data published previously^{6,7,168,206,209}, corresponding to the 010, 110/200, 100/203 and 102/210 plane reflections, respectively^{6,7,210}. The appearance of crystals in PLA after 3 days of exposure to ethanol solutions indicates that increasing chain mobility and crystallinity took place in the early stages. At all times, the diffraction peaks were the same, meaning the same kind of crystals were formed during crystallization and were present during the entire degradation of the amorphous regions^{6,67}. As shown in Figure 17 (B), the intensity of all the diffraction peaks of the composites showed an increase followed by a reduction. During hydrolysis, the degradation proceeded preferentially in amorphous regions while cleavage in the molecular chains enhanced their mobility, altogether increasing crystallinity. However, a prolonged degradation eventually affected the crystalline regions, leading to a decrease in crystallinity^{79,210}. These results can be correlated with DSC thermograms. In another study at the same conditions, Iñiguez et al.⁶⁷ showed the XRD profiles of PLA-nanocomposite with organo-modified montmorillonite (PLA-OMMT) film under the same conditions and the diffraction peaks observed were in accordance with the formation of PLA α -crystals. Therefore, during hydrolytic degradation of the amorphous region of the polymer matrix the same form of crystals was present, meaning that the incorporation of nanoclay into the PLA films did not interfere in the crystallization of the polymer. The presence of nanoclay increased the sorption of ethanol, which was sorbed between the clay galleries, where the clay acted as an anchor restricting the movement of the polymer chains. Crystallization was not affected, and consequently, the hydrolytic degradation was not affected by the presence of the clay⁶⁷.

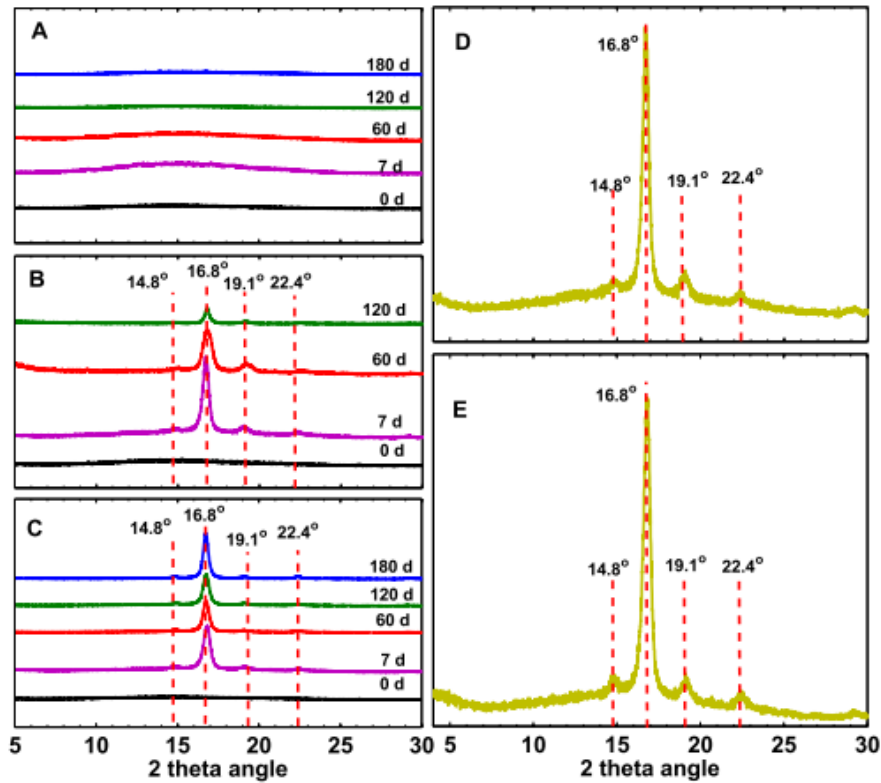


Figure 17. XRD profiles of PLA films during hydrolytic degradation in (A) water, (B) 50% ethanol, (C) 95% ethanol and in the 3rd day of immersion in (D) 50% ethanol and (E) 95% ethanol at 40 °C. The number on each profile indicate days immersed ⁶.

Under other conditions, Beltrán et al. ⁷ reported results after immersion in PBS at 58 °C and showed PLLA and PLLA based nanocomposites with neat halloysite (PLLA-Ha) develop lower degrees of crystallinity than PLLA-OMMT. At short immersion times, the higher content of the more stable α form was found in the nanocomposite with C30, due to the catalytic effect of this clay on the hydrolytic degradation of PLLA. Additionally, a small but noticeable PLLA crystallization (after 84 days of immersion) is observed at 37 °C only in the nanocomposite with the C30 clay. This result is considered important because it demonstrates that significant structural changes may occur even at 37 °C when the immersion times are long and in the presence of certain additives. Thus, the above results confirm the need to properly select the additives for PLLA when this polymer is in contact with water since some of them may promote structural changes in hydrated PLLA that can substantially modify the mechanical, optical, and barrier properties of the material ⁷. As mentioned above, polymer chain mobility increases with medium temperature, increasing the crystalline phases within the polymer chain. It is the case of

Felfel et al.¹⁶⁸ studies. A significant increase in their crystallinity was observed after degradation in PBS at higher temperatures (50, 65, 75 and 85 °C) due to a reduction in the molecular weight and degradation of the amorphous polymer chain regions. Two sharp peaks were detected at $2\theta = 16.5^\circ$ and 19° ¹⁶⁸, which correlates well with the crystallinity data obtained via DSC scans.

In studies carried out by Valapa et al.⁷⁴ under basic pH condition, the intensity of the peak ($2\theta = 16.7^\circ$) corresponding to the crystalline structure of PLA increases with increasing the degradation time, and the increment in crystallinity for PLA is further enhanced at higher degradation temperature (55 °C)⁷⁴. Besides, for the PLA reinforced with sucrose palmitate (PLA-SP) (before degradation) the peak observed at $2\theta = 2.27^\circ$ reveals the presence of SP incorporated in the PLA matrix and tends to almost disappear after the degradation process. This is because, at elevated temperature, due to the improvement in the mobility of PLA chains, water might diffuse into the interface between PLA and SP and initiate the hydrolysis of PLA, thereby, leading to oozing out of SP from PLA matrix⁷⁴.

3.4. Fourier Transform Infrared Spectrometry (FTIR)

Fourier transform infrared spectroscopy (FTIR) provides a rapid, nondestructive technique for detecting changes in the chemical structure of polymers after being subjected to photo-oxidative and hydrolytic degradation. Analysis of the infrared (IR) spectra enables identifying functional groups through the vibrations generated within bonds in the sample. The different peaks in a spectrum represent absorptions corresponding to vibrational transitions with different energy²⁰⁵.

A major attraction of the technique is that it can identify and following the loss or growth of particular functional groups quantitatively. This technique has successfully followed the alterations in carbonyl groups are the main indicators of degradation in PLA samples.²¹¹

Some authors obtained the FTIR spectra in the wavenumber range from 500 to 4000 cm^{-1} at a spectral resolution of 4 cm^{-1} ^{16,108,124,139,141,161,191,212} Also, in order to obtain accurate results, 64 scans were performed. The reference spectra of PLA samples obtained in the literature were used to compare changes in peaks after degradation, as detailed in Table 8.

Table 8. Peak band assignment for reference PLA^{19,84,139}.

<i>Assignments</i>	<i>Position (cm⁻¹)</i>
-CH- stretch	2995 (asym.); 2948 (sym.)
-C=O carbonyl stretch	1755
-CH ₃ bend	1456
-CH- asymmetric; symmetric deformation	1382, 1360
-CH- bend	1315-1300
-C-O- stretch	1265
-C=O bend	1211
-C-O- stretch	1180, 1129, 1090
-OH bend	1044
-CH ₃ rocking mode	955, 916
-C-C- stretch crystalline phase	871
Amorphous phase	755

Degradation of PLA leads to the scission of polymer chains as external water attacks the ester group (-C=O) and breaks it down to an acid (-COOH), and alcohol (-OH) terminated residue⁹. Under photolysis, the photo-cleavage reaction resulted in C=C double bond and hydroperoxide (O-H) at the new PLA chain terminals¹⁰⁸. It leads to decreased molecular weight due to chain scission. A single scission at the middle of the chain has a greater impact than many terminal scissions as the former reduces the molecular weight significantly. Hence it is assumed that random scissions control the molecular weight reduction and subsequently the degradation⁹. An analysis of the most relevant works is carried out to describe the alterations in the chemical bond structure.

For instance, Varsavas et al.¹⁰⁸ reported significant differences in the spectra for the neat PLA specimens after accelerated weathering. In the literature, it is well established that the chemical bond structure of PLA has distinctive IR bands, as shown in Table 8. Figure 18 indicates that, due to the significant level of chain scissions in the ester backbone structure of PLA, IR intensities of C-C and C-O stretching peaks and all other typical PLA peaks decrease significantly with increasing accelerated weathering period. These peaks all faded away, becoming very broad after 400 h of degradation. It has been discussed that the mechanism of photolysis deteriorates significantly at the C-C and C-O bonds of the ester backbone structure of PLA by photon absorption. Moreover, according to the Norrish II mechanism, photo-degradation results in decreased molecular weight by chain scission and leads to the C=C double bond formation and hydro-peroxide (O-H) at the new PLA chain terminals. Thus, it is seen in Figure 18 that these new peaks of C=C

and O-H appears at 1651 cm^{-1} and 3742 cm^{-1} , respectively since 100 h weathering period. Apart from new peak formations, it is known that, chain scissions via photolysis reactions also lead to shifting of the IR peaks of the typical PLA bands to lower wavenumbers. For instance, Figure 18 reveals that, after weathering, the C-O stretching peaks shifted from 1080 cm^{-1} to 1025 cm^{-1} , and 1262 cm^{-1} to 1091 cm^{-1} ; while the C=O carbonyl stretching peaks shifted from 1749 cm^{-1} to 1743 cm^{-1} ¹⁰⁸.

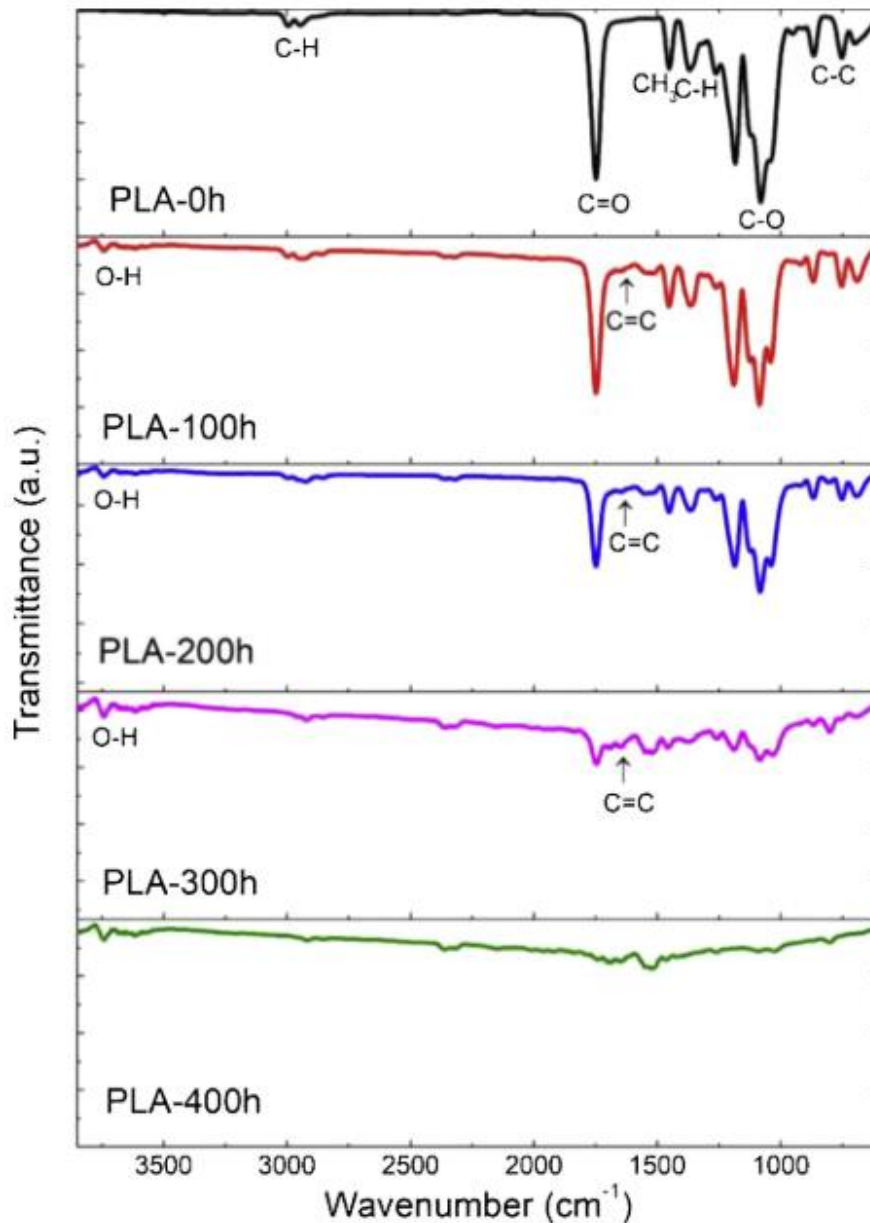


Figure 18. Alterations in FTIR spectra of the neat PLA specimens after each accelerated weathering period ¹⁰⁸.

Likewise, Wan et al.¹⁴¹ reported significant differences in peak intensities after degradation in alkali solution. During hydrolysis, C-O ester linkages of PLA structure experience cleavage, leading to significant decreases in the molecular weight. The peaks of the ester C–O– stretching vibrations anti-symmetric (1185 cm^{-1}) and symmetric (1087 cm^{-1}) were evidently weakened in intensity, whereas the intensity of the peak at 3298 cm^{-1} ascribed to hydroxyl group increased, indicating the hydrolysis of ester group during degradation of PLA²¹³. New peaks for the stretching vibration of $-\text{CH}_3$, symmetric stretching vibration of C=O, and symmetric and antisymmetric stretching vibrations of ester C–O– appeared. These characteristic peaks of the hydrolysates of PLA¹⁴¹, correspond to the hydrolytic reaction of PLA shown in Figure 19.

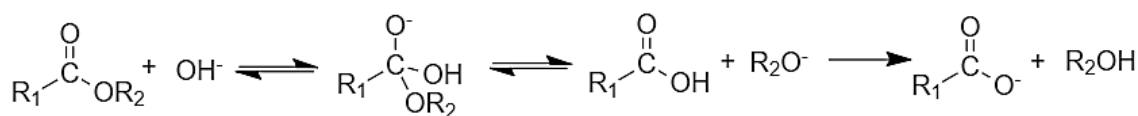


Figure 19. Hydrolysis reaction equation of PLA in alkali solution¹⁴¹.

On the other hand, some authors studied the changes in the chemical structure of PLA blends with other polymers or with the addition of fillers. Studies carried out by Luo et al.⁹⁹ reported the chemical modifications occurring upon UV radiation in PLA and PLA/TiO₂ nanocomposites during accelerated weathering and the FTIR spectra is shown in Figure 20⁹⁹. Accelerated weathering deteriorates the structure of PLA via polymer cleavage leading to chain scission, especially at the C–O (observed at 1262 cm^{-1} and 1180 cm^{-1}) and C–C (866 cm^{-1}) ester bonds from the PLA backbone structure, which indicates the oxidation and destruction of PLA under the influence of UV¹⁵¹. First, it can be seen that, the infrared bands after degradation change intensities or shift to lower wavenumbers. The FTIR spectrum indicated that UV irradiation resulted in the form of three absorption bands. The narrow band with a maximum at 1760 cm^{-1} assigned to C=O band; the broad band centered at 3400 cm^{-1} attributed to OH band from carboxylic acid; the third one in the region of $2800\text{--}2900\text{ cm}^{-1}$ could be assigned to asymmetric and symmetric in methylene chains ($-\text{CH}_2-$).

With the increase of the irradiation time, the intensity of these stretching bands increased, indicating that degradation of samples was taking place gradually. A new band only for PLA/TiO₂ nanocomposites in the region of 1610 cm^{-1} is observed, which could be

assigned to the conjugated double bond (C=C), that proves that the photo-degradation via a Norrish II type mechanism¹¹, was improved by the presence of TiO₂¹⁰⁷, which showed that the photodegradation mechanism was different from PLA. Also, the induced color change of polymer surface could be ascribed to the C=C double under the effects of TiO₂ by irradiation²¹².

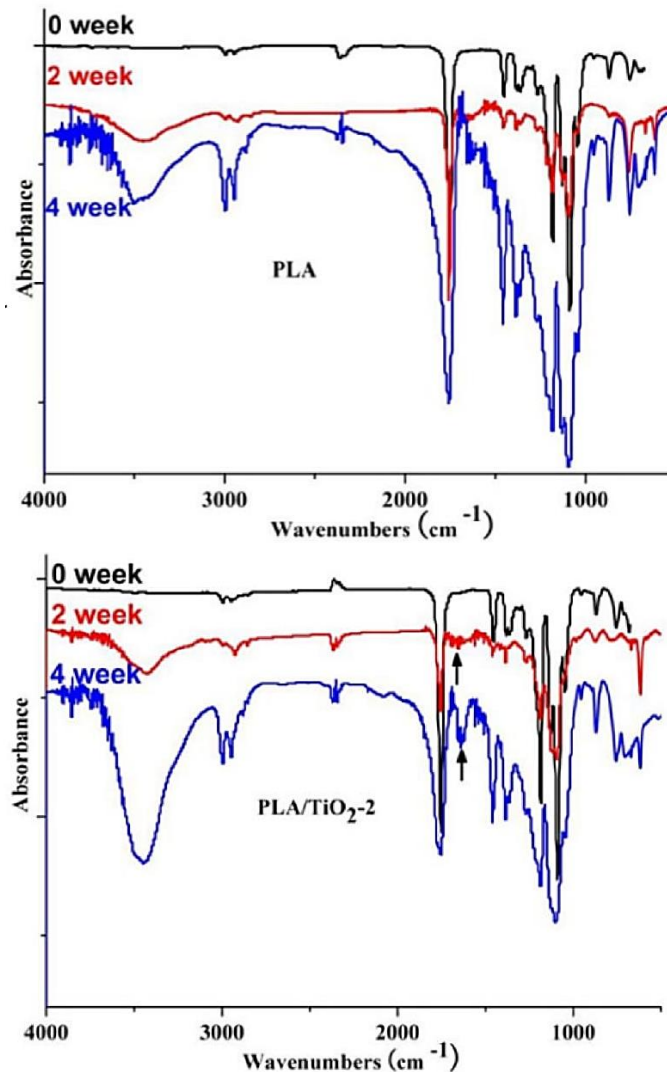


Figure 20. FTIR spectra for pure PLA and PLA/TiO₂ at different irradiation time⁹⁹.

Similar results showed Mucha et al.¹⁵⁴ during photo-degradation of PLA/Ag. The addition of Ag improved the photo-degradation. The large decrease of bands attributed to C=O (at 1756 cm^{-1}) and C-O (at 1190 and 1093 cm^{-1}) stretching vibrations was found. Absorbance at 868 cm^{-1} attributed to C-C skeletal vibrations confirms that chain scission is dominant by photolysis. Simultaneously, the clear band at 1725 cm^{-1} is formed, suggesting the creation of new carbonyl groups in PLA. Moreover, the presence of a signal at 1845 cm^{-1} is associated with the presence of photo-degradation by-products

containing C=O bonds, mainly anhydride compounds¹⁵⁴. Low intensive band components were found at 1845 and 1645 cm^{-1} , which can be attributed to peracid/perester groups and double bonds (probably at the chain ends), respectively¹⁰².

In like manner, IR spectra of PLA/Halloysite nanotubes nanocomposite (PLA-HNT) evidenced significant changes after irradiation by the presence of the band at 1845 cm^{-1} ascribed to the formation of anhydrides and broad band in the hydroxyl domain at 3420 cm^{-1} . This indicates that the same PLA photo-oxidation products are formed in the presence of HNT filler. Also HNT has a pro-degradant effect on the photo-oxidation of PLA, a process attributed to the presence of chromophoric impurities that can have an inducing effect on the radical oxidation mechanism of PLA and/or to the presence of traces of iron¹⁵³.

In studies carried out by Zare et al.¹³¹ the hydrolytic degradation and sensing behavior of poly (lactic acid) (PLA)/poly (ethylene oxide) (PEO)/carbon nanotubes (CNTs) nanocomposites in PBS solution is analyzed by FTIR. The results showed that all peaks decrease after degradation demonstrating that the degradation removes the chemical bonds of both PLA and PEO. The least variations of peaks are observed for the C=O bond in PLA at 1746 cm^{-1} because the degradation slightly change the structure of PLA in the samples. However, the peaks for C–H bonds in PEO (2900 cm^{-1}) suffer much reduction after degradation due to the high degradation of PEO phase in the samples. also, the PLA/PEO/CNT degraded nanocomposites demonstrate the smaller peaks compared to the degraded blends confirming that CNTs accelerate the degradation of polymers in PBS solution¹³¹. Similar results reported Li et al.¹⁴⁵ for PLA after in vitro degradation in phosphate-buffered saline (PBS)¹⁴⁵.

On the other hand, Lee et al.¹⁵⁰ reported the FTIR analysis of pure PLA and the results did not exhibit structural changes is PLA samples exposure in natural seawater. In this study, no significant variation after aging in FTIR analysis even after a biodegradation period of 30 days, which indicated that the inside of the PLA structure was not hydrolyzed by biodegradation. The conditions under which it can be degraded require longer immersion times under non-natural conditions (pH, temperature, moisture, and oxygen) to be completely degraded. Seeing the absence of such conditions in marine environments, whether PLA will degrade considerably faster than ordinary plastics in the ocean, is questionable¹⁶⁵.

Additionally, Beltrán et al.⁷ reveal important results about crystallization of PLLA during the immersion in water at 58 °C through IR spectra. An increase in intensity is observed for the absorption bands centered at 1212, 1182 and 1130 cm^{-1} while a decrease in intensity is noticeable in bands centered at 1265 and 1090 cm^{-1} . The rise in intensity for the bands at 1212 and 1182 cm^{-1} has been associated in literature with the formation of crystalline polymorphs during the annealing of PLLA at high temperatures. Likewise, the decrease in intensity for the absorptions at 1265 and 1090 cm^{-1} has been attributed to the reduction of the amorphous phase. As well, it can be observed in the spectra that the immersion leads to an important increase of the intensity of the band at 920 cm^{-1} , characteristic of the α and α' crystalline forms^{7,62} together with a decrease in the intensity of the band assigned to the amorphous phase at 956 cm^{-1} . Hence, IR spectra provides information on the nature of the crystalline polymorphs. The crystallization can be explained by the effects of water as a plasticizing agent, favoring the segmental mobility, and as a reagent for hydrolytic degradation, which produces shorter chains and favors conformational rearrangements, results discussed before in XRD analysis⁷.

3.5. Nuclear Magnetic Resonance (NMR) Spectroscopy

High-resolution solid-state NMR is a method to observe individual carbon and proton atoms along the main chain and side chains of polymers. This feature makes it possible to characterize in detail the microstructure, the conformation, and the molecular organization in the solid²¹⁴. In the study of polymer degradation, ¹H NMR is an available tool used to characterize degradation products by visualizing the differences in the degradation product pattern released from PLA. Also, this technique is used in the molecular weight analysis of polymers⁹⁴. A complementary technique that provides structural information about PLA crystallinity is ¹³C NMR. Solid-state NMR spectra provide a “fingerprint” of the α -polymorph of L-poly lactide²¹⁵. ¹³C NMR showed that amorphous PLA yielded the α crystalline form during hydrolytic degradation¹¹².

The experimental conditions of some authors showed the spectra were acquired at ambient temperature operating at 600 MHz. The polymers are dissolved in CDCl₃ (H: $\delta=7.285$ ppm), and tetramethylsilane (TMS, $\delta=0.00$ ppm) is used as an internal chemical shift reference²¹⁶. The blend composition was determined with ¹H NMR spectra, based on the integration of protons from the methine group of the PLA component (at $\delta = 5.20$

ppm)¹²¹. The chemical shift of ¹³C spectra was determined by taking the carbonyl carbon of solid glycine (176.03 ppm) as an external reference standard²¹⁷.

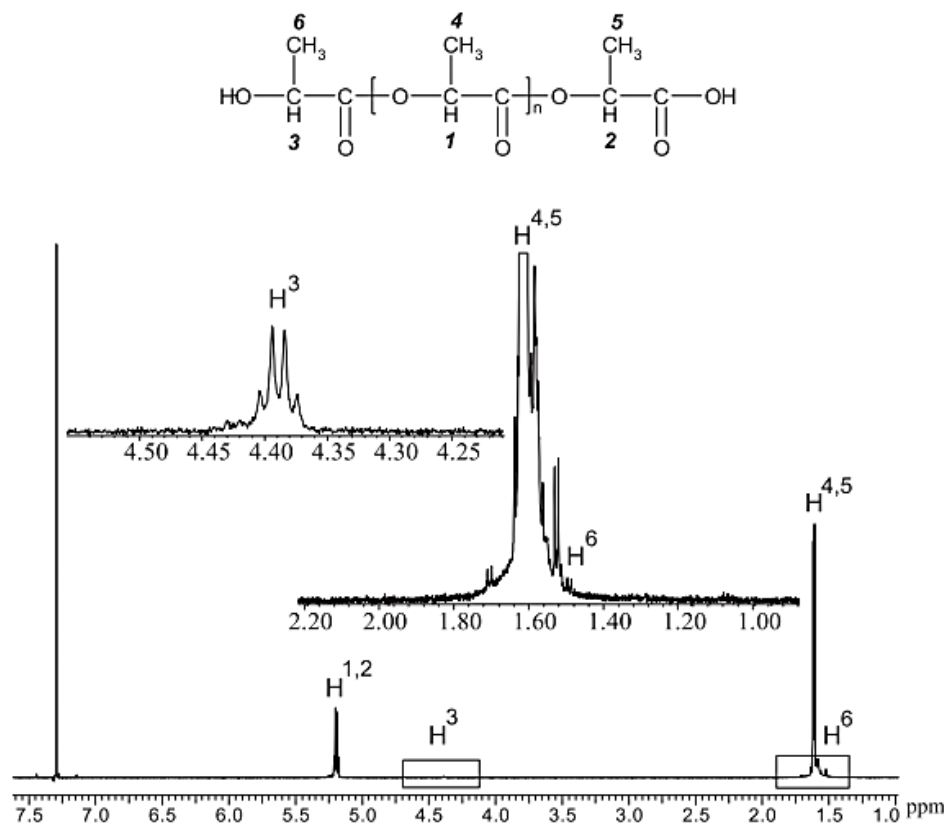


Figure 21. ¹H NMR spectrum (700 MHz, CDCl₃) of PLA after 16h of UV exposure at 254 nm¹⁸⁵.

Kruszkowska et al.¹⁸⁵ calculated the average molecular weight (\bar{M}_n) distribution by means of the ¹H NMR technique of PLA samples before and after 16 hours of UV exposure and after different time of hydrolytic degradation and showed the similar results^{94,185}. The ¹H NMR spectra after 16 hours of UV exposure of the PLA sample have been depicted in Figure 21. The resonances of chain methine (H¹) and methyl (H⁴) have been observed at 5.18 and 1.61 ppm, respectively. The $-CH(CH_3)-OH$ methine (H³) and $-CH(CH_3)-OH$ methyl (H⁶) result in a quadruplet at 4.40 ppm and a doublet at 1.51 ppm, respectively. The signals H² and H⁵ corresponding to the $-CH(CH_3)-COOH$ end units overlap with the peaks of methine (H¹) and methyl (H⁴) chain units¹⁸⁵.

The average number degree of polymerization (n) and number average molecular weight (\bar{M}_n) of PLA was determined based on the ratio of H^{1,2} to H³ integrals according to the equations presented below (8-9)^{185,218}.

$$n = \frac{I_{1,2} - I_3}{2I_3} \quad (8)$$

$$\bar{M}_n = (C_j * n) + C_{k1} + C_{k2} \quad (9)$$

Where:

C_j : molar mass of $-\text{CH}(\text{CH}_3) - \text{COO}-$ chain units (g/mol)

C_{k1} : molar mass of $-\text{CH}(\text{CH}_3) - \text{COOH}$ end units (g/mol)

C_{k2} : molar mass of $-\text{CH}(\text{CH}_3) - \text{COH}$ end units (g/mol)

The value attributed to particular end units has been shown in Figure 22.

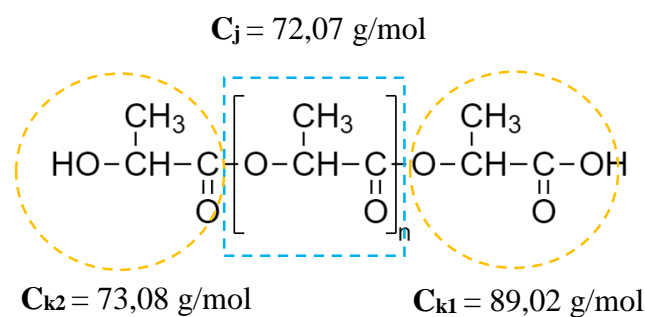


Figure 22. Molar mass of particular groups in PLA used for calculating \bar{M}_n ¹⁸⁵.

Results indicate that \bar{M}_n of PLA decreases about 75% after 16 h of UV exposure and about 92% after 30 days of degradation phosphate-citric buffer solution. This phenomenon is related to the formation of lactic acid monomers and oligomers during degradation^{94,185}. The tendency of \bar{M}_n to decrease is in accordance with the results obtained by means of GPC, that showed that upon exposure to UV radiation the polylactide undergoes chain scission and transforms into low molecular weight species.

Musiol et al.¹²⁰ used ¹H NMR to calculate the composition changes in PLA/poly(butylene adipate-*co*-terephthalate) (PLA/PBAT) and polylactide (PLA) with synthetic poly[(R,S)-3-hydroxybutyrate (PLA/(R,S)-PHB) after 21 days incubation in distilled water at 70°C. NMR analysis confirmed that the lactic acid, hydroxybutyric dimer acid, and oligomers (OHB) were formed during the hydrolytic degradation of the 85PLA/15(R,S) PHB sample studied¹²⁰. The quantitative estimation of mixture content after 70 days of degradation as measured integrals corresponding to methyl groups indicates 48 mol% lactic acid and 14 mol% of 3-hydroxybutyric acid. It confirms the mass decrease in the other techniques due to lactic acid and its dimer in the degradation medium that caused the autocatalytic effect that occurs during hydrolysis of the PLA

component^{120,121}. Similarly, for the PLA/PBAT sample, it observed the decrease of PLA content (mol%) indicates that the hydrolytic degradation occurs by random cleavage of the ester groups along the polyester chain¹²¹.

Furthermore, Zhang et al.²¹⁷ used ¹³C NMR technique to investigate phase structures of polymers and obtained information about their crystallinity. The chemical shift of ¹³C spectra was determined by taking the carbonyl carbon of solid glycine (176.03 ppm) as an external reference standard. Figure 23 (a) shown the three carbon resonances of PLA, corresponding to the C=O (170.8 ppm), the (–CH) carbon (70.5 ppm), and the (–CH₃) group (18.1 ppm). After degradation, when the crystallinity of PLA increased, the crystalline component with high regularity in the environment led to a narrower line width²¹⁷. For PLA degraded over 19 days, a shoulder appeared for the C=O resonance at 172 ppm when the line width became narrower (Figure 23(b)), while the other two resonances remained as single peaks. According to the literature, five peaks were obtained for the C=O resonances of PLA with high crystallinity, representing five crystallographically sites in the α -form homo-crystal structures²¹⁵. Most likely, the crystalline structures formed during degradation displayed a relatively low regularity. Thus, only a shoulder at 172 ppm was detected (Figure 23(b)), corresponding to the two peaks 172.3 ppm and 171.8 ppm in Ref.²¹⁹. Also, the methine and methyl carbons of PLA residues showed as a single peak as reported in the highly crystalline PLA. These results indicated the crystalline structures formed for PLA after degradation, which was confirmed by DSC and XRD.

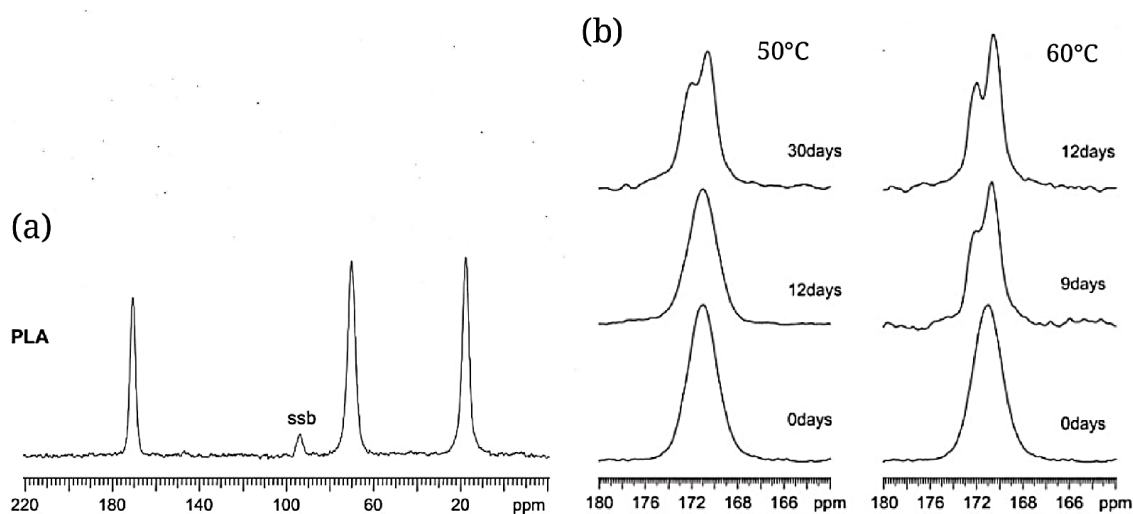


Figure 23. (a) ¹³C NMR spectra of PLA before degradation and (b) ¹³C NMR spectra of the C=O peaks of PLA after degradation at 50 °C and 60 °C under neutral pH condition²¹⁷.

3.6. Scanning electron microscopy (SEM)

The morphology of the samples is observed using SEM. Studying the microstructures and morphologies of samples is crucial to understanding the subsequent photolytic and hydrolytic degradation behaviors¹²³. In general, morphological changes are observed using a scanning electron microscope with an acceleration voltage of 15 kV. Samples are firstly immersed into liquid nitrogen, and then they are cryogenically fractured¹⁶³.

Analyzing the work of Wang et al.⁵⁶, the morphologies of Poly(lactic acid)/Poly(butylene succinate) (PLA/PBS) blends before degradation (Figure 24(a)) exhibit the typical sea-island structures and it observes clear interfaces between PLA matrix and dispersed PBS particles⁵⁶. As shown in Figure 24 (b), some dispersed PBS particles are completely exposed to the sample surface after degradation. Besides that, the gaps between PBS particles and the PLA matrix become more apparent than those observed in the samples before hydrolytic degradation. This indicates that the hydrolytic degradation of PLA matrix occurs firstly in the interface regions between the two components. Moreover, in Figure 24 (c) and (d), one can see that the hydrolytic degradation of PLA/PBS blends mainly occurs on the surface of the sample, and with increasing hydrolytic degradation time, the inner part of the sample begins⁵⁶.

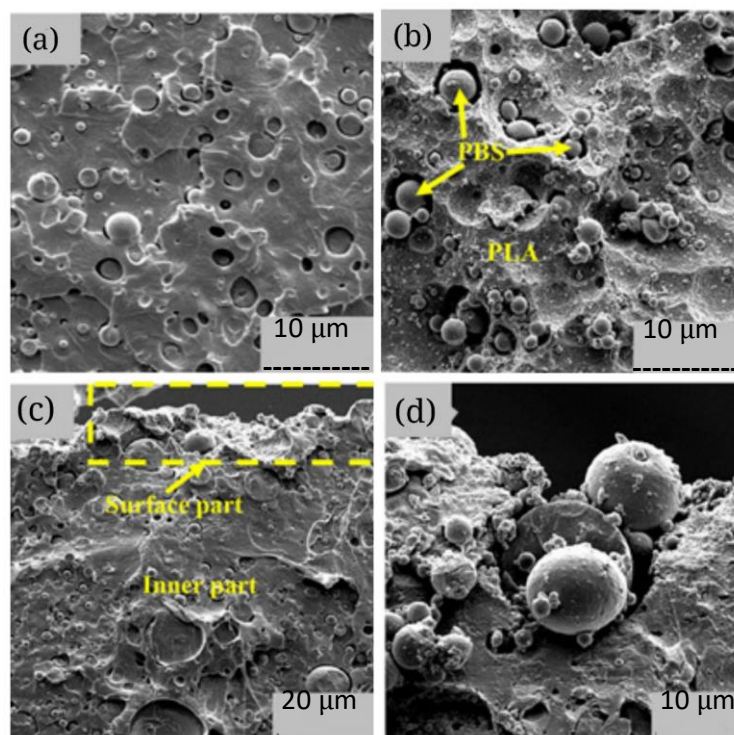


Figure 24. SEM of PLA/PBS with 30 wt% of PBS. (a) before degradation, (b) after being degraded at 37 °C for 312 h. Cross-section direction of sample degraded at low (c) and high magnifications (d)⁵⁶.

To well understand the hydrolytic degradation behavior of PLA/PBS blends, Figure 25 is shown an illustration. For pure PLA, the hydrolytic degradation proceeds mainly via a surface-erosion mechanism⁸⁸, and the sample size and shape gradually change with increasing hydrolytic degradation time. For PLA/PBS blends, the hydrolytic degradation is similar to that of pure PLA; that is to say, the blends still obey the surface-erosion mechanism. However, once the sample surface is degraded, PBS particles are exposed, and water has more chance to penetrate the gaps between PBS particles and PLA matrix, and consequently, the hydrolytic degradation of PLA matrix is greatly accelerated⁵⁶.

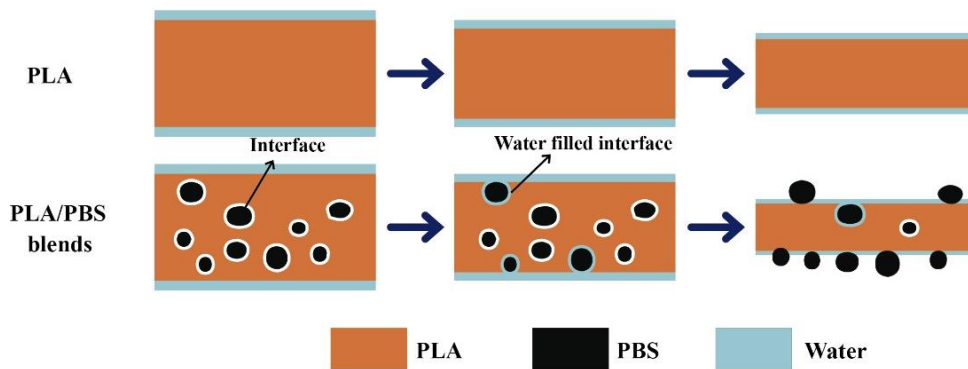


Figure 25. Schematic representations of the hydrolytic degradation process of pure PLA and PLA/PBS blends⁵⁶.

To observe the degradation mechanism of PLA fibers as a function of the hydrolysis time, Pacheco et al.⁵⁰ analyzed by SEM the surface of PLA fibers. As seen in Figure 26 (a), the fiber fragments showed a homogeneous cylindrical shape and with a smooth appearance before the degradation process. Figure 26 (b)–(d) shows that after a few weeks of being immersed in the hydrolysis medium, the surface presents changes in roughness. For the acidic and neutral pH, this change was not significant. However, in Figure 26 (d), for the alkaline pH solution, it seemed that a more significant degradative process on the PLA. The formation of microcracks in the fiber is observed, providing evidence of the hydrolytic degradation process. Subsequently, from these cracks, the fragmentation of the filaments occurred. These cracks were randomly distributed on the surface, propagate circumferentially around the fibers. The hydrolytic attack started on the surface and went through the interior of the fiber. Thus, the presence of hydroxyl species (-OH) could induce a more significant chemical attack on the electrophilic groups present in the chains of the polymer PLA⁵⁰. This attack results in a weight loss, decreasing the molecular weight with a mechanical strength loss, corroborated in the techniques mentioned above.

The same tendency was observed by other authors, where PLA present evidence of surface erosion ^{51,55,60,74,124,141,145,168,172,220}. Valapa et al. ⁷⁴ used SEM analysis to analyze PLA and PLA-SP nanocomposite morphology under degradation at higher degradation temperature (55 °C). Surface erosion and the number of cavities in the amorphous domains increased due to the faster degradation phenomenon⁷⁴. In this regard, SEM and XRD results indicate that the loss of amorphous regions occurs during the hydrolytic degradation process for PLA composites while the crystalline regions are retained ⁷⁴. Nevertheless, the least noticeable changes in the surface morphology have been observed for the samples stored in lake water¹²³.

In another study, Girdthep et al. ⁷⁰ analyzed the composite morphology (PLA/PBAT/AgKT). After being aged for one year in ambient condition and relative humidity, the surface did not show any noticeable difference in morphology. This observation supports the result of DSC analysis, where a discussion that a more ordered (crystalline) structure is due to induced crystallization by the silver-loaded kaolinite (AgKT) ⁷⁰.

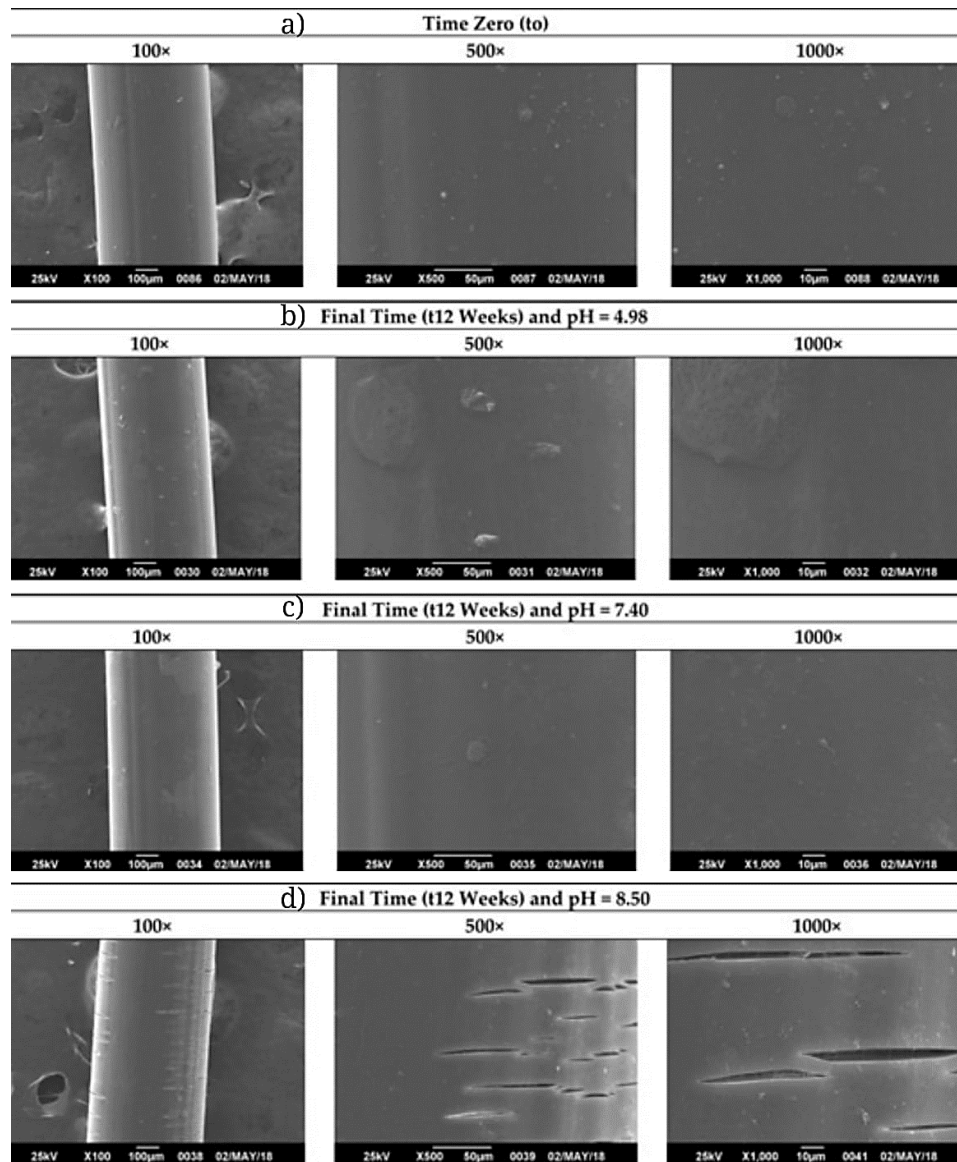


Figure 26. SEM micrographs of PLA fiber surface morphology. (a) non- degraded PLA fibers, (b) degraded fiber for 12 weeks at pH = 4.98 and $T = 25\text{ }^{\circ}\text{C}$, (c) degraded fiber for 12 weeks at pH = 7.40 and $T = 25\text{ }^{\circ}\text{C}$ and (d) degraded fiber for 12 weeks at pH = 8.50 and $T = 25\text{ }^{\circ}\text{C}$ ⁵⁰.

3.7. Mechanical test

The mechanical response of PLA is highly non-linear due to a strong dependence on temperature, molecular weight, molecular orientation, and crystallinity²²¹. Due to biodegradable applications, numerous studies dealing with hydrolytic and photo-oxidative aging are available. Ideally, composite materials and their structures that are intended for long-term use should be tested in real-time and with realistic in-service environments²³. It intends to determine the durability of PLA in terms of mechanical properties. It is critically important to understand these behaviors and how they influence the material response to design them correctly. The mechanical properties of lactic acid-based polymers can be varied to a large extent ranging from soft and elastic plastics to

stiff and high strength materials ²³. The mechanical properties of PLA that are the most intensively studied include tensile properties: tensile strength (σ), tensile modulus (E), ultimate strain (ϵ), and elongation at break (%). Data of mechanical properties of different stereochemical forms of PLA reported in the literature are summarized in Table 7 ²³.

First, we need to explain some of the physical concepts behind the mechanical properties. The main one is stress. Stress indicates how big is a force applies to an area and is primarily expressed in MPa's. The formula for stress is ²²²:

$$\sigma = \frac{F}{A} \quad (10)$$

; where F is force (N) and A is area (mm^2).

The second important concept is strain. The strain has no unit as it is a ratio of the initial and final lengths. It is calculated as follows ²²²:

$$\epsilon = \frac{l - l_0}{l_0} \quad (11)$$

; where l_0 is starting or initial length (mm) and l is stretched length (mm).

Below the proportionality limit of the stress-strain curve (Figure 27), the relationship between stress and strain is linear. The slope of this linear portion of the stress-strain curve is Young's modulus. The bigger its value, the stiffer the material; in the same way, the lesser value means that the material is more elastic ²²³.

The formula for Young's modulus ²²²:

$$E = \frac{\sigma}{\epsilon} \quad (12)$$

As shown from the stress-strain curve (Figure 27), yield strength is the value in MPa it can take before plastic deformation. This place is called the yield point. Before it, a material regains its former shape when lifting the load. After exceeding the yield point, the deformation is permanent. Tensile strength is the next step from yield strength. Also measured in MPa, this value indicates the maximum stress a material can withstand before fracturing. Moreover, toughness is related to the area under the stress-strain curve and is the amount of energy per unit volume that a material can absorb before rupturing. Finally, elongation at break (%), also known as fracture strain, is the ratio between changed length and initial length after breakage of the test specimen ²²³.

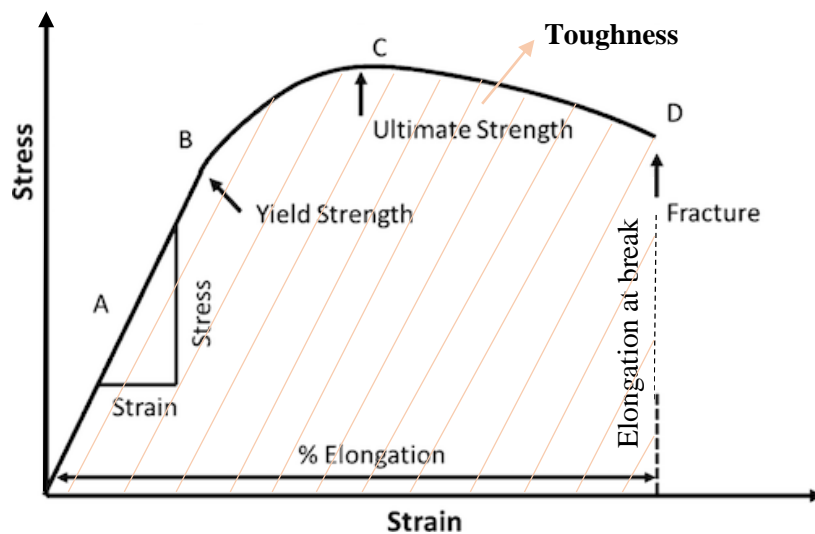


Figure 27. Stress-strain curve.

Additionally, a flexural strength of a material is defined as its ability to resist deformation under load. A rectangular cross-section of the desired testing specimen is rested in two supports, and a force is applied by a loading nose midway between the supports. The flexural strength would be the same as the tensile strength if the material were uniform. In figure 28, is shown a schematic illustration of the flexural strength test of a material ²²⁴.

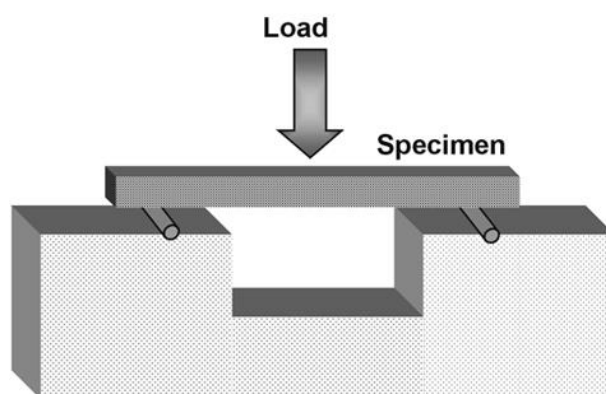


Figure 28. Schematic illustration of flexural strength test of a material ²²⁴.

Mechanical properties of the samples were evaluated before and after degradation and several authors using a universal testing machine. In López et al.⁹⁷ the load cell used had a maximum capacity of 100 N and the test speed was 5mm/min. All tests were carried out at room temperature. Elastic modulus (E) was thus calculated as the initial slope of stress-

strain curves; tensile strength (σ) and the elongation at break (ϵ) were evaluated as the maximum values of stress and strain for each curve ²²⁵.

Table 9. Mechanical properties of different stereochemical forms of PLA^{23,226}

Properties	Units	Amorphous PLA	PLLA	PLDA
Tensile strength	MPa	59	66	44
Elongation at break	%	7	4	5.4
Modulus of elasticity	MPa	3750	4150	3900
Yield strength	MPa	70	70	53
Flexural strength	MPa	106	119	88
Unnotched izod impact	J/m	195	350	150
Notched izod impact	J/m	26	66	18
Heat deflection temperature	°C	55	61	50
Vicat penetration	°C	59	165	52

The aging behavior of PLA and jute/PLA composites in a hydrothermal environment was studied by Jiang et al ⁶⁹. Figure 29 (a) shows the tensile strengths and Young's modulus of PLA and jute/PLA composites immersed in deionized water at 50°C ⁶⁹. After adding jute fibers, a gradual decline in the mechanical properties was observed because the decrease in T_g , observed in the DSC test, implies an increase in molecular mobility, which would also influence the reduction of the elastic modulus⁹⁷. The tensile strength of pure PLA and jute/PLA composites was reduced with the increase of aging time. However, the tensile strength of PLA showed a slight increase after 7 days of aging. This increase is because the water acted as an effective plasticizer, which increased the aggregation of PLA chains and promoted nucleation and crystallization of the PLA molecules ²²⁷. Jute/PLA composites had a slower decline in mechanical properties than PLA; due to the mobility of PLA molecular chains, they were hindered by addition of jute fibers, thus showing slower hydrolysis. Moreover, the gradual decline in the mechanical properties was due to the water absorption capacity of jute fibers. After absorbing water, swelling of jute fibers was caused, which led to residual stresses in jute/PLA composites. The stresses would result in micro-cracking in the fiber-matrix interface ²²⁸, which resulted in a decline in tensile strength⁶⁹.

The change in Young's modulus is shown in Figure 29 (b). The Young's modulus of unaged jute/PLA composites is higher than those of PLA due to the high modulus of jute fibers. There was no significant change in Young's modulus of pure PLA. However, the decrease in the jute/PLA modulus can be attributed to the plasticizing effect of water molecules. As the degradation advance, the formation of lactic acid molecules occurs, which embrittled the jute/PLA composites. Also, the appearance of voids and cracking induced with aging time led to a decrease of Young's modulus of jute/PLA composites⁶⁹.

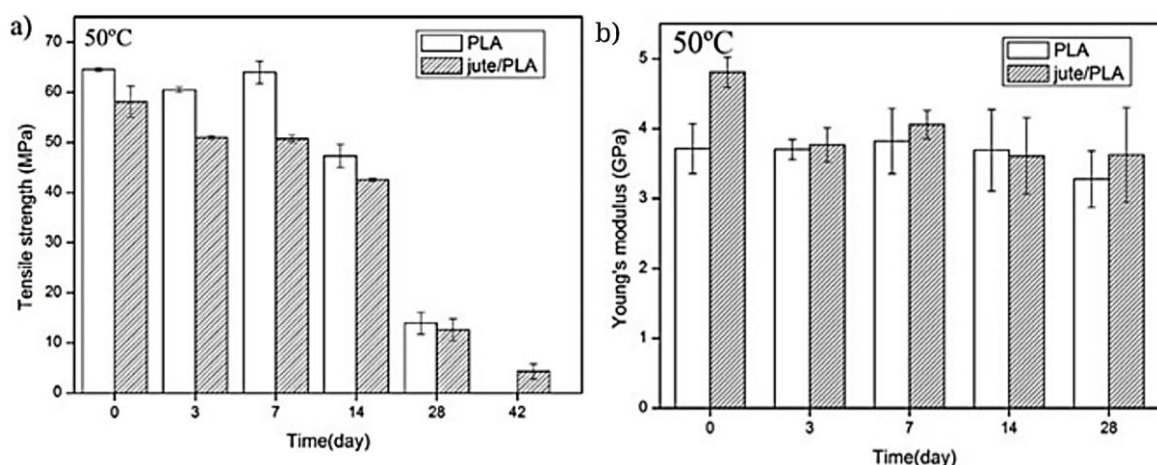


Figure 29. Effect of hydrolysis time on mechanical properties of PLA and jute/PLA composites, a) tensile strength and b) Young's modulus at 50 °C⁶⁹.

To analyzing other studies, the results of Felfel et al.¹⁶⁸ showed that the mechanical properties for PLA reinforced with phosphate glass fibre (PGF) decreased dramatically after 56 days of degradation in PBS at 50 °C. First, the high temperature (above T_g) assists the active molecular motion, facilitating water diffusivity into PLA matrix and the fiber-matrix interfacial¹⁶⁸, and second, the mechanical properties decreased after immersion in PBS as a result of the plasticization effect of water within the composite, which demonstrated the faster degradation of the fiber/matrix interfaces^{168,229}.

In the work of Varsavas et al.¹⁰⁸ the reduction in mechanical values of the PLA reinforced with glass fiber (PLA/GF) was less compared to neat PLA. Due to the very effective stiffening, it was strengthening, toughening actions of the GF. also due to the “barrier” actions of the glass fibers decreasing the very detrimental effects of the photolysis and hydrolysis reactions on the PLA matrix¹⁰⁸. In the same way, Lopéz et al.⁹⁷ analyzed the mechanical properties of PLA/TPS blends subjected to photodegradation the rupture and yield stress for PLA/TPS blends; slight changes were observed in the exposure times

evaluated. In this case, it was concluded that during degradation occurs to modify the lamellar thicknesses. This modification leads to a reduction in mechanical properties due to the decrease in interconnecting chains²³⁰. On the other hand, the decrease in elongation at break occurred drastically for neat PLA and blends with lower TPS content. In the case of neat PLA, this can be considered the effect of a rapid decrease in its molecular weight due to UV irradiation and to random mechanisms of chain cleavage²³¹. Blends with high TPS content showed higher resistance to photodegradation, possibly due to the great content of glycerol increasing its protective effect^{97,230}.

Following the same trend, Kaynak et al.¹⁶¹ reported that Young's modulus and flexural modulus values of PLA increase with the incorporation of talc particles. Fracture toughness values of brittle PLA are both improved, using 5wt% talc¹⁶¹. These improvements can be attributed to the toughening mechanisms of "crack deflection": increased pathway of cracks due to talc particles and energy absorption of the propagating cracks during the test¹⁶¹. Nevertheless, because of accelerated weathering, it observed a severe chemical degradation and molecular weight reduction of the matrix, resulting in drastic reductions in the strength and fracture toughness values¹⁶¹. The only mechanical property not deteriorated during the weathering period was flexural modulus due to the increased amount of crystallinity in the PLA matrix during weathering¹⁶¹.

Another study by Kaynak et al.¹⁹ shows that the incorporation of halloysites nanotubes (HNTs) into PLA matrix increased all mechanical properties. Increases in modulus were due to the stiffening effect of rigid HNTs, while increases in strength were due to the efficient load transfer mechanism from the matrix to HNTs, and the decrease of the mobility of PLA chains by the nanotubular structure of HNTs. After weathering, severe actions of photolysis and hydrolysis resulted in drastic reductions in the strength and fracture toughness values of the specimens. However, this reduction was slightly less than neat PLA¹⁹. It should be emphasized that the reduction in mechanical properties is lower in comparison with neat PLA. Other authors report an increase in mechanical properties due to the addition of nucleating agents, plasticizer^{23,70,118,134,172,180,232,233}, with a gradual reduction after degradation compared with neat PLA.

However, in the case of PLA/TiO₂ samples, Antunes et al.¹⁰⁷ proved the lower stability of the PLA/TiO₂ in comparison neat PLA over the accelerated weathering time (2000 h). Although the addition of TiO₂ nanoparticles improved stiffness and Young's modulus

compared to the PLA, the extent of degradation was more significant for the PLA/TiO₂ sample. Young's modulus decreased drastically in comparison as neat PLA, showing that the addition of TiO₂ accelerated the degradation process of the samples in the surface area¹⁰⁷.

Additionally, Rasselet et al.²³⁴ shows the changes in the strain at break for PLA films exposed to oxidation at 100, 130, and 150 °C as a function of number average molar mass (\bar{M}_n)²³⁴ (Figure 30). It has been proposed that the average molar mass reduction affects the failure properties of polymers directly. Here, the elongation at break decreases sharply when \bar{M}_n decreases²³⁴.

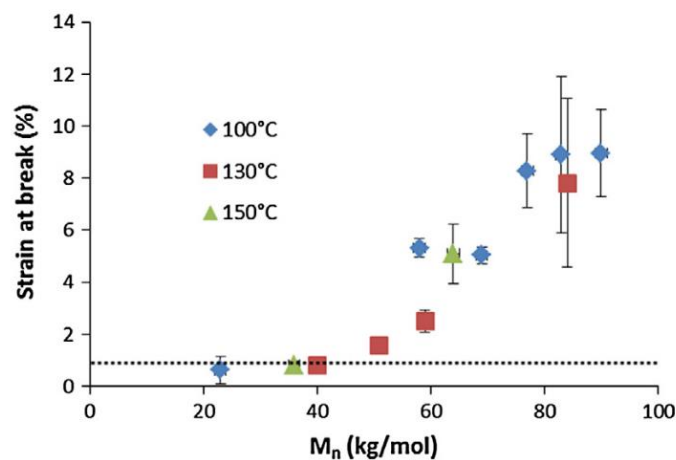


Figure 30. Strain at break of PLA as a function of number average molar mass (\bar{M}_n) during exposure at 100, 130 and 150 °C under air²³⁴.

In order to determine the most sensitive technique, each characterization technique and the changes in its physical and chemical properties at short degradation times were analyzed. According to Chen et al.,²³⁵ changes in mechanical properties of PLA/PBAT blends exposed to high humidity and temperature can be appreciated since the first day of degradation. As shown in Figure 31, degradation drastically decreases the tensile strain of the blends in early stages of degradation²³⁵. The same trend is reported by Varsavas et al.¹⁰⁸ alterations in the tensile stress-strain curves of the specimens after accelerated weathering period are reported since the second day of degradation. However, according to Muller et al.²³⁶, during the first days of degradation, a small amount of chain scission occurs; it can be corroborated by decreasing mechanical properties. These structural changes occur before being detected in DSC and other techniques. So, DSC provides data on the degradation of a polymer in later stages, when there are evident changes in the crystalline structure of the sample²³⁶. In the work of Rocca et al.⁵⁸, changes in T_g , T_m , are

observed for much longer stages, while Beltrán et al.¹⁶⁶ observed no significant changes in melting enthalpy and crystallinity in PLA-based samples that were underwater conditions during the experiment¹⁶⁶. Likewise, the study of Li et al.²³² reported the mass loss and tensile strength as a function of degradation time for Polyoxymethylene/ Poly(l-lactic acid) (POM/PLLA). The PLA/POM fibers show a significant loss in tensile strength after soaked in the alkali medium for 12 h, whereas the mass is maintained unchanged for the fiber samples. With the extension of soaking time, the mass tends to decrease rapidly. This observation suggests that the beginning of the PLA hydrolysis only damaged the structure of filaments and therefore deteriorates the tensile performance, while the mass loss is observed in longer degradation stages²³².

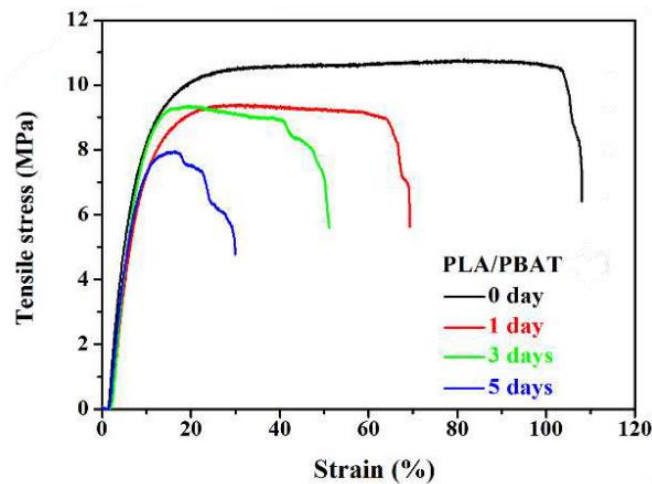


Figure 31. Tensile stress curves of the PLA/PBAT with different degradation days ²³⁵.

Finally, it is concluded that mechanical tests after degradation provide relevant information in the earliest stages of degradation. The first step of degradation is observed on the surface of the samples, so we can be estimated by measuring the degradation of mechanical strength. Principally, the authors reported a loss in tensile tests, being the breaking point the most sensitive in degradation studies.

4. CONCLUSIONS

A complete degradation review study of Polylactide (PLA) under different abiotic environments has been carried out. Principally, samples of PLA that have been subjected to hydrolytic and photolytic degradation to understand the degradation mechanism. The changes in the many properties of the specimens were characterized by combining the use of several analytical techniques. For instance, the degradation leads to a decrease in the molecular weight which is reflected in Gel Permeation Chromatography and Nuclear Magnetic Resonance.

The thermal transitions were studied in detail by DSC. The glass transition, the crystallization, and melting processes of the different degraded samples yielded valuable information regarding the different degradation processes. The results reported by several authors show an increase in the melting and cold crystallization enthalpy of PLA, while T_{cc} , T_g , and T_m decreasing as the degradation proceeds. Moreover, DSC monitors the evolution of the crystallinity. Changes in DSC are observed only when the degradation advances to the point of modifying the crystalline region. Likewise, XRD and ^{13}C NMR is used to confirm that the degradation process affected the crystalline regions of the studied polymer. Showing the importance of the crystalline phase formed as an indicator of the degradation degree and as a distinctive characteristic for each degradation process.

On the other hand, TGA is used to study the thermal stability and the fraction of volatile components in a sample by monitoring the change in mass as it is heated. In general, the profile of all the temperatures follows a decreasing pattern with molar mass regardless of the degradation process. This gradual decrease in thermal stability implies the reduction of structural stability and breaking of bonds in PLA during degradation.

Additionally, FTIR is capable of identifying and following the loss or growth of particular functional groups quantitatively. This technique has successfully followed the alterations in carbonyl groups are the main indicators of degradation in PLA samples. The scission of polymer chains is observed in the ester group ($-\text{C}=\text{O}$) at 1760 cm^{-1} that breaks it down to an acid ($-\text{COOH}$), and alcohol ($-\text{OH}$) terminated residue, appearing broadband at $3400\text{--}3700\text{ cm}^{-1}$ approximately. Apart from new peak formations, chain scissions also lead to shifting of the IR peaks of the typical PLA bands to lower wavenumbers. It leads to decreased molecular weight due to chain scission in the ester backbone structure of PLA.

Moreover; photo-degradation leads to the C=C double bond formation and hydroperoxide (O-H) at the new PLA chain terminals.

During the degradation process, changes in the morphology of samples are observed through SEM. The hydrolytic degradation proceeds mainly via a surface-erosion mechanism, and the sample size and shape gradually change with increasing hydrolytic degradation time.

Finally, a gradual decline in the mechanical properties was observed. Principally, tensile tests were drastically reduced in most studies, while there was no significant change in Young's modulus. Also, it has been reported that the average molar mass reduction directly affects the failure properties of polymers. Significantly the breaking point decrease, chain scission occurs in the amorphous areas reduce the amount of interconnecting chains which can be detected in the early stages of degradation. Thus, mechanical tests were shown to be the most sensitive technique applied since they evidenced early structural changes during degradation.

Future Research

This review study of PLA can be applied to compare the degradation of several polymers. Furthermore, the protocol could be complemented by implementing alternative techniques such as chromatography, ESI-MS, WAXD, DMA, UV-VIS, and a new method is needed to explore more in-depth information. For instance, Positron annihilation lifetime spectroscopy (PALS) has attracted much attention due to the applications in the microstructure of polymers and polymeric blends. PALS method might be an excellent technique to give some deeper information about microstructure change during the degradation process. PALS is used to know how inside free volume holes change during the degradation process, and to further investigate the inside changing during degradation²³⁵.

Moreover, other possible strategies to continue and broaden this research line can be focused on studying sensitive techniques that provide relevant information in the earliest stages of degradation. For example, the Successive Self-nucleation and Annealing (SSA) technique designed by Muller et al.²³⁶ provides evidence of structural changes in polymers during the early stages of degradation. The SSA results also showed differences in X_c , which indicates that a small amount of chain scission did occur after only 3 days of

aging while GPC and FTIR and tensile tests (i.e., strain at break) were not sensitive enough to detect it ²³⁶.

5. REFERENCES

1. Karamanlioglu, M. & Robson, G. D. The influence of biotic and abiotic factors on the rate of degradation of poly(lactic) acid (PLA) coupons buried in compost and soil. *Polym. Degrad. Stab.* **98**, 2063–2071 (2013). <https://doi.org/10.1016/j.polymdegradstab.2013.07.004>
2. Rodrigues, C. A., Tofanello, A., Nantes, I. L. & Rosa, D. S. Biological Oxidative Mechanisms for Degradation of Poly(lactic acid) Blended with Thermoplastic Starch. *ACS Sustain. Chem. Eng.* **3**, 2756–2766 (2015). <https://doi.org/10.1021/acssuschemeng.5b00639>
3. Ozdemir, E., Lekesiz, T. O. & Hacaloglu, J. Polylactide/organically modified montmorillonite composites; effects of organic modifier on thermal characteristics. *Polym. Degrad. Stab.* **134**, 87–96 (2016). <https://doi.org/10.1016/j.polymdegradstab.2016.09.028>
4. Satti, S. M. & Shah, A. A. Polyester-based biodegradable plastics: an approach towards sustainable development. *Lett. Appl. Microbiol.* **70**, 413–430 (2020). <https://doi.org/10.1111/lam.13287>
5. Qi, X., Ren, Y. & Wang, X. New advances in the biodegradation of Poly(lactic) acid. *Int. Biodeterior. Biodegrad.* **117**, 215–223 (2017). <https://doi.org/10.1016/j.ibiod.2017.01.010>
6. Iñiguez-Franco, F. *et al.* Concurrent solvent induced crystallization and hydrolytic degradation of PLA by water-ethanol solutions. *Polymer.* **99**, 315–323 (2016). <https://doi.org/10.1016/j.polymer.2016.07.018>
7. Beltrán, F. R. *et al.* Water-induced structural changes in poly(lactic acid) and PLLA-clay nanocomposites. *Polymer.* **107**, 211–222 (2016). <https://doi.org/10.1016/j.polymer.2016.11.031>
8. Elsayy, M. A., Kim, K. H., Park, J. W. & Deep, A. Hydrolytic degradation of polylactic acid (PLA) and its composites. *Renew. Sustain. Energy Rev.* **79**, 1346–1352 (2017). <https://doi.org/10.1016/j.rser.2017.05.143>
9. Alex, A., Ilango, N. K. & Ghosh, P. Comparative Role of Chain Scission and Solvation in the Biodegradation of Polylactic Acid (PLA). *J. Phys. Chem. B* **122**, 9516–9526 (2018). <https://doi.org/10.1021/acs.jpcc.8b07930>
10. Murariu, M. & Dubois, P. PLA composites: From production to properties. *Adv. Drug Deliv. Rev.* **107**, 17–46 (2016). <https://doi.org/10.1016/j.addr.2016.04.003>
11. Ishikawa, D. *et al.* High-speed monitoring of the crystallinity change in poly(lactic acid) during photodegradation by using a newly developed wide area NIR imaging system (Compovision). *Anal. Bioanal. Chem.* **407**, 397–403 (2015). <https://doi.org/10.1007/s00216-014-8211-z>
12. Xiao, L., Wang, B., Yang, G. & Gauthier, M. Poly(Lactic Acid)-Based Biomaterials: Synthesis, Modification and Applications. *Biomed. Sci. Eng. Technol.* (2012) <https://doi.org/10.5772/23927>.
13. Cosate de Andrade, M. F., Souza, P. M. S., Cavalett, O. & Morales, A. R. Life Cycle Assessment of Poly(Lactic Acid) (PLA): Comparison Between Chemical

- Recycling, Mechanical Recycling and Composting. *J. Polym. Environ.* **24**, 372–384 (2016). <https://doi.org/10.1007/s10924-016-0787-2>
14. Larrañaga, A. & Lizundia, E. A review on the thermomechanical properties and biodegradation behaviour of polyesters. *Eur. Polym. J.* **121**, 109296 (2019). <https://doi.org/10.1016/j.eurpolymj.2019.109296>
 15. Morão, A. & de Bie, F. Life Cycle Impact Assessment of Polylactic Acid (PLA) Produced from Sugarcane in Thailand. *J. Polym. Environ.* **27**, 2523–2539 (2019). <https://doi.org/10.1007/s10924-019-01525-9>
 16. Van Cong, D., Trang, N. T. T., Giang, N. V., Lam, T. D. & Hoang, T. Effect of TiO₂-Crystal Forms on the Photo-Degradation of EVA/PLA Blend Under Accelerated Weather Testing. *J. Electron. Mater.* **45**, 2536–2546 (2016). <https://doi.org/10.1007/s11664-016-4409-5>
 17. Karamanlioglu, M., Preziosi, R. & Robson, G. D. Abiotic and biotic environmental degradation of the bioplastic polymer poly(lactic acid): A review. *Polym. Degrad. Stab.* **137**, 122–130 (2017). <https://doi.org/10.1016/j.polymdegradstab.2017.01.009>
 18. Siakeng, R., Jawaid, M., Asim, M. & Siengchin, S. Accelerated weathering and soil burial effect on biodegradability, colour and texture of coir/pineapple leaf fibres/PLA biocomposites. *Polymers.* **12**, (2020). <https://doi.org/10.3390/polym12020458>
 19. Kaynak, C. & Kaygusuz, I. Consequences of accelerated weathering in polylactide nanocomposites reinforced with halloysite nanotubes. *J. Compos. Mater.* **50**, 365–375 (2016). <https://doi.org/10.1177/0021998315575038>
 20. Garlotta, D. A literature review of poly(lactic acid). *J. Polym. Environ.* **9**, 63–84 (2001). <https://doi.org/10.1023/A:1020200822435>
 21. Zaaba, N. F. & Jaafar, M. A review on degradation mechanisms of polylactic acid: Hydrolytic, photodegradative, microbial, and enzymatic degradation. *Polym. Eng. Sci.* **60**, 2061–2075 (2020). <https://doi.org/10.1002/pen.25511>
 22. Sharif, A., Mondal, S. & Hoque, M. E. Polylactic acid (PLA)-based nanocomposites: Processing and properties. *Bio-based Polym. Nanocomposites Prep. Process. Prop. Perform.* 233–254 (2019) https://doi.org/10.1007/978-3-030-05825-8_11
 23. Farah, S., Anderson, D. G. & Langer, R. Physical and mechanical properties of PLA, and their functions in widespread applications — A comprehensive review. *Adv. Drug Deliv. Rev.* **107**, 367–392 (2016). <https://doi.org/10.1016/j.addr.2016.06.012>
 24. Avérous, L. Polylactic acid: Synthesis, properties and applications. *Monomers, Polym. Compos. from Renew. Resour.* 433–450 (2008) <https://doi.org/10.1016/B978-0-08-045316-3.00021-1>.
 25. Henton, D. E., Gruber, P., Lunt, J. & Randall, J. Natural Fibers, Biopolymers, and Biocomposites. 16. Polylactic acid technology. *Nat. Fibers, Biopolym. Biocomposites* 527–578 (2005).
 26. Singhvi, M. S., Zinjarde, S. S. & Gokhale, D. V. Polylactic acid: synthesis and

- biomedical applications. *J. Appl. Microbiol.* **127**, 1612–1626 (2019). <https://doi.org/10.1111/jam.14290>
27. Davachi, S. M. & Kaffashi, B. Polylactic Acid in Medicine. *Polym. - Plast. Technol. Eng.* **54**, 944–967 (2015). <https://doi.org/10.1080/03602559.2014.979507>
28. Anders Södergard, M. S. Poly (Lactic Acid). *Bio-Based Plast. Mater. Appl.* 27–41 (2010). <https://doi.org/10.1002/0471440264.pst275>
29. Gan, I. & Chow, W. S. Antimicrobial poly(lactic acid)/cellulose bionanocomposite for food packaging application: A review. *Food Packag. Shelf Life* **17**, 150–161 (2018). <https://doi.org/10.1016/j.fpsl.2018.06.012>
30. Jin, T. & Zhang, H. Biodegradable polylactic acid polymer with nisin for use in antimicrobial food packaging. *J. Food Sci.* **73**, (2008). <https://doi.org/10.1111/j.1750-3841.2008.00681.x>
31. Arrieta, M. P., López, J., Ferrándiz, S. & Peltzer, M. A. Characterization of PLA-limonene blends for food packaging applications. *Polym. Test.* **32**, 760–768 (2013). <https://doi.org/10.1016/j.polymertesting.2013.03.016>
32. Muller, J., González-Martínez, C. & Chiralt, A. Combination Of Poly(lactic) acid and starch for biodegradable food packaging. *Materials.* **10**, 1–22 (2017). <https://doi.org/10.3390/ma10080952>
33. Spiridon, I., Ursu, R. G. & Spiridon, I. A. C. New Polylactic Acid Composites for Packaging Applications: Mechanical Properties, Thermal Behavior, and Antimicrobial Activity. *Int. J. Polym. Anal. Charact.* **20**, 681–692 (2015). <https://doi.org/10.1080/1023666X.2015.1081131>
34. Nazrin, A. *et al.* Nanocellulose Reinforced Thermoplastic Starch (TPS), Polylactic Acid (PLA), and Polybutylene Succinate (PBS) for Food Packaging Applications. *Front. Chem.* **8**, (2020). <https://doi.org/10.3389/fchem.2020.00213>
35. Swaroop, C. & Shukla, M. Nano-magnesium oxide reinforced polylactic acid biofilms for food packaging applications. *Int. J. Biol. Macromol.* **113**, 729–736 (2018). <https://doi.org/10.1016/j.ijbiomac.2018.02.156>
36. Arrieta, M. P., Samper, M. D., Aldas, M. & López, J. On the use of PLA-PHB blends for sustainable food packaging applications. *Materials .* **10**, 1–26 (2017). <https://doi.org/10.3390/ma10091008>
37. Lagarón, J.-M. Polylactic acid (PLA) nanocomposites for food packaging applications. *Multifunct. Nanoreinforced Polym. Food Packag.* 485–497 (2011) <https://doi.org/10.1533/9780857092786.4.485>.
38. Tawakkal, I. S. M. A., Cran, M. J., Miltz, J. & Bigger, S. W. A review of poly(lactic acid)-based materials for antimicrobial packaging. *J. Food Sci.* **79**, (2014). <https://doi.org/10.1111/1750-3841.12534>
39. Tyler, B., Gullotti, D., Mangraviti, A., Utsuki, T. & Brem, H. Polylactic acid (PLA) controlled delivery carriers for biomedical applications. *Adv. Drug Deliv. Rev.* **107**, 163–175 (2016). <https://doi.org/10.1016/j.addr.2016.06.018>
40. Pillai, O. & Panchagnula, R. Polymers in Drug Delivery. *Curr. Opin. Chem. Biol.*

- 5, 447–451 (2001). [https://doi.org/10.1016/S1367-5931\(00\)00227-1](https://doi.org/10.1016/S1367-5931(00)00227-1)
41. Dev, A. *et al.* Preparation of poly(lactic acid)/chitosan nanoparticles for anti-HIV drug delivery applications. *Carbohydr. Polym.* **80**, 833–838 (2010). <https://doi.org/10.1016/j.carbpol.2009.12.040>
 42. Gavasane, A. J. Synthetic Biodegradable Polymers Used in Controlled Drug Delivery System: An Overview. *Clin. Pharmacol. Biopharm.* **3**, (2014). <http://dx.doi.org/10.4172/2167-065X.1000121>
 43. Saini, P., Arora, M. & Kumar, M. N. V. R. Poly(lactic acid) blends in biomedical applications. *Adv. Drug Deliv. Rev.* **107**, 47–59 (2016). <https://doi.org/10.1016/j.addr.2016.06.014>
 44. Liu, S. *et al.* Current applications of poly(lactic acid) composites in tissue engineering and drug delivery. *Compos. Part B Eng.* **199**, 108238 (2020). <https://doi.org/10.1016/j.compositesb.2020.108238>
 45. Calzoni, E. *et al.* Biocompatible polymer nanoparticles for drug delivery applications in cancer and neurodegenerative disorder therapies. *J. Funct. Biomater.* **10**, 1–15 (2019). <https://doi.org/10.3390/jfb10010004>
 46. Savioli Lopes, M., Jardini, A. L. & Maciel Filho, R. Poly (lactic acid) production for tissue engineering applications. *Procedia Eng.* **42**, 1402–1413 (2012). <https://doi.org/10.1016/j.proeng.2012.07.534>
 47. Lasprilla, A. J. R., Martinez, G. A. R., Lunelli, B. H., Jardini, A. L. & Filho, R. M. Poly-lactic acid synthesis for application in biomedical devices - A review. *Biotechnol. Adv.* **30**, 321–328 (2012). <https://doi.org/10.1016/j.biotechadv.2011.06.019>
 48. Santoro, M., Shah, S. R., Walker, J. L. & Mikos, A. G. Poly(lactic acid) nanofibrous scaffolds for tissue engineering. *Adv. Drug Deliv. Rev.* **107**, 206–212 (2016). <https://doi.org/10.1016/j.addr.2016.04.019>
 49. Hamad, K., Kaseem, M., Ayyoob, M., Joo, J. & Deri, F. Polylactic acid blends: The future of green, light and tough. *Prog. Polym. Sci.* **85**, 83–127 (2018). <https://doi.org/10.1016/j.progpolymsci.2018.07.001>
 50. Correa-Pacheco, Z. N. *et al.* Preparation and characterization of bio-based PLA/PBAT and cinnamon essential oil polymer fibers and life-cycle assessment from hydrolytic degradation. *Polymers.* **12**, 1–32 (2020). <https://doi.org/10.3390/polym12010038>
 51. Porfyris, A. *et al.* Accelerated ageing and hydrolytic stabilization of poly(lactic acid) (PLA) under humidity and temperature conditioning. *Polym. Test.* **68**, 315–332 (2018). <https://doi.org/10.1016/j.polymertesting.2018.04.018>
 52. Gai, S., Xu, J., Zhang, H., Yin, R. & Zhang, W. Effects of nanofillers on the hydrolytic degradation of polyesters. *Tissue Eng. - Part B Rev.* **26**, 484–495 (2020). <https://doi.org/10.1089/ten.teb.2019.0260>
 53. Valverde, C., Lligadas, G., Ronda, J. C., Galià, M. & Cádiz, V. Hydrolytic and enzymatic degradation studies of aliphatic 10-undecenoic acid-based polyesters. *Polym. Degrad. Stab.* **155**, 84–94 (2018). <https://doi.org/10.1016/j.polymdegradstab.2018.07.012>

54. Musioł, M. *et al.* (Bio)degradation studies of degradable polymer composites with jute in different environments. *Fibers Polym.* **16**, 1362–1369 (2015). <https://doi.org/10.1007/s12221-015-1362-5>
55. Taiatele, I. *et al.* Abiotic Hydrolysis and Compostability of Blends Based on Cassava Starch and Biodegradable Polymers. *J. Polym. Environ.* **27**, 2577–2587 (2019). <https://doi.org/10.1007/s10924-019-01541-9>
56. Wang, Y. peng *et al.* Accelerated hydrolytic degradation of poly(lactic acid) achieved by adding poly(butylene succinate). *Polym. Bull.* **73**, 1067–1083 (2016). <https://doi.org/10.1007/s00289-015-1535-9>
57. Karimpour-Motlagh, N. *et al.* An experimental and theoretical mechanistic analysis of thermal degradation of polypropylene/polylactic acid/clay nanocomposites. *Polym. Adv. Technol.* **30**, 2695–2706 (2019). <https://doi.org/10.1002/pat.4699>
58. Rocca-Smith, J. R. *et al.* Beyond Biodegradability of Poly(lactic acid): Physical and Chemical Stability in Humid Environments. *ACS Sustain. Chem. Eng.* **5**, 2751–2762 (2017). <https://doi.org/10.1021/acssuschemeng.6b03088>
59. Kultravut, K., Kuboyama, K. & Ougizawa, T. Annealing effect on tensile property and hydrolytic degradation of biodegradable poly(lactic acid) reactive blend with poly(trimethylene terephthalate) by two-step blending procedure. *Polym. Degrad. Stab.* **179**, 109228 (2020). <https://doi.org/10.1016/j.polymdegradstab.2020.109228>
60. Ren, Y., Hu, J., Yang, M. & Weng, Y. Biodegradation Behavior of Poly (Lactic Acid) (PLA), Poly (Butylene Adipate-Co-Terephthalate) (PBAT), and Their Blends Under Digested Sludge Conditions. *J. Polym. Environ.* **27**, 2784–2792 (2019). <https://doi.org/10.1007/s10924-019-01563-3>
61. Stloukal, P., Jandikova, G., Koutny, M. & Sedlařík, V. Carbodiimide additive to control hydrolytic stability and biodegradability of PLA. *Polym. Test.* **54**, 19–28 (2016). <https://doi.org/10.1016/j.polymertesting.2016.06.007>
62. Xu, H., Yang, X., Xie, L. & Hakkarainen, M. Conformational Footprint in Hydrolysis-Induced Nanofibrillation and Crystallization of Poly(lactic acid). *Biomacromolecules* **17**, 985–995 (2016). <https://doi.org/10.1021/acs.biomac.5b01636>
63. Kucharczyk, P., Pavelková, A., Stloukal, P. & Sedlařík, V. Degradation behaviour of PLA-based polyesterurethanes under abiotic and biotic environments. *Polym. Degrad. Stab.* **129**, 222–230 (2016). <https://doi.org/10.1016/j.polymdegradstab.2016.04.019>
64. Cristina, A. M. *et al.* Degradation of Post-consumer PLA: Hydrolysis of Polymeric Matrix and Oligomers Stabilization in Aqueous Phase. *J. Polym. Environ.* **26**, 4396–4404 (2018). <https://doi.org/10.1007/s10924-018-1312-6>
65. Chamas, A. *et al.* Degradation Rates of Plastics in the Environment. *ACS Sustain. Chem. Eng.* **8**, 3494–3511 (2020). <https://doi.org/10.1021/acssuschemeng.9b06635>
66. Jafari, S. M. A., Khajavi, R., Goodarzi, V., Kalaei, M. R. & Khonakdar, H. A.

- Development of degradable poly(ethylene terephthalate)-based nanocomposites with the aid of polylactic acid and graphenic materials: Thermal, thermo-oxidative and hydrolytic degradation characteristics. *J. Appl. Polym. Sci.* **137**, 1–11 (2020). <https://doi.org/10.1002/app.48466>
67. Iñiguez-Franco, F. *et al.* Effect of nanoparticles on the hydrolytic degradation of PLA-nanocomposites by water-ethanol solutions. *Polym. Degrad. Stab.* **146**, 287–297 (2017). <https://doi.org/10.1016/j.polymdegradstab.2017.11.004>
68. Olewnik-Kruszkowska, E., Kasperska, P. & Koter, I. Effect of poly(ϵ -caprolactone) as plasticizer on the properties of composites based on polylactide during hydrolytic degradation. *React. Funct. Polym.* **103**, 99–107 (2016). <https://doi.org/10.1016/j.reactfunctpolym.2016.03.026>
69. Jiang, N. *et al.* Effect of short jute fibers on the hydrolytic degradation behavior of poly(lactic acid). *Polym. Degrad. Stab.* **178**, (2020). <https://doi.org/10.1016/j.polymdegradstab.2020.109214>
70. Girdthep, Sg., Worajittiphon, P., Leejarkpai, T., Molloy, R. & Punyodom, W. Effect of silver-loaded kaolinite on real ageing, hydrolytic degradation, and biodegradation of composite blown films based on poly(lactic acid) and poly(butylene adipate-co-terephthalate). *Eur. Polym. J.* **82**, 244–259 (2016). <https://doi.org/10.1016/j.eurpolymj.2016.07.020>
71. Zare, Y. & Rhee, K. Y. Following the morphological and thermal properties of PLA/PEO blends containing carbon nanotubes (CNTs) during hydrolytic degradation. *Compos. Part B Eng.* **175**, 107132 (2019). <https://doi.org/10.1016/j.compositesb.2019.107132>
72. Zare, Y. & Rhee, K. Y. Experimental data and modeling of electrical conductivity for polymer carbon nanotubes nanobiosensor during degradation in neutral phosphate-buffered saline (PBS). *Mater. Sci. Eng. B Solid-State Mater. Adv. Technol.* **252**, 114482 (2020). <https://doi.org/10.1016/j.mseb.2019.114482>
73. Gorrasi, G. & Pantani, R. Hydrolysis and Biodegradation of Poly(lactic acid). *Adv. Polym. Sci.* **279**, 119–151 (2018). https://doi.org/10.1007/12_2016_12
74. Valapa, R. babu, Pugazhenthii, G. & Katiyar, V. Hydrolytic degradation behaviour of sucrose palmitate reinforced poly(lactic acid) nanocomposites. *International Journal of Biological Macromolecules* vol. 89 (2016). <https://doi.org/10.1016/j.ijbiomac.2016.04.040>
75. Rowe, M. D., Eyiler, E. & Walters, K. B. Hydrolytic degradation of bio-based polyesters: Effect of pH and time. *Polym. Test.* **52**, 192–199 (2016). <https://doi.org/10.1016/j.polymertesting.2016.04.015>
76. Simmons, H. & Kontopoulou, M. Hydrolytic degradation of branched PLA produced by reactive extrusion. *Polym. Degrad. Stab.* **158**, 228–237 (2018). <https://doi.org/10.1016/j.polymdegradstab.2018.11.006>
77. Woodard, L. N. & Grunlan, M. A. Hydrolytic Degradation of PCL-PLLA Semi-IPNs Exhibiting Rapid, Tunable Degradation. *ACS Biomater. Sci. Eng.* **5**, 498–508 (2019). <https://doi.org/10.1021/acsbomaterials.8b01135>
78. Ma, M. & Zhou, W. Improving the Hydrolysis Resistance of Poly(lactic acid) Fiber

- by Hydrophobic Finishing. *Ind. Eng. Chem. Res.* **54**, 2599–2605 (2015). <https://doi.org/10.1021/ie504814x>
79. Li, H. *et al.* In vitro degradation of self-reinforced poly(lactic acid) with beta-tricalcium phosphate composite prepared by equal channel angular pressing. *Polym. Compos.* **41**, 4054–4063 (2020). <https://doi.org/10.1002/pc.25692>
80. Davachi, S. M., Kaffashi, B., Torabinejad, B. & Zamanian, A. In-vitro investigation and hydrolytic degradation of antibacterial nanocomposites based on PLLA/triclosan/nano-hydroxyapatite. *Polymer.* **83**, 101–110 (2016). <https://doi.org/10.1016/j.polymer.2015.12.015>
81. Wan, L. & Zhang, Y. Jointly modified mechanical properties and accelerated hydrolytic degradation of PLA by interface reinforcement of PLA-WF. *J. Mech. Behav. Biomed. Mater.* **88**, 223–230 (2018). <https://doi.org/10.1016/j.jmbbm.2018.08.016>
82. Kumar, A., Venkatappa Rao, T., Ray Chowdhury, S. & Ramana Reddy, S. V. S. Optimization of mechanical, thermal and hydrolytic degradation properties of Poly (lactic acid)/Poly (ethylene-co-glycidyl methacrylate)/Hexagonal boron nitride blend-composites through electron-beam irradiation. *Nucl. Instruments Methods Phys. Res. Sect. B Beam Interact. with Mater. Atoms* **428**, 38–46 (2018). <https://doi.org/10.1016/j.nimb.2018.05.011>
83. Gil-Castell, O. *et al.* Polylactide-based self-reinforced composites biodegradation: Individual and combined influence of temperature, water and compost. *Polym. Degrad. Stab.* **158**, 40–51 (2018). <https://doi.org/10.1016/j.polymdegradstab.2018.10.017>
84. Scaffaro, R., Lopresti, F. & Botta, L. Preparation, characterization and hydrolytic degradation of PLA/PCL co-mingled nanofibrous mats prepared via dual-jet electrospinning. *Eur. Polym. J.* **96**, 266–277 (2017). <https://doi.org/10.1016/j.eurpolymj.2017.09.016>
85. Shalumon, K. T., Anjana, J., Mony, U., Jayakumar, R. & Chen, J. P. Process study, development and degradation behavior of different size scale electrospun poly(caprolactone) and poly(lactic acid) fibers. *J. Polym. Res.* **25**, (2018). <https://doi.org/10.1007/s10965-018-1475-9>
86. Zare, Y., Rhee, K. Y. & Park, S. J. Simple model for hydrolytic degradation of poly(lactic acid)/poly(ethylene oxide)/carbon nanotubes nanobiosensor in neutral phosphate-buffered saline solution. *J. Biomed. Mater. Res. - Part A* **107**, 2706–2717 (2019). <https://doi.org/10.1002/jbm.a.36774>
87. Li, X. *et al.* Study on the degradation behavior and mechanism of Poly(lactic acid) modification by ferric chloride. *Polymer.* **188**, (2020). <https://doi.org/10.1016/j.polymer.2019.121991>
88. Haider, T. P., Völker, C., Kramm, J., Landfester, K. & Wurm, F. R. Plastics of the Future? The Impact of Biodegradable Polymers on the Environment and on Society. *Angew. Chemie - Int. Ed.* **58**, 50–62 (2019). <https://doi.org/10.1002/anie.201805766>
89. Schedl, L. Why degradable polymers undergo surface erosion or bulk erosion. *Biomaterials* **23**, 4221–4231 (2002). <https://doi.org/10.1016/S0142->

9612(02)00170-9

90. Chen, Q., Liang, S. & Thouas, G. A. Elastomeric biomaterials for tissue engineering. *Prog. Polym. Sci.* **38**, 584–671 (2013). <https://doi.org/10.1016/j.progpolymsci.2012.05.003>
91. Zhang, Z., Kuijjer, R., Bulstra, S. K., Grijpma, D. W. & Feijen, J. The in vivo and in vitro degradation behavior of poly(trimethylene carbonate). *Biomaterials* **27**, 1741–1748 (2006). <https://doi.org/10.1016/j.biomaterials.2005.09.017>
92. Sailema-Palate, G. Patricia, et al. "A comparative study on Poly (ϵ -caprolactone) film degradation at extreme pH values." *Polymer Degradation and Stability*. (2016). <https://doi.org/10.1016/j.polymdegradstab.2016.06.005>
93. Cifuentes, S. C., Lieblich, M., Saldaña, L., González-Carrasco, J. L. & Benavente, R. In vitro degradation of biodegradable polylactic acid/Mg composites: Influence of nature and crystalline degree of the polymeric matrix. *Materialia* **6**, 100270 (2019). <https://doi.org/10.1016/j.mtla.2019.100270>
94. Olewnik-Kruszkowska, E. Influence of the type of buffer solution on thermal and structural properties of polylactide-based composites. *Polym. Degrad. Stab.* **129**, 87–95 (2016). <https://doi.org/10.1016/j.polymdegradstab.2016.04.009>
95. Tsuji, H., Echizen, Y. & Nishimura, Y. Photodegradation of biodegradable polyesters: A comprehensive study on poly(l-lactide) and poly(ϵ -caprolactone). *Polym. Degrad. Stab.* **91**, 1128–1137 (2006). <https://doi.org/10.1016/j.polymdegradstab.2005.07.007>
96. Lu, T., Solis-Ramos, E., Yi, Y. & Kumosa, M. UV degradation model for polymers and polymer matrix composites. *Polym. Degrad. Stab.* **154**, 203–210 (2018). <https://doi.org/10.1016/j.polymdegradstab.2018.06.004>
97. López, C., Medina, K., D'Ambrosio, R. & Michell, R. M. PLLA and cassava thermoplastic starch blends: crystallinity, mechanical properties, and UV degradation. *J. Polym. Res.* **28**, 26 (2021). <https://doi.org/10.1007/s10965-020-02368-y>
98. Spiridon, I., Leluk, K., Resmerita, A. M. & Darie, R. N. Evaluation of PLA-lignin bioplastics properties before and after accelerated weathering. *Compos. Part B Eng.* **69**, 342–349 (2015). <https://doi.org/10.1016/j.compositesb.2014.10.006>
99. Luo, Y., Cao, Y. & Guo, G. Effects of TiO₂ nanoparticles on the photodegradation of poly(lactic acid). *J. Appl. Polym. Sci.* **135**, 1–8 (2018). <https://doi.org/10.1002/app.46509>
100. Sakai, W. & Tsutsumi, N. Photodegradation and Radiation Degradation. *Poly(Lactic Acid) Synth. Struct. Prop. Process. Appl.* 413–421 (2010) <https://doi.org/10.1002/9780470649848.ch24>.
101. Salač, J. *et al.* Photodegradation and biodegradation of poly(lactic) acid containing orotic acid as a nucleation agent. *Materials*. **12**, (2019). <https://doi.org/10.3390/ma12030481>
102. Mucha, M., Bialas, S. & Kaczmarek, H. Effect of nanosilver on the photodegradation of poly(lactic acid). *J. Appl. Polym. Sci.* **131**, 1–8 (2014). <https://doi.org/10.1002/app.40144>

103. Litauszki, K., Kovács, Z., Mészáros, L. & Kmetty, Á. Accelerated photodegradation of poly(lactic acid) with weathering test chamber and laser exposure – A comparative study. *Polym. Test.* **76**, 411–419 (2019). <https://doi.org/10.1016/j.polymertesting.2019.03.038>
104. da Silva, A. P., Pereira, M. de P., Passador, F. R. & Montagna, L. S. PLA/Coffee Grounds Composites: A Study of Photodegradation and Biodegradation in Soil. *Macromol. Symp.* **394**, 1–9 (2020). <https://doi.org/10.1002/masy.202000091>
105. Olewnik-Kruszkowska, E. Effect of UV irradiation on thermal properties of nanocomposites based on polylactide. *J. Therm. Anal. Calorim.* **119**, 219–228 (2015). <https://doi.org/10.1007/s10973-014-4103-x>
106. It, A. Uv Degradation & Stabilization of Polymers & Rubbers. *Handb. UV Degrad. Stab.* 187–321 (2020) <https://doi.org/10.1016/b978-1-927885-57-4.50010-3>
107. Antunes, A., Popelka, A., Aljarod, O., Hassan, M. K. & Luyt, A. S. Effects of rutile-TiO₂ nanoparticles on accelerated weathering degradation of poly(Lactic Acid). *Polymers.* **12**, 21–23 (2020). <https://doi.org/10.3390/polym12051096>
108. Varsavas, S. D. & Kaynak, C. Weathering degradation performance of PLA and its glass fiber reinforced composite. *Mater. Today Commun.* **15**, 344–353 (2018). <https://doi.org/10.1016/j.mtcomm.2017.11.008>
109. Lesaffre, N. *et al.* Recent advances on the ageing of flame retarded PLA: Effect of UV-light and/or relative humidity. *Polym. Degrad. Stab.* **139**, 143–164 (2017). <https://doi.org/10.1016/j.polymdegradstab.2017.04.007>
110. Jandas, P. J., Prabakaran, K., Mohanty, S. & Nayak, S. K. Evaluation of biodegradability of disposable product prepared from poly (lactic acid) under accelerated conditions. *Polym. Degrad. Stab.* **164**, 46–54 (2019). <https://doi.org/10.1016/j.polymdegradstab.2019.04.004>
111. Chávez-Montes, W. M. *et al.* Effect of artificial weathering on PLA/Nanocomposite molecular weight distribution. *Polymers.* **7**, 760–776 (2015). <https://doi.org/10.3390/polym7040760>
112. Nishida, M., Tanaka, T., Tanaka, T. & Hayakawa, Y. Nucleating and plasticization effects in drawn poly(lactic acid) fiber during accelerated weathering degradation. *Polymers.* **10**, (2018). <https://doi.org/10.3390/polym10040365>
113. Islam, M. S., Pickering, K. L. & Foreman, N. J. Influence of Hygrothermal Ageing on the Physico-Mechanical Properties of Alkali Treated Industrial Hemp Fibre Reinforced Polylactic Acid Composites. *J. Polym. Environ.* **18**, 696–704 (2010). <https://doi.org/10.1007/s10924-010-0225-9>
114. Sikorska, W. *et al.* Prediction studies of environment-friendly biodegradable polymeric packaging based on PLA. Influence of specimens' thickness on the hydrolytic degradation profile. *Waste Manag.* **78**, 938–947 (2018). <https://doi.org/10.1016/j.wasman.2018.07.014>
115. Gonzalez Ausejo, J. *et al.* A comparative study of three-dimensional printing directions: The degradation and toxicological profile of a PLA/PHA blend. *Polym. Degrad. Stab.* **152**, 191–207 (2018). <https://doi.org/10.1016/j.polymdegradstab.2018.04.024>

116. Gonzalez Ausejo, J. *et al.* Three-dimensional printing of PLA and PLA/PHA dumbbell-shaped specimens of crisscross and transverse patterns as promising materials in emerging application areas: Prediction study. *Polym. Degrad. Stab.* **156**, 100–110 (2018). <https://doi.org/10.1016/j.polymdegradstab.2018.08.008>
117. de Macedo, J. R. N., dos Santos, D. J. & dos Santos Rosa, D. Poly(lactic acid)–thermoplastic starch–cotton composites: Starch-compatibilizing effects and composite biodegradability. *J. Appl. Polym. Sci.* **136**, 1–10 (2019). <https://doi.org/10.1002/app.47490>
118. Le Duigou, A., Bourmaud, A. & Baley, C. In-situ evaluation of flax fibre degradation during water ageing. *Ind. Crops Prod.* **70**, 190–200 (2015). <https://doi.org/10.1016/j.indcrop.2015.03.049>
119. Sikorska, W. *et al.* Forensic engineering of advanced polymeric materials-part VII: Degradation of biopolymer welded joints. *Polymers.* **12**, (2020). <https://doi.org/10.3390/polym12051167>
120. Musioł, M. *et al.* (Bio)degradable polymers as a potential material for food packaging: studies on the (bio)degradation process of PLA/(R,S)-PHB rigid foils under industrial composting conditions. *Eur. Food Res. Technol.* **242**, 815–823 (2016). <https://doi.org/10.1007/s00217-015-2611-y>
121. Musioł, M. *et al.* (Bio)degradable polymeric materials for a sustainable future – part 1. Organic recycling of PLA/PBAT blends in the form of prototype packages with long shelf-life. *Waste Manag.* **77**, 447–454 (2018). <https://doi.org/10.1016/j.wasman.2018.04.030>
122. Iñiguez-Franco, F. *et al.* Chemical recycling of poly(lactic acid) by water-ethanol solutions. *Polym. Degrad. Stab.* **149**, 28–38 (2018). <https://doi.org/10.1016/j.polymdegradstab.2018.01.016>
123. Olewnik-Kruszkowska, E., Burkowska-But, A., Tarach, I., Walczak, M. & Jakubowska, E. Biodegradation of polylactide-based composites with an addition of a compatibilizing agent in different environments. *Int. Biodeterior. Biodegrad.* **147**, 104840 (2020). <https://doi.org/10.1016/j.ibiod.2019.104840>
124. Pinto, A. M., Gonçalves, C., Gonçalves, I. C. & Magalhães, F. D. Effect of biodegradation on thermo-mechanical properties and biocompatibility of poly(lactic acid)/graphene nanoplatelets composites. *Eur. Polym. J.* **85**, 431–444 (2016). <https://doi.org/10.1016/j.eurpolymj.2016.10.046>
125. Ye, S. *et al.* Evaluating platelet activation related to the degradation of biomaterials using molecular markers. *Colloids Surfaces B Biointerfaces* **184**, 110516 (2019). <https://doi.org/10.1016/j.colsurfb.2019.110516>
126. Jiang, S. *et al.* Release behavior of tetracycline hydrochloride loaded chitosan/poly(lactic acid) antimicrobial nanofibrous membranes. *Mater. Sci. Eng. C* **59**, 86–91 (2016). <https://doi.org/10.1016/j.msec.2015.10.005>
127. Behrens, A. M. *et al.* Rapid fabrication of poly(DL-lactide) nanofiber scaffolds with tunable degradation for tissue engineering applications by air-brushing. *Biomed. Mater.* **11**, 35001 (2016). <https://doi.org/10.1088/1748-6041/11/3/035001>
128. Zhang, W. *et al.* Strengthened corrosion control of poly (lactic acid) (PLA) and

- poly (ϵ -caprolactone) (PCL) polymer-coated magnesium by imbedded hydrophobic stearic acid (SA) thin layer. *Corros. Sci.* **112**, 327–337 (2016). <https://doi.org/10.1016/j.corsci.2016.07.027>
129. Wang, Y. Y., Yu, H. Y., Yang, L., Abdalkarim, S. Y. H. & Chen, W. L. Enhancing long-term biodegradability and UV-shielding performances of transparent polylactic acid nanocomposite films by adding cellulose nanocrystal-zinc oxide hybrids. *Int. J. Biol. Macromol.* **141**, 893–905 (2019). <https://doi.org/10.1016/j.ijbiomac.2019.09.062>
130. Siafaka, P. I., Barmbalexis, P. & Bikiaris, D. N. Novel electrospun nanofibrous matrices prepared from poly(lactic acid)/poly(butylene adipate) blends for controlled release formulations of an anti-rheumatoid agent. *Eur. J. Pharm. Sci.* **88**, 12–25 (2016). <https://doi.org/10.1016/j.ejps.2016.03.021>
131. Zare, Y., Garmabi, H. & Rhee, K. Y. Degradation biosensing performance of polymer blend carbon nanotubes (CNTs) nanocomposites. *Sensors Actuators, A Phys.* **295**, 113–124 (2019). <https://doi.org/10.1016/j.sna.2019.05.040>
132. Kim, S., Zare, Y., Garmabi, H. & Rhee, K. Y. Variations of tunneling properties in poly (lactic acid) (PLA)/poly (ethylene oxide) (PEO)/carbon nanotubes (CNT) nanocomposites during hydrolytic degradation. *Sensors Actuators, A Phys.* **274**, 28–36 (2018). <https://doi.org/10.1016/j.sna.2018.03.004>
133. Liu, C. *et al.* Melt-compounded polylactic acid composite hybrids with hydroxyapatite nanorods and silver nanoparticles: Biodegradation, antibacterial ability, bioactivity and cytotoxicity. *RSC Adv.* **5**, 72288–72299 (2015). <https://doi.org/10.1039/C5RA14155A>
134. Kumar, A., Tumu, V. R., Ray Chowdhury, S. & Ramana, R. R. A green physical approach to compatibilize a bio-based poly (lactic acid)/lignin blend for better mechanical, thermal and degradation properties. *Int. J. Biol. Macromol.* **121**, 588–600 (2019). <https://doi.org/10.1016/j.ijbiomac.2018.10.057>
135. Vergnol, G. *et al.* In vitro and in vivo evaluation of a polylactic acid-bioactive glass composite for bone fixation devices. *J. Biomed. Mater. Res. - Part B Appl. Biomater.* **104**, 180–191 (2016). <https://doi.org/10.1002/jbm.b.33364>
136. Jandíková, G. *et al.* Effect of a Hybrid Zinc Stearate-Silver System on the Properties of Polylactide and Its Abiotic and the Biotic Degradation and Antimicrobial Activity Thereof. *Chinese J. Polym. Sci.* **36**, 925–933 (2018). <https://doi.org/10.1007/s10118-018-2120-0>
137. Li, X. *et al.* Biodegradable poly-lactic acid based-composite reinforced unidirectionally with high-strength magnesium alloy wires. *Biomaterials* **49**, 135–144 (2015). <https://doi.org/10.1016/j.biomaterials.2015.01.060>
138. Rajesh, G., Ratna Prasad, A. V. & Gupta, A. V. S. S. K. S. Water Absorption Characteristics of Successive Alkali Treated Jute/Polylactic Acid Composites. *Mater. Today Proc.* **5**, 24414–24421 (2018). <https://doi.org/10.1016/j.matpr.2018.10.237>
139. Granados-Hernández, M. V. *et al.* In vitro and in vivo biological characterization of poly(lactic acid) fiber scaffolds synthesized by air jet spinning. *J. Biomed. Mater. Res. - Part B Appl. Biomater.* **106**, 2435–2446 (2018).

- <https://doi.org/10.1002/jbm.b.34053>
140. Wan, L., Zhou, S. & Zhang, Y. Parallel advances in improving mechanical properties and accelerating degradation to polylactic acid. *Int. J. Biol. Macromol.* **125**, 1093–1102 (2019). <https://doi.org/10.1016/j.ijbiomac.2018.12.148>
 141. Wan, L., Li, C., Sun, C., Zhou, S. & Zhang, Y. Conceiving a feasible degradation model of polylactic acid-based composites through hydrolysis study to polylactic acid/wood flour/polymethyl methacrylate. *Compos. Sci. Technol.* **181**, 107675 (2019). <https://doi.org/10.1016/j.compscitech.2019.06.002>
 142. Ma, H. *et al.* Novel platform for visualization monitoring of hydrolytic degradation of bio-degradable polymers based on aggregation-induced emission (AIE) technique. *Sensors Actuators, B Chem.* **304**, 127342 (2020). <https://doi.org/10.1016/j.snb.2019.127342>
 143. Cuevas-Carballo, Z. B., Duarte-Aranda, S. & Canché-Escamilla, G. Properties and Biodegradation of Thermoplastic Starch Obtained from Grafted Starches with Poly(lactic acid). *J. Polym. Environ.* **27**, 2607–2617 (2019). <https://doi.org/10.1007/s10924-019-01540-w>
 144. Chitrattha, S. & Phaechamud, T. Porous poly(dl-lactic acid) matrix film with antimicrobial activities for wound dressing application. *Mater. Sci. Eng. C* **58**, 1122–1130 (2016). <https://doi.org/10.1016/j.msec.2015.09.083>
 145. Li, R. *et al.* Controlled in vitro degradation behavior of highly oriented long-chain-branched poly(lactic acid) produced by solid-phase die drawing. *J. Biomed. Mater. Res. - Part A* 1522–1531 (2019) <https://doi.org/10.1002/jbm.a.36665>.
 146. Wang, W. *et al.* Development of X-ray opaque poly(lactic acid) end-capped by triiodobenzoic acid towards non-invasive micro-CT imaging biodegradable embolic microspheres. *Eur. Polym. J.* **108**, 337–347 (2018). <https://doi.org/10.1016/j.eurpolymj.2018.09.018>
 147. Huang, C. H., Lee, S. Y., Horng, S., Guy, L. G. & Yu, T. Bin. In vitro and in vivo degradation of microfiber bioresorbable coronary scaffold. *J. Biomed. Mater. Res. - Part B Appl. Biomater.* **106**, 1842–1850 (2018). <https://doi.org/10.1002/jbm.b.33987>
 148. Thanh, D. T. M. *et al.* Effects of porogen on structure and properties of poly lactic acid/hydroxyapatite nanocomposites (PLA/HAp). *J. Nanosci. Nanotechnol.* **16**, 9450–9459 (2016). <https://doi.org/10.1166/jnn.2016.12032>
 149. Li, X. *et al.* In vitro degradation kinetics of pure PLA and Mg/PLA composite: Effects of immersion temperature and compression stress. *Acta Biomater.* **48**, 468–478 (2017). <https://doi.org/10.1016/j.actbio.2016.11.001>
 150. Lee, J. C. *et al.* Biodegradability of poly(lactic acid) (PLA)/lactic acid (LA) blends using anaerobic digester sludge. *Macromol. Res.* **24**, 741–747 (2016). <https://doi.org/10.1007/s13233-016-4100-y>
 151. Podzorova, M. V., Tertyshnaya, Y. V., Pantyukhov, P. V., Popov, A. A. & Nikolaeva, S. G. Influence of ultraviolet on polylactide degradation. *AIP Conf. Proc.* **1909**, 1–5 (2017). <https://doi.org/10.1063/1.5013854>
 152. Shi, J. *et al.* Biodegradable PLA Nonwoven Fabric with Controllable Wettability

- for Efficient Water Purification and Photocatalysis Degradation. *ACS Sustain. Chem. Eng.* **6**, 2445–2452 (2018). <https://doi.org/10.1021/acssuschemeng.7b03897>
153. Therias, S., Murariu, M. & Dubois, P. Bionanocomposites based on PLA and halloysite nanotubes: From key properties to photooxidative degradation. *Polym. Degrad. Stab.* **145**, 60–69 (2017). <https://doi.org/10.1016/j.polymdegradstab.2017.06.008>
154. Rodríguez-Tobías, H., Morales, G., Maldonado-Textle, H. & Grande, D. Photodegradation of electrospun composite mats based on poly(D,L-lactide) submicron fibers and zinc oxide nanoparticles. *Polym. Degrad. Stab.* **152**, 95–104 (2018). <https://doi.org/10.1016/j.polymdegradstab.2018.04.002>
155. Kuo, C. F. J., Lan, W. L., Chen, C. Y. & Tsai, H. C. Property modification and process parameter optimization design of polylactic acid composite materials. Part I: Polylactic acid toughening and photo-degradation modification and optimized parameter design. *Text. Res. J.* **85**, 13–25 (2015). <https://doi.org/10.1177/0040517514540766>
156. Mosnáčková, K. *et al.* Complex study of the physical properties of a poly(lactic acid)/poly(3-hydroxybutyrate) blend and its carbon black composite during various outdoor and laboratory ageing conditions. *RSC Adv.* **7**, 47132–47142 (2017). <https://doi.org/10.1039/C7RA08869H>
157. Rocca-Smith, J. R. *et al.* Effect of the state of water and relative humidity on ageing of PLA films. *Food Chem.* **236**, 109–119 (2017). <https://doi.org/10.1016/j.foodchem.2017.02.113>
158. Feng, L., Bian, X., Li, G., Chen, Z. & Chen, X. Compatibility, mechanical properties and stability of blends of polylactide and polyurethane based on poly(ethylene glycol)-b-polylactide copolymers by chain extension with diisocyanate. *Polym. Degrad. Stab.* **125**, 148–155 (2016). <https://doi.org/10.1016/j.polymdegradstab.2015.12.017>
159. Kalita, N. K., Bhasney, S. M., Kalamdhad, A. & Katiyar, V. Influence of Hygrothermal Ageing on the Physico-Mechanical Properties of Alkali Treated Industrial Hemp Fibre Reinforced Polylactic Acid Composites. *J. Environ. Manage.* **261**, 1–8 (2020). <https://doi.org/10.1007/s10924-010-0225-9>
160. Diani, J. & Gall, K. Degradation of PLA Fibers at Elevated Temperature and Humidity. *Society* (2006). <https://doi.org/10.1002/pen>
161. Kaynak, C. & Erdogan, A. R. Mechanical and thermal properties of polylactide/talc microcomposites: Before and after accelerated weathering. *Polym. Adv. Technol.* **27**, 812–822 (2016). <https://doi.org/10.1002/pat.3721>
162. Lin, H. Y., Tsai, S. Y., Yu, H. T. & Lin, C. P. Degradation of Polylactic Acid by Irradiation. *J. Polym. Environ.* **26**, 122–131 (2018). <https://doi.org/10.1007/s10924-016-0928-7>
163. Zembouai, I. *et al.* Electron beam radiation effects on properties and ecotoxicity of PHBV/PLA blends in presence of organo-modified montmorillonite. *Polym. Degrad. Stab.* **132**, 117–126 (2016). <https://doi.org/10.1016/j.polymdegradstab.2016.03.019>

164. Yang, X., Clénet, J., Xu, H., Odelius, K. & Hakkarainen, M. Two step extrusion process: From thermal recycling of PHB to plasticized PLA by reactive extrusion grafting of PHB degradation products onto PLA chains. *Macromolecules* **48**, 2509–2518 (2015). <https://doi.org/10.1021/acs.macromol.5b00235>
165. Nazareth, M., Marques, M. R. C., Leite, M. C. A. & Castro, Í. B. Commercial plastics claiming biodegradable status: Is this also accurate for marine environments? *J. Hazard. Mater.* **366**, 714–722 (2019). <https://doi.org/10.1016/j.jhazmat.2018.12.052>
166. Beltrán-Sanahuja, A., Casado-Coy, N., Simó-Cabrera, L. & Sanz-Lázaro, C. Monitoring polymer degradation under different conditions in the marine environment. *Environ. Pollut.* **259**, 113836 (2020). <https://doi.org/10.1016/j.envpol.2019.113836>
167. Zhao, Y. *et al.* Effects of magnesium oxide (MgO) shapes on in vitro and in vivo degradation behaviors of PLA/MgO composites in long term. *Polymers (Basel)*. **12**, 1–13 (2020). <https://doi.org/10.3390/polym12051074>
168. Felfel, R. M., Hossain, K. M. Z., Parsons, A. J., Rudd, C. D. & Ahmed, I. Accelerated in vitro degradation properties of polylactic acid/phosphate glass fibre composites. *J. Mater. Sci.* **50**, 3942–3955 (2015). <https://doi.org/10.1007/s10853-015-8946-8>
169. Russell, D. A., Meunier, L. & Hutchinson, R. A. Characterization of degradation products from a hydrolytically degradable cationic flocculant. *Polym. Degrad. Stab.* **174**, 109097 (2020). <https://doi.org/10.1016/j.polymdegradstab.2020.109097>
170. Xin, Q. *et al.* Poly[2-(methacryloyloxy)ethyl choline phosphate] functionalized polylactic acid film with improved degradation resistance both in vitro and in vivo. *Colloids Surfaces B Biointerfaces* **185**, 110630 (2020). <https://doi.org/10.1016/j.colsurfb.2019.110630>
171. Schusser, S. *et al.* An application of field-effect sensors for in-situ monitoring of degradation of biopolymers. *Sensors Actuators, B Chem.* **207**, 954–959 (2015). <https://doi.org/10.1016/j.snb.2014.10.058>
172. Butt, M. S. *et al.* Mechanical and degradation properties of biodegradable Mg strengthened poly-lactic acid composite through plastic injection molding. *Mater. Sci. Eng. C* **70**, 141–147 (2017). <https://doi.org/10.1016/j.msec.2016.08.051>
173. Shi, H. *et al.* Poly(glycerol sebacate)-modified polylactic acid scaffolds with improved hydrophilicity, mechanical strength and bioactivity for bone tissue regeneration. *RSC Adv.* **5**, 79703–79714 (2015). <https://doi.org/10.1039/C5RA13334C>
174. Pogorielov, M. *et al.* In vitro degradation and in vivo toxicity of NanoMatrix3D® polycaprolactone and poly(lactic acid) nanofibrous scaffolds. *J. Biomed. Mater. Res. - Part A* **106**, 2200–2212 (2018). <https://doi.org/10.1002/jbm.a.36427>
175. Chu, C. *et al.* Degradation behaviors of PLA-matrix composite with 20 vol% magnesium alloy wires under static loading conditions. *J. Mater. Sci.* **54**, 4701–4709 (2018). <https://doi.org/10.1007/s10853-018-03199-5>

176. Samami, H. & Pan, J. Detection of degradation in polyester implants by analysing mode shapes of structure vibration. *J. Mech. Behav. Biomed. Mater.* **62**, 299–309 (2016). <https://doi.org/10.1016/j.jmbbm.2016.05.002>
177. Li, X. *et al.* A study on Mg wires/poly-lactic acid composite degradation under dynamic compression and bending load for implant applications. *J. Mech. Behav. Biomed. Mater.* **105**, 103707 (2020). <https://doi.org/10.1016/j.jmbbm.2020.103707>
178. Wen, W., Zou, Z., Luo, B. & Zhou, C. In vitro degradation and cytocompatibility of g -MgO whiskers / PLLA composites. *J. Mater. Sci.* (2016) <https://doi.org/10.1007/s10853-016-0525-0>.
179. Li, M., Kim, S., Choi, S., Goda, K. & Lee, W. Effect of reinforcing particles on hydrolytic degradation behavior of poly (lactic acid) composites. *Compos. Part B* **96**, 248–254 (2016). <https://doi.org/10.1016/j.compositesb.2016.04.029>
180. Jandas, P. J., Prabakaran, K., Mohanty, S. & Nayak, S. K. Evaluation of biodegradability of disposable product prepared from poly (lactic acid) under accelerated conditions. *Polym. Degrad. Stab.* **164**, 46–54 (2019). <https://doi.org/10.1016/j.polymdegradstab.2019.04.004>
181. Shaikh, T., Rathore, A. & Kaur, H. Poly (Lactic Acid) Grafting of TiO₂ Nanoparticles : A Shift in Dye Degradation Performance of TiO₂ from UV to Solar Light. *Chemistry Select* **2**, 6901–6908 (2017). <https://doi.org/10.1002/slct.201701560>
182. Riaz, U. & Ashraf, S. M. Characterization of Polymer Blends with FTIR Spectroscopy. *Charact. Polym. Blends Miscibility, Morphol. Interfaces* **9783527331**, 625–678 (2015). <https://doi.org/10.1002/9783527645602.ch20>
183. Neira-Velázquez, M. G., Rodríguez-Hernández, M. T., Hernández-Hernández, E. & Ruiz-Martínez, A. R. Y. Polymer Molecular Weight Measurement. *Handb. Polym. Synth. Charact. Process.* 355–366 (2013) <https://doi.org/10.1002/9781118480793.ch17>.
184. Pattanasuttichonlakul, W., Sombatsompop, N. & Prapagdee, B. Accelerating biodegradation of PLA using microbial consortium from dairy wastewater sludge combined with PLA-degrading bacterium. *Int. Biodeterior. Biodegrad.* **132**, 74–83 (2018). <https://doi.org/10.1016/j.ibiod.2018.05.014>
185. Olewnik-Kruszkowska, E., Koter, I., Skopińska-Wiśniewska, J. & Richert, J. Degradation of polylactide composites under UV irradiation at 254 nm. *J. Photochem. Photobiol. A Chem.* **311**, 144–153 (2015). <https://doi.org/10.1016/j.jphotochem.2015.06.029>
186. Fukushima, K. *et al.* Effect of temperature and nanoparticle type on hydrolytic degradation of poly (lactic acid) nanocomposites. *Polym. Degrad. Stab.* **96**, 2120–2129 (2011). <https://doi.org/10.1016/j.polymdegradstab.2011.09.018>
187. Gleadall, A., Pan, J., Krufft, M. A. & Kellomäki, M. Degradation mechanisms of bioresorbable polyesters. Part 1. Effects of random scission, end scission and autocatalysis. *Acta Biomater.* **10**, 2223–2232 (2014). <https://doi.org/10.1016/j.actbio.2013.12.039>

188. Kelen, T. & Reinhold, V. N. *Polymer Degradation*. **266**, 956–958 (1982). https://doi.org/10.1007/978-3-642-69376-2_2
189. Menczel, J. D. & Prime, R. B. *Thermal Analysis of Polymers: Fundamentals and Applications*. Thermal Analysis of Polymers: Fundamentals and Applications (2008). <https://doi.org/10.1002/9780470423837>.
190. Schick, C. Differential scanning calorimetry (DSC) of semicrystalline polymers. *Anal. Bioanal. Chem.* **395**, 1589–1611 (2009). <https://doi.org/10.1007/s00216-009-3169-y>
191. Cuadri, A. A. & Martín-Alfonso, J. E. Thermal, thermo-oxidative and thermomechanical degradation of PLA: A comparative study based on rheological, chemical and thermal properties. *Polym. Degrad. Stab.* **150**, 37–45 (2018). <https://doi.org/10.1016/j.polymdegradstab.2018.02.011>
192. Tsuji, H., Mizuno, A. & Ikada, Y. Properties and morphology of poly(L-lactide). III. Effects of initial crystallinity on long-term in vitro hydrolysis of high molecular weight poly(L-lactide) film in phosphate-buffered solution. *J. Appl. Polym. Sci.* **77**, 1452–1464 (2000). [https://doi.org/10.1002/1097-4628\(20000815\)77:7<1452::AID-APP7>3.0.CO;2-S](https://doi.org/10.1002/1097-4628(20000815)77:7<1452::AID-APP7>3.0.CO;2-S)
193. Vasanthan, N. & Ly, O. Effect of microstructure on hydrolytic degradation studies of poly (l-lactic acid) by FTIR spectroscopy and differential scanning calorimetry. *Polym. Degrad. Stab.* **94**, 1364–1372 (2009). <https://doi.org/10.1016/j.polymdegradstab.2009.05.015>
194. Kong, Y. & Hay, J. N. The measurement of the crystallinity of polymers by DSC. *Polymer*. **43**, 3873–3878 (2002). [https://doi.org/10.1016/S0032-3861\(02\)00235-5](https://doi.org/10.1016/S0032-3861(02)00235-5)
195. Akash, M. S. H., Rehman, K., Akash, M. S. H. & Rehman, K. *Ultraviolet-Visible (UV-VIS) Spectroscopy. Essentials of Pharmaceutical Analysis* (2020). https://doi.org/10.1007/978-981-15-1547-7_3.
196. Jamshidi, K., Hyon, S. H. & Ikada, Y. Thermal characterization of polylactides. *Polymer*. **29**, 2229–2234 (1988). [https://doi.org/10.1016/0032-3861\(88\)90116-4](https://doi.org/10.1016/0032-3861(88)90116-4)
197. SolarSKI, S., Ferreira, M. & Devaux, E. Characterization of the thermal properties of PLA fibers by modulated differential scanning calorimetry. *Polymer*. **46**, 11187–11192 (2005). <https://doi.org/10.1016/j.polymer.2005.10.027>
198. Murariu, M. *et al.* Characterization of degradation products from a hydrolytically degradable cationic flocculant. *Polym. Degrad. Stab.* **11**, 109097 (2018). <https://doi.org/10.1016/j.polymdegradstab.2020.109097>
199. Wilkie, C. A. TGA/FTIR: An extremely useful technique for studying polymer degradation. *Polym. Degrad. Stab.* **66**, 301–306 (1999). [https://doi.org/10.1016/S0141-3910\(99\)00054-3](https://doi.org/10.1016/S0141-3910(99)00054-3)
200. MacCallum, J. R. Thermogravimetric analysis of polymers for assessing thermal degradation. *Thermochim. Acta* **96**, 275–281 (1985). [https://doi.org/10.1016/0040-6031\(85\)80068-X](https://doi.org/10.1016/0040-6031(85)80068-X)
201. Wilkie, C. A. & Mittleman, M. L. Thermogravimetric Analysis—IR Spectroscopy: An Important Technique for the Study of Polymer Degradation. 116–128 (1994) <https://doi.org/10.1021/bk-1994-0581.ch009>.

202. Doyle, C. D. Estimating thermal stability of experimental polymers. *Anal. Chem.* **33**, 77–79 (1961). <https://doi.org/10.1021/ac60169a022>
203. Villetti, M. A. *et al.* Thermal degradation of natural polymers. *J. Therm. Anal. Calorim.* **67**, 295–303 (2002). <https://doi.org/10.1023/a:1013902510952>
204. Ng, H. M. *et al.* Thermogravimetric Analysis of Polymers. *Encycl. Polym. Sci. Technol.* 1–29 (2018) <https://doi.org/10.1002/0471440264.pst667>
205. Blasco, L. S. & Greus, A. R. Contribution to the study of thermal, biological and photo degradation of polylactide. *Universitat Politècnica de València.* (2012). <http://hdl.handle.net/10251/16470>
206. Agarwal, M., Koelling, K. W. & Chalmers, J. J. Characterization of the Degradation of Polylactic Acid Polymer in a Solid Substrate Environment. 517–526 (1998). <https://doi.org/10.1021/bp980015p>
207. Boey, T. H. L. E. E. F. Y. C. & Khor, K. A. X-Ray Diffraction Analysis Technique for Determining the Polymer Crystallinity in a Polyphenylene Sulfide Composite. **16**, 481–488 (1995). <https://doi.org/10.1002/pc.750160606>
208. Sasaki, S. & Asakura, T. Helix distortion and crystal structure of the α -form of poly(L-lactide). *Macromolecules* **36**, 8385–8390 (2003). <https://doi.org/10.1021/ma0348674>
209. Kaczmarek, H., Nowicki, M. & Vukovi, I. Crosslinked blends of poly (lactic acid) and polyacrylates : AFM , DSC and XRD studies. (2013) <https://doi.org/10.1007/s10965-013-0091-y>
210. Lv, S. *et al.* Microstructure analysis of polylactic acid-based composites during degradation in soil. *Int. Biodeterior. Biodegrad.* **122**, 53–60 (2017). <https://doi.org/10.1016/j.ibiod.2017.04.017>
211. Hamid, S. H. & Prichard, W. H. Polymer-Plastics Technology and Engineering Application of Infrared Spectroscopy in Polymer Degradation. *Polymer-Plastics Technology and Engineering.* (2006). <https://doi.org/10.1080/03602558808070112>
212. Hollande, S. & Laurent, J. L. Study of discolouring change in PVC, plasticizer and plasticized PVC films. *Polym. Degrad. Stab.* **55**, 141–145 (1997). [https://doi.org/10.1016/S0141-3910\(96\)00165-6](https://doi.org/10.1016/S0141-3910(96)00165-6)
213. Oliveira, M. *et al.* The role of shear and stabilizer on PLA degradation. *Polym. Test.* **51**, 109–116 (2016). <https://doi.org/10.1016/j.polymertesting.2016.03.005>
214. Mirau, P. A., Heffner, S. A., Koegler, G. & Bovey, F. A. 2D and 3D NMR for polymer characterization. *Polym. Int.* **26**, 29–34 (1991). <https://doi.org/10.1002/pi.4990260106>
215. Pawlaka, T. & Jaworskaa, Magdalena Potrzebowski, M. J. NMR crystallography of α -Poly(L-lactide). *J. Mater. Chem. C* **3**, 10715–10722 (2015). <https://doi.org/10.1039/C2CP43174B>
216. Suganuma, K. *et al.* NMR analysis of poly(lactic acid) via statistical models. *Polymers.* **11**, 1–8 (2019). <https://doi.org/10.3390/polym11040725>
217. Zhang, X., Espiritu, M., Bilyk, A. & Kurniawan, L. Morphological behaviour of

- poly(lactic acid) during hydrolytic degradation. *Polym. Degrad. Stab.* **93**, 1964–1970 (2008). <https://doi.org/10.1016/j.polymdegradstab.2008.06.007>
218. Olewnik, E. *et al.* Synthesis and structural study of copolymers of l-lactic acid and bis(2-hydroxyethyl terephthalate). *Eur. Polym. J.* **43**, 1009–1019 (2007). <https://doi.org/10.1016/j.eurpolymj.2006.11.025>
219. Okihara, T. *et al.* Crystal Structure of Stereocomplex of Poly(L-lactide) and Poly(D-lactide). *J. Macromol. Sci. Part B* **30**, 119–140 (1991). <https://doi.org/10.1080/00222349108245788>
220. Xin, Q. *et al.* Poly [2- (methacryloyloxy) ethyl choline phosphate] functionalized polylactic acid film with improved degradation resistance both in vitro and in vivo. *Colloids Surfaces B Biointerfaces* **110630** (2019). <https://doi.org/10.1016/j.colsurfb.2019.110630>.
221. Bergström, J. S. & Hayman, D. An Overview of Mechanical Properties and Material Modeling of Polylactide (PLA) for Medical Applications. *Ann. Biomed. Eng.* **44**, 330–340 (2016). <https://doi.org/10.1007/s10439-015-1455-8>
222. Swallowe, G. M. Mechanical Properties and Testing of Polymers: An A–Z Reference. (1999).
223. Shrivastava, A. 1 - Introduction to Plastics Engineering. in *Introduction to Plastics Engineering* 1–16 (2018). <https://doi.org/10.1016/B978-0-323-39500-7.00001-0>
224. Shrivastava, A. 3 - Plastic Properties and Testing. in *Introduction to Plastics Engineering* 49–110 (2018). doi:<https://doi.org/10.1016/B978-0-323-39500-7.00003-4>
225. Scaffaro, R., Maio, A., Gulino, E. F., Morreale, M. & Mantia, F. P. La. The effects of nanoclay on the mechanical properties, carvacrol release and degradation of a PLA/PBAT blend. *Material.* **13**, (2020). <https://doi.org/10.3390/ma13040983>
226. Kaplan, D. L. "Introduction to biopolymers from renewable resources." *Biopolymers from renewable resources*. (1998). https://doi.org/10.1007/978-3-662-03680-8_1
227. Acioli-Moura, R. & Sun, X. S. Thermal Degradation and Physical Aging of Poly(lactic acid) and its Blends With Starch. *Polym. Eng. Sci.* 1–8 (2008). <https://doi.org/10.1002/pen.21019>
228. Yussuf, A. A., Massoumi, I. & Hassan, A. Comparison of polylactic Acid/Kenaf and polylactic Acid/Rise husk composites: The influence of the natural fibers on the mechanical, thermal and biodegradability properties. *J. Polym. Environ.* **18**, 422–429 (2010). <https://doi.org/10.1007/s10924-010-0185-0>
229. Felfel, R. M., Ahmed, I., Parsons, A. J., Walker, G. S. & Rudd, C. D. In vitro degradation, flexural, compressive and shear properties of fully bioresorbable composite rods. *J. Mech. Behav. Biomed. Mater.* **4**, 1462–1472 (2011). <https://doi.org/10.1016/j.jmbbm.2011.05.016>
230. Campos, A., Marconcini, J. M., Martins-Franchetti, S. M. & Mattoso, L. H. C. The influence of UV-C irradiation on the properties of thermoplastic starch and polycaprolactone biocomposite with sisal bleached fibers. *Polymer Degradation and Stability* vol. 97 1948–1955 (2012).

- <https://doi.org/10.1016/j.polymdegradstab.2011.11.010>
231. Ikada, E. Photo- and bio-degradable polyesters. photodegradation behaviors of aliphatic polyesters. *J. Photopolym. Sci. Technol.* **10**, 265–270 (1997). <https://doi.org/10.2494/photopolymer.10.265>
 232. Li, J., Wang, Y., Wang, X. & Wu, D. Crystalline characteristics, mechanical properties, thermal degradation kinetics and hydration behavior of biodegradable fibers melt-spun from polyoxymethylene/poly(L-lactic acid) blends. *Polymers.* **11**, (2019). <https://doi.org/10.3390/polym11111753>
 233. Fukushima, K., Tabuani, D., Arena, M., Gennari, M. & Camino, G. Effect of clay type and loading on thermal, mechanical properties and biodegradation of poly(lactic acid) nanocomposites. *React. Funct. Polym.* **73**, 540–549 (2013). <https://doi.org/10.1016/j.reactfunctpolym.2013.01.003>
 234. Rasselet, D. *et al.* Oxidative degradation of polylactide (PLA) and its effects on physical and mechanical properties. *Eur. Polym. J.* **50**, 109–116 (2014). <https://doi.org/10.1016/j.eurpolymj.2013.10.011>
 235. Chen, W., Qi, C., Li, Y. & Tao, H. The degradation investigation of biodegradable PLA/PBAT blend: Thermal stability, mechanical properties and PALS analysis. *Radiat. Phys. Chem.* **180**, 109239 (2021). <https://doi.org/10.1016/j.radphyschem.2020.109239>
 236. Benítez, A. *et al.* Abiotic degradation of LDPE and LLDPE formulated with a pro-oxidant additive. *Polym. Degrad. Stab.* **98**, 490–501 (2013). <https://doi.org/10.1016/j.polymdegradstab.2012.12.011>